SAND--80-2677

DE82 018632

Distribution
TID-4500-R66-UC-66C

SAND80-2677
Unlimited Release
Printed June 1982

STUDIES OF THE FRICTIONAL HEATING OF POLYCRYSTALLINE DIAMOND COMPACT DRAG TOOLS DURING ROCK CUTTING

Alfonso Ortega
David A. Glowka
Sandia National Laboratories
Albuquerque, New Mexico 87185

ABSTRACT

A numerical-analytical model is developed to analyze temperatures in Polycrystalline Diamond Compact (PDC) drag tools subject to localized frictional heating at a worn flat area and convective cooling at exposed lateral surfaces. Experimental measurements of convective heat transfer coefficients of PDC cutters in a uniform crossflow are presented and used in the model to predict temperatures under typical drilling conditions with fluid flow. The analysis compares favorably with measurements of frictional temperatures in controlled cutting tests on Tennessee marble. It is found that average temperatures at the wearflat contact zone vary directly with frictional force per unit area and are proportional to the one-half power of the cutting speed at the velocities investigated. Temperatures are found to be much more sensitive to decreases in the dynamic friction by lubrication than to increases in convective cooling rates beyond currently achievable levels with water or drilling fluids. It is shown that use of weighted drilling fluids may actually decrease cooling rates compared to those achieved with pure water. It is doubtful that tool temperatures can be kept below critical levels (750°C) if air is employed as the drilling fluid. The degree of tool wear is found to have a major influence on the thermal response of the friction contact zone, so that for equal heating per contact area, a worn tool will run much hotter than a sharp tool. It is concluded that tool temperatures may be kept below critical levels with conventional water or mud cooling as long as the fluid provides good cutter-rock lubrication. In cases where friction between the cutter and rock is high, such as with air drilling, it is doubtful that temperatures can be kept subcritical at high rotary speeds unless direct forced cooling of the friction contact zone can be achieved.

DISCLAIMER

TABLE OF CONTENTS

LIST OF FIGURES

LIST OF TABLES

NOMENCLATURE

A	Area (cm^2)
Co	Cobalt
c_f	Fluid specific heat (kJ/kg-°C)
c	Specific heat of cutter materials (J/gm-°C)
D	Cylinder or PDC stud diameter (cm)
d	Simple slider thickness or PDC wearflat length (cm)
F	Instantaneous cutter force (N)
f	Temperature response function, eqn. 24 (°C/W/cm^2)
h	Heat transfer coefficient (W/cm^2-°C)
i	Measured electric current through heat transfer gage (amps)
k	Thermal conductivity (W/cm-°C)
ℓ	Simple slider half-thickness
L	Total height of PDC cutter or length of finite slider
Nu	Nusselt number = hD/k_f
Pe	Peclet number = $V\ell/2\chi$ or $Vd/4\chi$
P_E	Electrical power supplied to heat transfer gauge (W)
P_T	Thermal power of heat transfer gauge (W)
Pr	Prandtl number = $c_f\ \mu_f/k_f$
Q	Total rate of heat generation (W) or volume flow rate (gpm)
$Q\ell$	Electrical lead and mounting surface heat losses (W)
Q_c	Convected heat rate (W)
q	Wearflat heat flux, Q/A_w, (W/cm^2)
r	Radial location of PDC cutter on bit (cm)
R_G	Electrical resistance of heat transfer gage (Ω)
Re_D	Reynolds number = $\rho_f\ u\ D/\mu_f$
T_G	Temperature of heat transfer gage (°C)
T_w	Average wearflat temperature (°C)
T_f	Average fluid temperature (°C)
u	Corrected flow channel test section velocity (m/s)
$\bar{u}$	Mean flow channel test section velocity (m/s)

u_c	Centerline flow channel test section velocity (m/s)
u_u	Unobstructed flow channel test section velocity (m/s)
V	Sliding velocity (m/s or cm/s)
WC	Tungsten carbide

Greek Symbols

α	Energy partitioning fraction
θ	Cutter rake angle (deg)
$\bar{\theta}$	Average temperature elevation $T_w - T_f$, (°C)
κ	Specific thermal conductance of heat transfer gage phenolic layer (W/°C)
μ	Dynamic friction coefficient
μ_c	Cutting friction coefficient F_c/F_{th}
μ_f	Fluid viscosity (cp)
ρ	Density of cutter materials (gm/cm^3)
ρ_f	Fluid density (kg/m^3)
ϕ	Angle between leading edge of cylinder and heat transfer gage location (degrees)
χ	Thermal diffusivity (cm^2/s)
ω	Bit rotational speed (s^{-1})

Subscripts

c	Cutter force
f	Refers to fluid property
m	Refers to mean area for blocked flow
n	Normal force
r	Rock reaction force
th	Thrust force
u	Refers to unobstructed flow area
w	Refers to wearflat area
1	Refers to slider
2	Refers to rock or fixed semi-infinite solid

INTRODUCTION

One of the principal goals of drilling technology research at Sandia National Laboratories is to develop and evaluate advanced drilling systems to reduce the cost of drilling for geothermal resources. The high cost of geothermal drilling is due primarily to the more severe environment of higher temperatures and harder formations than those normally found in traditional oil and gas well drilling, for which the majority of drilling technology has been developed. The development of methods for drilling faster and longer in these severe environments has thus been a primary objective of the Sandia program.

The most common oil field drilling systems employ roller-cone rock bits and standard drilling muds for chip removal, bit cleaning and lubrication. There are two disadvantages with this system in geothermal applications. First, roller-cone bits require bearings and seals which have greatly reduced lives in high temperature environments. Secondly, many geothermal formations are underpressured, requiring the use of light-weight drilling fluids, such as air, mist or foam. The most stringent requirements for a geothermal drill bit are thus a good penetration rate and an acceptable lifetime in hard, fractured rock at elevated temperatures and the ability to operate with low density fluids which may provide minimal cooling and cleaning [1].

One type of bit which does not employ bearings or seals and, therefore, could possibly meet the above criteria is the drag bit. Drag bits have been in use in the drilling and mineral excavation industries for more than 20 years [2,3,4]; however, their applicability has been generally restricted to soft, nonabrasive rock, due to excessive tool wear in hard formations. The relatively recent development of cutters fabricated of wear-resistant tungsten carbide-cobalt alloys has extended the widespread use of drag bits to harder formations in mineral excavation [12]. Even with the employment of these alloys and single crystal diamonds, however, the use of these bits in wellbore drilling

has not been extended to harder formations due to the greater sensitivity of well cost to bit life in this application.

In 1975 the General Electric Company began exploring the suitability of using their man-made polycrystalline diamond compact (PDC) cutting element, Stratapax®, for rock cutting [7]. It was found that the material's superior hardness and toughness greatly enhanced the cutting tool life as compared to cemented tungsten carbide tools or single crystal diamond tools. In addition, it was found that when mounted at negative rake angles as shown in Figures 1 and 2, diamond chipping is minimized and the tool maintains a sharp cutting edge even as wear progresses. In contrast, conventional drag tools dull by wearing and rounding off the cutting edge when cutting hard rock, effectively increasing the required tool forces to maintain the same rate of penetration. The drilling performance rapidly degrades when this occurs, and therefore the ability to maintain a sharp cutting edge is a significant advance in drag bit technology [1].

Since approximately 1976, Sandia has been involved in the design and development of advanced drag bits employing PDC cutting elements. The development of design criteria for these bits has consisted of a coordinated plan of experimental and analytic studies carried out in collaboration with the General Electric Company Corporate Research and Development Laboratories and various commercial bit manufacturers and users. The experimental program includes single point tests of individual cutters, laboratory tests of full-size prototype bits, and field tests of full-scale bit designs based on laboratory data [5]. In an effort to characterize some of the fundamental aspects of rock cutting by PDC tools, finite-difference and finite element numerical codes have been used by Yarrington [6] and Swenson [11] to simulate the behavior of the rock-tool mechanical interaction.

One of the results of the experimental program is that, even though PDC elements tend to maintain sharp cutting edges, various

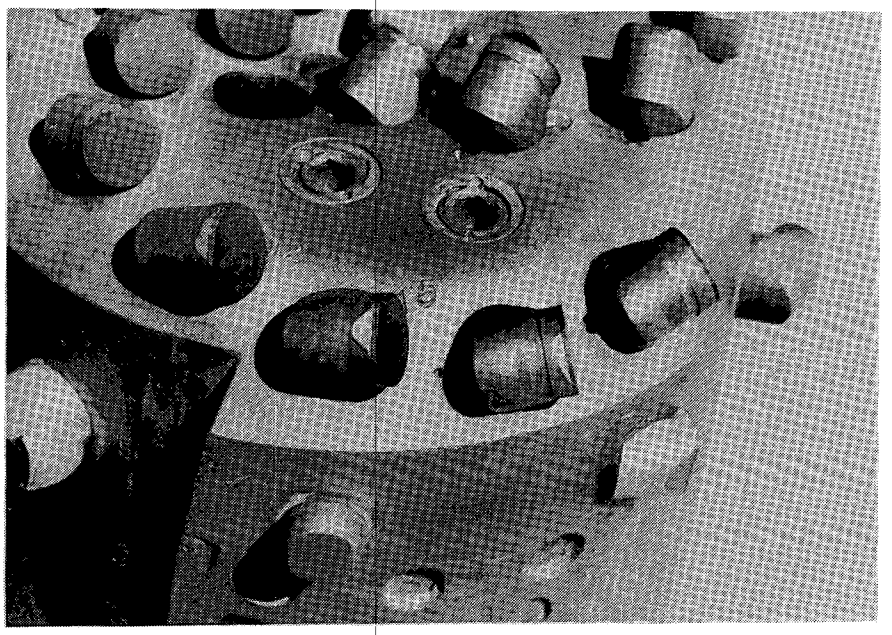

Figure 1. 6-1/2" Sandia PDC Drag Bit After Cutting in Crab Orchard Sandstone and Sierra White Granite - Water Cooling

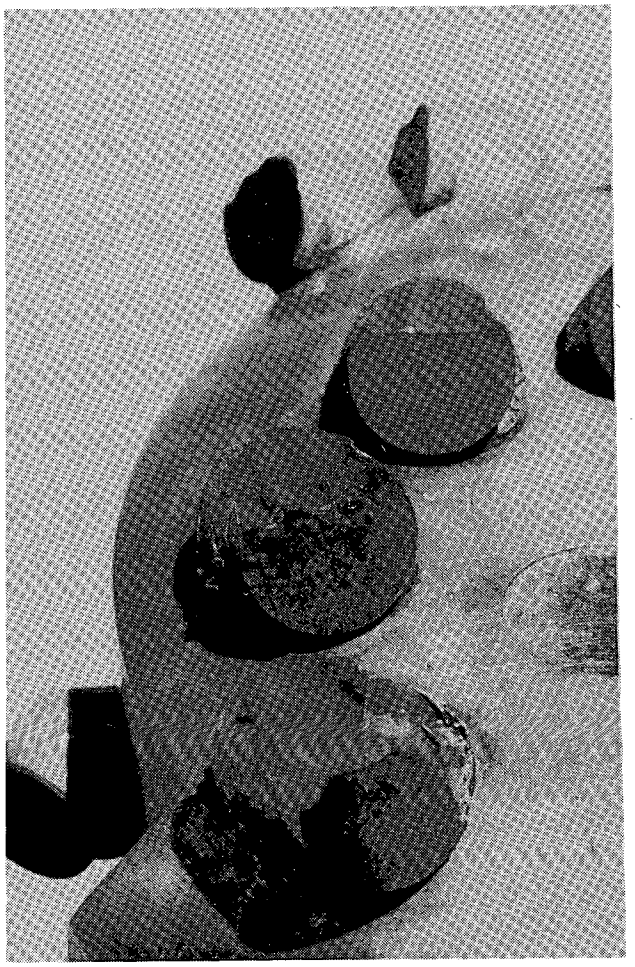

Figure 2. 6-1/2" Sandia PDC Drag Bit After Cutting in Sierra White Granite - Water Cooling

degrees of abrasive wear, chipping, spalling and gross plastic deformation of the PDC element and the steel or tungsten carbide studs to which they are mounted can occur, depending on the cutting conditions. The rate at which tool performance is diminished because of wear and failure is a function of the imposed cutter forces, cutting speed, rock type, and degree of lubrication and cooling. Because of previous experiences in the field of metal cutting and postmortem examination of laboratory and field PDC cutters [13,15,16,17], it has been suggested that cutter temperatures induced by frictional heating can become excessive during cutting in hard rock, thus accelerating wear and increasing the probability of catastrophic tool failure by strength deterioration.

The work described in this report was initiated as part of an effort to systematically model by analytical and numerical means the mechanical and thermal-fluid dynamic phenomena associated with rock-cutting. It is felt that the results of such modeling will improve the evaluation of laboratory data and provide a means of extrapolating relevant input parameters to predict PDC tool performance in field applications where the ability to obtain detailed data is virtually nonexistent. In particular, the goals of this study were:

1. To investigate the severity of frictional heating during PDC drag cutting in rock,
2. To provide thermal input for calculation of thermal stresses to couple with the mechanical analysis,
3. To develop the analytic capability of predicting tool temperatures and their relationship to drilling variables and
4. To be able to recommend methods for alleviating the potential heating problem.

During the course of the study it became apparent that parameters associated with convective cooling of tools could only be obtained by experimental measurement, and appropriate bench-scale experiments were performed to obtain that necessary physical information. In addition,

laboratory measurements of tool temperatures during single-point cutter tests were initiated during the course of this study in collaboration with L. E. Hibbs, Jr. of the GE Corporate Research and Development Laboratories, and some results from this experimental program were fortunately available for comparison with analytical results at the time of issue of this report.

ASPECTS OF FRICTION AND WEAR DURING ROCK CUTTING

Before embarking on an examination of the frictional heating of polycrystalline diamond compact drag tools it is appropriate to discuss some general fundamentals of the rock mechanics of drag cutting and the inevitable irreversible wear associated with the process. Since the surface wear and gross failure of drag tools are inextricably tied to the surface and bulk tool temperatures during cutting [14], it is important to motivate the study of frictional temperatures by understanding their importance in this context.

Rock Cutting Mechanics

The cutting action of drag cutters in hard rock has been widely investigated [5,7,9,10,12,16,27], both analytically and by study of high speed films of the process. It has been generally observed, for example by Fairhurst and Lacabanne [5], that rock cutting is a discontinuous process as shown in Figure 3 [9]. After a major rock chip has been removed the cutter accelerates forward until it impacts the rock, crushing and forming small chips. As the bit contacts the rock, forces build up in the tool and rock until fracture occurs from the bit tip to the rock surface. A major chip is thus formed, and the cycle is repeated. Because of the discontinuous nature of the chip formation-removal process, the resulting tool forces rapidly oscillate, producing intermittent high stress conditions at the tool surface. In the case of drag tools with zero or negative rake angles, Hood [10] has observed that the front face of the tool is not in contact with the rock and thus does not affect the cutting process. The overriding consensus of the various investigations is that rock drilling is much more severe than metal cutting.

In Figure 4 the various forces acting on a PDC drag tool have been represented on a free-body diagram. The instantaneous thrust and cutting forces imposed on the tool are balanced by the rock reaction force on the leading edge and the friction and normal forces on the wear flat.

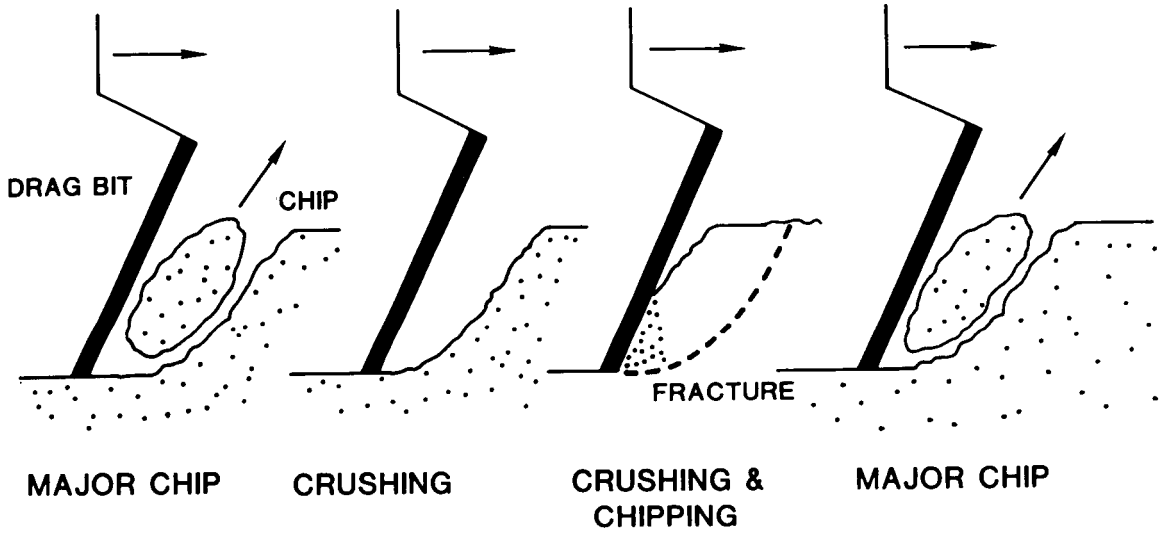

Figure 3. Ideal Cutting Sequence for Drag Cutting in Rock (after Goodrich [9])

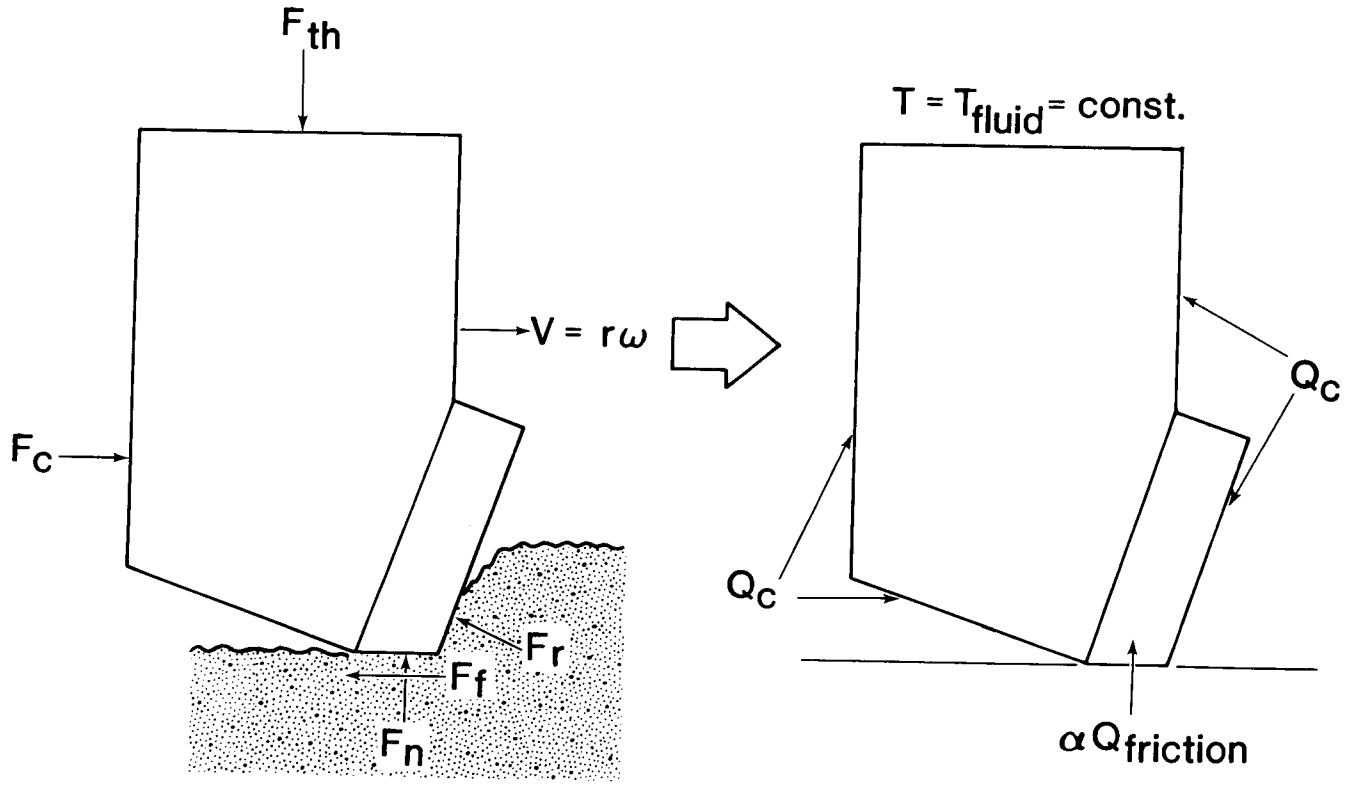

Figure 4. Cutter Forces in Relation to Frictional Heating

Stud-mounted PDC cutters are designed so that an evenly worn area, termed the "wearflat", develops behind the diamond cutting edge and a sharp edge is maintained even as wear progresses. The parabolic wearflats are clearly visible on the cutters in Figure 1 and are idealized in Figure 5. If θ is the rake angle between the vertical and the leading face of the cutter the forces are related simply by:

$$F_c = F_r (\cos\theta - \mu \sin\theta) + \mu F_n \quad (1)$$

$$F_{th} = F_r (\mu \cos\theta + \sin\theta) + F_n \quad (2)$$

It should be apparent that as the thrust and cutting forces vary, so too will the friction and normal forces on the flat. Although the relationship between tool thrust force, torque, speed and rate of penetration with state of wear is not yet well understood for polycrystalline diamond compact drag tools, it has been shown experimentally [2] that in cutting hard, brittle rock such as marble and granite, the required weight on bit for a given penetration rate increases significantly with wear, whereas the torque is only slightly affected. In the same study it is concluded that the frictional forces between worn cutters and brittle specimens during cutting consume a large fraction of the drilling energy. Needless to say, the state of wear of the tool bit is a major factor not only in determining energy requirements during drilling but in determining the degree of frictional heating of the tool as well.

Friction, Wear, and Failure Processes

In laboratory cutting experiments and full scale bit tests, PDC cutters have experienced various modes of wear and failure, including:

1. Separation of compact and stud at the joint.
2. Gross plastic deformation and shear failure of the compact and/or stud.
3. Chipping and spalling of diamond at the leading edge.
4. Micro-chipping of diamond grains and whole grain pullout from

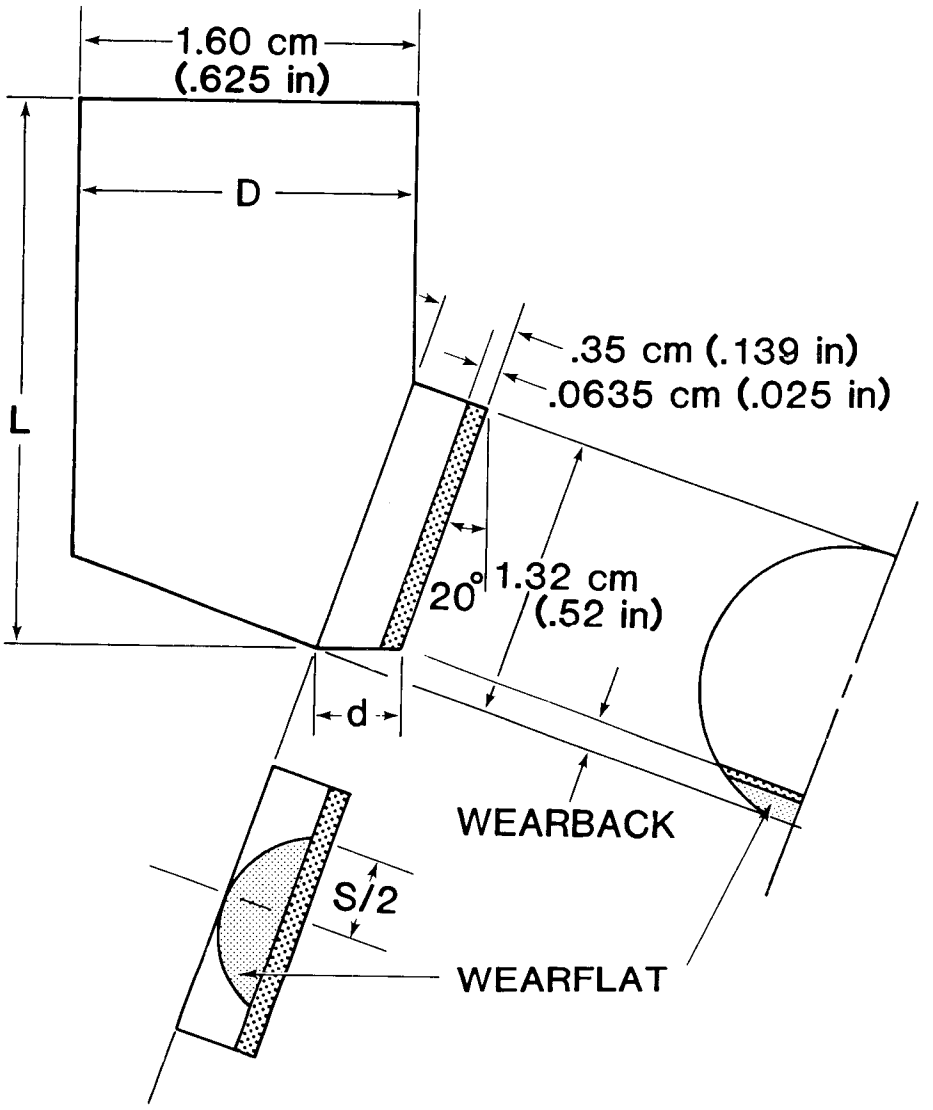

Figure 5. PDC Cutter Dimensions

the matrix at the wearflat.

5. Abrasive wear of tungsten carbide or steel stud over the wearflat area.
6. Heat checking and thermal fatigue of surface layers in high pressure sliding contact.

The resulting damage from some of these processes is shown in Figures 1 and 2 on Sandia-designed Stratapax® bits after laboratory cutting tests. The catastrophic failure of cutters by separation of compact and stud or by plastic deformation and shear failure results from the severe mechanical stresses of cutting coupled with cutting temperatures reaching the level where material strength deteriorates. As a general rule the tungsten carbides used for PDC studs begin to lose their hot hardness at temperatures on the order of 800°C and by 950°C are certainly susceptible to plastic deformation and flow under surface shear [23].

With respect to the contribution of elevated frictional temperatures to the wear of PDC cutters, especially by those processes numbered 3-6 on the preceding list, it is important to distinguish between wear and failure of the sintered diamond leading edge of the compact and the tungsten carbide or steel posts to which they are attached since both materials are in sliding contact at the tool wearflat. Hibbs and Lee [13,14,15] of the GE Corporate Research and Development Laboratories investigated the wear of Stratapax® PDC tools during rock cutting by use of SEM micrographs of the worn cutting edges of polycrystalline diamond compacts. Cutting was principally done on Jack Fork Sandstone, an abrasive, high compressive strength material, at cutting speeds up to 1.5 m/s. Copious cooling was used to prevent thermal damage. The principal conclusions were that the diamond-diamond grain boundaries are sufficiently strong to sustain severe stress and abrasion conditions so that each grain acts like a single diamond cutter and there is no massive particle pullout. Failure of diamond grains was either by crushing, where small segments were chipped away, or by brittle fracture

of large pieces of the diamond grains. Occasionally, gross fracture of the edge was observed under high impact conditions. In a companion study the effect of cutting speed on wear was investigated by cutting at speeds up to 3.3 m/s. It was found that volumetric wear rate greatly increased with cutting speed and, presumably, temperature. It was noted that polycrystalline sintered diamond compacts are subject to gross thermal damage if heated above approximately 750°C due to the stress generated by the difference in thermal expansion between the diamond and trapped islands of residual metal inclusions along diamond grain boundaries. Boundary failure can occur under these conditions, resulting in whole grain pullout. Gross thermal damage of this type has been observed under conditions of dry cutting, where frictional temperatures were estimated to be on the order of 750°C [15]. With good cooling and speeds up to 3.3 m/s, no evidence of bulk thermal damage was detected, and the principal wear mechanism was still diamond grain microchipping. A suggested explanation for the increase in wear with temperature was a decrease in the diamond grain fracture strength with increasing temperature.

The wear of the tungsten carbide substrate to which the sintered diamond edge is bonded and the tungsten carbide or steel studs to which the compacts are attached, is ideally confined to a wearflat whose area increases with distance travelled. The wear of hard metals during rock cutting has been investigated by various researchers primarily interested in improving mineral excavation techniques [10,12,18,19,20,21], and the wear and failure of PDC drag tools share many of the characteristics found for all-metal tools. Larsen-Basse [12], in surveying the literature of hard metal wear, concludes that in rock cutting with hard metal tools the predominant wear mechanisms are impact spalling, impact fatigue spalling, sliding abrasion and thermal fatigue. The spalling mechanisms do not apply to the metal components of PDC tools since the sintered diamond edge receives the leading impact during cutting.

Abrasion and thermal fatigue, however, are without doubt the principal contributors to the metal wear at the wearflat. It is also concluded by Larsen-Basse that tool bit surfaces attain high temperatures and that tool performance is intimately related to thermal conductivity and to the mechanical properties of the tool at the elevated temperature rather than to the room-temperature mechanical properties. It is further suggested by Osburn [20] that aside from mechanical micro-machining and surface scratching which is the predominant abrasion-wear mechanism, frictional wear may become important at higher temperatures where momentary localized welding may occur between points of contact on the metal and rock. Both of these mechanisms involve plastic deformation of the surface layer of the metal. It is concluded by Osburn that microfracturing of surface layers is favored as the predominant form of wear in rock cutting tools. In nonabrasive rocks, surface cracking or heat checking, found where sintered carbides are subjected to thermal fatigue in combination with high contact pressure, would be expected to be of most importance.

In summary, it appears that high frictionally induced temperatures accelerate the occurence and severity of all aspects of polycrystalline diamond compact wear and failure in rock cutting. At tool temperatures up to 700°C the hot hardness and strength of the compact and stud decrease with increasing temperatures so as to accelerate impact wear of the diamond and abrasive wear of the tungsten carbide substrate. At temperatures on the order of 750°C to 800°C, the wear resistance of the tool decreases drastically. The sintered diamond leading edge experiences gross thermal deterioration and whole diamond grain pullout, leading to severe wear. The mechanical strength of the tungsten carbide substrate and stud decreases to the point where gross plastic deformation and shear failure may occur, as well as rapidly accelerated abrasive and frictional wear. At temperatures above 950°C tungsten carbide studs will flow and deform plastically under moderate loads; therefore,

this temperature represents the upper limit for maintaining any measurable tool life.

PREVIOUS RESEARCH

Although the effects of frictional temperatures have been cited as important considerations in various studies of the wear of hard metals and polycrystalline diamond compacts during rock cutting, few in-depth investigations of the heating problem have been reported in the rock cutting literature as compared to the numerous contributions made to the metal cutting and grinding problem. The applications of hard metal drag cutting in mineral excavation and mining have for the most part not warranted detailed consideration of the thermal problem since the heating can be successfully controlled by water cooling if it becomes excessive. A number of researchers have instrumented hard metal drag tools with thermocouples and measured temperatures near cutting surfaces, but no meaningful attempt has been made to correlate the temperatures with drilling variables and rock characteristics.

In a detailed study of hard metal drag tools used for cutting hard rock in mineral excavation applications, Hood [10] concluded that thermal deterioration of the bit, bit-insert, braze joint and the tungsten carbide insert were major causes of failure during dry cutting. Temperatures measured at the tool holder-tungsten carbide insert interface during cutting in a test rig were consistently above 400°C with no cooling water and on the order of 100°C with cooling. It was further suggested that temperatures at the rubbing zone could be greater than 2000°C based on numerical calculation of a cutter geometry with a constant strength heat flux imposed at the wearflat. No details were given as to the predicted effect of cooling.

Whitbread [25] measured the temperatures on the back side of hard metal inserts used in dry rotary drilling of sandstone. With little or no cooling, temperature equilibrium was reached in approximately five minutes and the average temperature for all tests was 150°C. The highest temperature measured was 490°C, and temperatures above 300°C were common. Fish [26] measured temperatures of 405 to 500°C in the vicinity of hard

metal inserts in dry percussive rotary drilling in sandstone, but few details were given as to the cutting conditions. Rae [18] ran WC-Co sliders dry against sandstone wheels in order to investigate temperatures achievable at high sliding velocities. He observed that a glassy layer formed on the wheel indicating that the temperature of fusion of quartz, 1250°C, was achieved at the sliding interface.

In most cases temperatures have been measured at some distances from the sliding wearflat-rock interface and the maximum bulk temperatures at the interface have been inferred, as by Rae [18], or have been found by using a numerical model of the tool to extrapolate measured temperatures to the surface, as done by Hood [10]. Even though each application that has been investigated differs substantially from the use of PDC's mounted on tungsten carbide holders which are in turn mounted on a bit body, the results clearly indicate that in the much more severe application envisioned for this configuration in wellbore drilling, temperatures induced by frictional heating can easily be greater than 500°C and may approach the temperature of deterioration of the sintered diamond in the compacts. As part of the present study, Hibbs [15] has performed a number of single point cutting tests with carefully prepared pre-ground PDC cutters instrumented with miniature thermocouples placed near the rubbing wearflat surface. Discussion of these experimental results will be deferred to a later section where they will be compared with analytical predictions of mean surface frictional temperatures developed in the following sections.

THEORETICAL FRICTIONAL TEMPERATURE MODELS

The rock cutting sequence suggested by Goodrich [9], shown in Figure 3, is realistically a highly idealized sequence that is approached in practice only in carefully controlled single cutter tests. It has been suggested that because of the interaction of cutters in full-scale PDC bits, and because of drill string dynamics, the individual cutters may not be in constant normal contact with the rock but in fact may become temporarily separated from the rock so that drilling fluid wets the wearflat surface. This operating sequence has not been substantiated in full bit tests but intuitively appears to be a valid possibility. Regardless of this departure from the simple cutting sequence, it is nonetheless both conservative and convenient to consider the effects of friction on a PDC cutter by allowing the cutter wearflat to be in constant sliding contact with the rock. A single idealized drag cutting tool is thus subjected to the conditions shown in Figure 4, in which the mechanical frictional force F_f accounts for a uniform surface heat flux at the wearflat and drilling fluid flowing around the cutter provides convective cooling at the lateral surfaces. In addition heat is conducted into the bit body at the upper contacting surfaces. For the purposes of analysis the PDC cutter is merely an element in constant sliding contact with rock whose lateral surfaces are non-isothermal.

The Flash Temperature Concept

Like all surfaces in sliding contact the real area of contact between the PDC cutter and the rock is significantly smaller than the apparent contact area of the wearflat. Microscopically both the tungsten carbide or steel and sintered diamond surfaces at the wearflat are rough and irregular, and contact is made only at the asperities, i.e. bumps, on the surface of the wearflat and on the equally rough rock surface. Frictional heat derives either from the breaking of adhered junctions between contacting asperities or by the thermodynamically irreversible process of plastic deformation of surface layers in the contacting

bodies. It is reasonable to assume that the heat is generated at the contacting asperities and in the immediate surface layers experiencing deformation.

If the surfaces were considered to be smooth and subjected to the equivalent uniformly distributed frictional heat flux generated at the interface, the resulting temperature would be some area-averaged macroscopic surface temperature. The temperature at real contact areas, however, are higher than this and are of short duration. They have thus been termed "flash temperatures" and have been the subject of study by numerous investigators [30,31,32,33,38,39]. Unfortunately, the calculation of flash temperatures requires detailed knowledge of the real contact area of contacting asperities which is extremely difficult to obtain. In the case of hard metal and sintered diamond materials in sliding contact with rock, flash temperatures have not been investigated but certainly are expected to be present as in any sliding pair. A useful rule of thumb is that the flash temperature at sliding surfaces is usually the melting temperature of the lower melting of the two sliding materials. As a matter of interest the fusion temperature of quartz is 1250°C, and the melting or transition temperature of a high grade tungsten carbide is on the order of 2800°C. The transition temperature of a pure diamond crystal is about 3550°C.

In the present analysis there are enough unknowns regarding the actual behavior of PDC cutters in rock sliding and cutting so that an attempt to quantify possible flash temperatures at the wearflat is clearly out of the question. Even though a macroscopic surface temperature is not an actual surface temperature, it does represent a temperature which is obtained at a distance below the surface at which the effects of individual temperature flashes are diffused. This quantity is a useful measure of the near-surface temperature response of the PDC wearflat and in any case more nearly represents that temperature which could conceivably be measured by a thermocouple imbedded near

the contacting surface. In this study the PDC contacting surface and the rock are considered to be smooth so that only the macroscopic average surface temperatures induced by friction are considered.

The Temperature of Moving Heat Sources

Theoretically, the sliding PDC cutter shown in Figure 4 is subjected to a uniform frictional heat flux which is stationary with respect to the cutter but which moves at the sliding velocity over the rock surface. The surface temperature is governed not only by the temperature response of the PDC cutter but also by the response of the rock to a moving source of heat. Assuming that all of the mechanical friction is manifested as heat at the interface, the total heat generated is

$$Q = \mu F_n V \tag{3}$$

where the fraction αQ is transmitted to the cutter or slider and $(1-\alpha)Q$ goes into the rock. The partitioning fraction α is central in determining the quantity of the total frictional heat which is used in calculating tool wearflat temperatures. It will be shown that it is principally a function of the thermal properties of the two surfaces and the sliding velocity. Analytically the principal tasks are to determine response characteristics of a PDC cutter exposed to localized wearflat heating and to evaluate the partitioning coefficient α.

The great majority of the investigations of friction temperatures have as theoretical basis the classic work of Blok [30,32], Jaeger [31] and Archard [33]. Analytical solutions have been derived for the governing transient Laplace equation for the response of a semi-infinite solid exposed to both stationary and moving sources of heat of various geometries. These results will be briefly reviewed here.

The solutions for the temperature field about square and band sources of heat moving over a semi-infinite constant property solid are given by Jaeger [31] for the case where no heat is lost from the surfaces not exposed to heating. For a band source of width 2ℓ moving with velo-

city V in the direction of increasing x, the temperature of the surface z = 0 is dependent on whether or not there is sufficient time for the temperature distribution of a stationary contact to be established in the semi-infinite body. The speed criterion is given in terms of the dimensionless group

$$Pe = \frac{V\ell}{2\chi_2} \tag{4}$$

where χ is the thermal diffusivity of the solid. This group has been called a Peclet number by some investigators even though its significance cannot be interpreted in the same vein as the Peclet number of convective heat transfer.

For slow moving band heat sources the solution is approximately given by the solution for a stationary band source, i.e., for:

$$Pe < 0.1 \qquad \bar{\theta} = \frac{4\ q_2\chi_2}{\pi\ k_2 V}\{-2.303\ Pe \log 2Pe + 1.616\ Pe\} \tag{5}$$

For a fast moving band heat source:

$$Pe > 5 \qquad \bar{\theta} = \frac{8q_2\chi_2 Pe^{1/2}}{3k_2 V\sqrt{\pi}} = \frac{1.064q_2}{k_2}\left(\frac{\chi_2\ell}{V}\right)^{1/2} \tag{6}$$

For a square source of heat of side 2ℓ moving at velocity V along the plane z = 0 the solution is given by:

$$Pe < 0.1 \qquad \bar{\theta} = \frac{8\ \chi_2 q_2\ Pe}{\pi\ k_2 V}\left\{\ell n(1+\sqrt{2}) - \frac{(\sqrt{2}-1)}{3}\right\} = 0.946\ \frac{q_2\ \ell}{k_2} \tag{7}$$

and

$$Pe > 5 \qquad \bar{\theta} \cong \frac{1.064q_2}{k_2}\left(\frac{\chi_2\ell}{V}\right)^{1/2} \tag{8}$$

Note that for Pe > 5, the solution for a square source of heat is given approximately by that for a band source. Archard [33] gives the solution for a fast moving circular source of heat of radius ℓ as

$$Pe = \left(\frac{V\ell}{2\chi_2}\right) > 5 \qquad \bar{\theta} = \frac{\pi\ q_2}{3.25\ k_2}\left(\frac{\chi_2\ell}{V}\right)^{1/2} = \frac{0.966\ q_2}{k_2}\left(\frac{\chi_2\ell}{V}\right)^{1/2} \tag{9}$$

In all cases $\bar{\theta}$ is the steady average wearflat temperature elevation over the fluid temperature. Even though these expressions were derived

in attempts to calculate flash temperatures at microscopic contacting regions, their applicability is not restricted to contacting surfaces of small proportions as long as the assumptions made in deriving them are not violated. In the case of a slider with an apparent contact area of the size of PDC wearflats, it is useful to remember that the assumption of a smooth surface implies that the apparent and real contact areas are one and the same. The significance of the macroscopic temperature thus calculated has already been discussed.

Partitioning of Frictional Heat

In any practical case the moving source of heat which might produce the temperatures given by Equations 5 through 9 is generated by friction from a physical slider, such as a polycrystalline diamond compact cutter, if it is assumed to slide in constant normal contact on the rock being cut at the wearflat. If the slider material is a perfect insulator the average temperature at the interface would be given exactly by Equations 5 through 9 for sliders of these cross-sectional geometries. When both the slider and the fixed material have finite conductivity the problem is more complicated since both bodies accept some of the frictional heat. Various methods have been used to partition the energy. Archard [33] has suggested that the true interface temperature can be approximated by first calculating the temperature of each body with the appropriate solution assuming that all of the heat is supplied to it. The true temperature is then calculated by

$$\frac{1}{\bar{\theta}} = \frac{1}{\bar{\theta}_A} + \frac{1}{\bar{\theta}_B} \quad , \tag{10}$$

where $\bar{\theta}_A$ and $\bar{\theta}_B$ are the average temperatures of the bodies from the independent solutions. Jaeger [31] calculated the energy partitioning fraction α by requiring that the average temperature calculated for the slider receiving αq of the frictional heat flux be equal to the average temperature over the area of contact for the moving source of

strength $(1-\alpha)q$. Recently a novel finite element approach has been used by Kennedy [40] in which the moving and stationary specimens are numerically modelled such that no approximation of the energy partitioning is required. In the present study the method of Jaeger has been adopted to approximate the partitioning fraction since it permits both the use of available fully closed form expressions for the average interface temperature of the sliding and fixed components, and applications of very simple expressions with first order parameters when only discrete thermal response characteristics are available.

Results for Simplified Sliders

Before examining the thermal response of PDC cutter geometries it is useful to derive the frictional temperature relations for simplified geometries in order to have a basis for comparison. In Figure 6 various two and three-dimensional sliders are shown in which k_1 and χ_1 are the thermal conductivity and thermal diffusivity of the slider and k_2 and χ_2 are the properties of the fixed semi-infinite solid, in this context, the rock. The slider is exposed to surface cooling by convection represented by the heat transfer coefficient h, and slides along the surface with constant velocity V.

For the semi-infinite two- and three-dimensional sliders, Figures 6b and 6a, the governing equation is the well known fin formulation:

$$\frac{d^2\theta}{dz^2} - m^2\theta = 0 \qquad (11)$$

$$z = 0 \qquad -k_1 \frac{d\theta}{dz} = q_1$$

$$z \to \infty \qquad \theta = 0$$

where z is in the direction towards the fin and z = 0 is the contact surface. θ is the temperature elevation over the ambient or fluid temperature. It is assumed to be constant over the cross-section.

a. For the semi-infinite square rod of side $2\ell = d$ (Figure 6a):

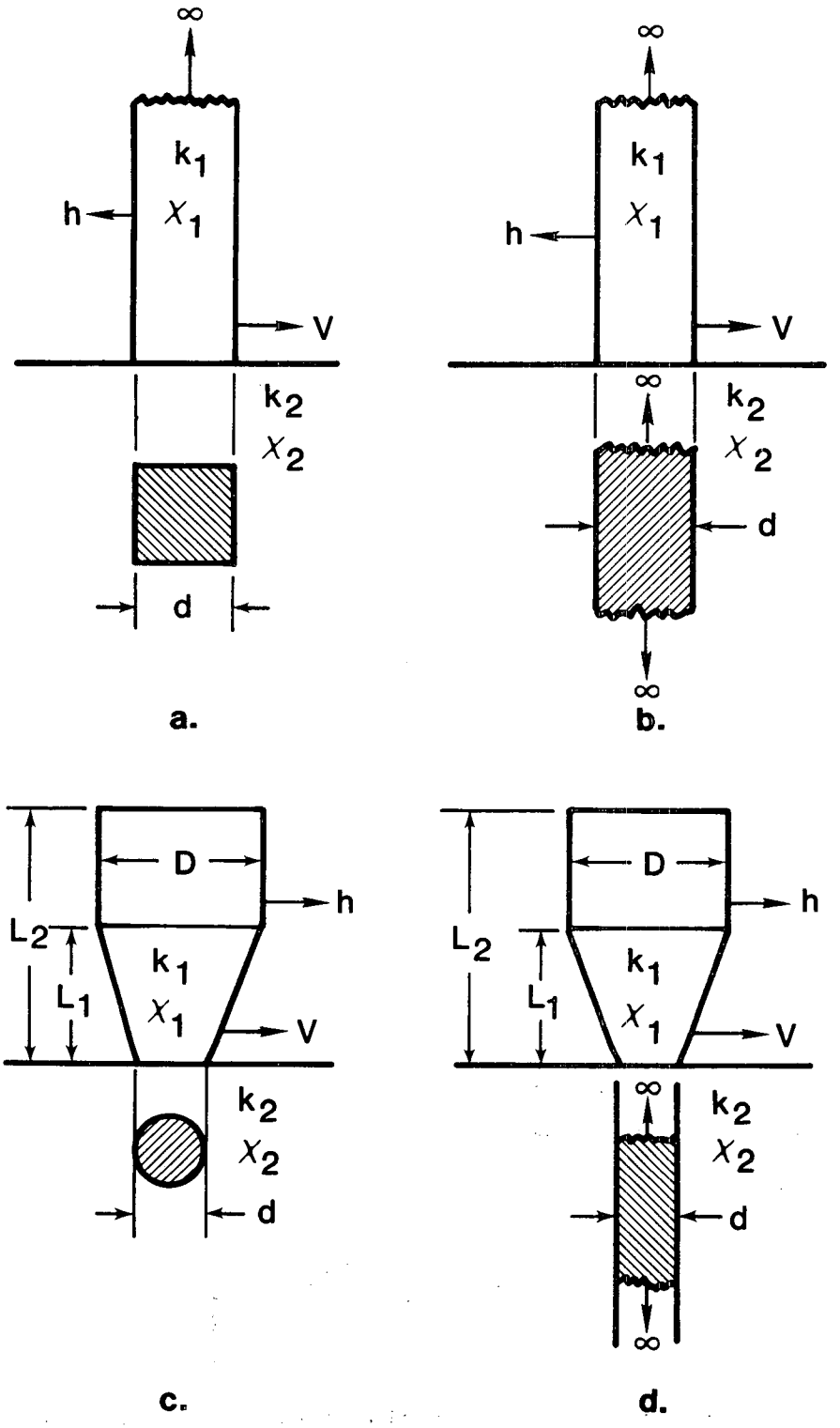

Figure 6. Simplified Frictional Sliders

$$m^2 = \frac{2h}{k_1 \ell} = \frac{4h}{k_1 d} \tag{12}$$

and:

$$\theta_o = q_1 \left(\frac{\ell}{2k_1 h} \right)^{1/2} = q_1 \left(\frac{d}{4k_1 h} \right)^{1/2} \tag{13}$$

where θ_o is the slider average end temperature.

b. For the semi-infinite two-dimensional slider of thickness $2\ell = d$ (Figure 6b):

$$m^2 = \frac{h}{k_1 \ell} = \frac{2h}{k_1 d} \tag{14}$$

$$\theta_o = q_1 \left(\frac{\ell}{k_1 h} \right)^{1/2} = q_1 \left(\frac{d}{2k_1 h} \right)^{1/2} \tag{15}$$

In order to derive the partitioning fraction α, it is required that the temperature of the slider receiving a portion of the frictional energy $q_1 = \alpha q$ be equal to the temperature of the fixed solid receiving $q_2 = (1-\alpha)q$ of the energy as the source moves over its surface. Note that $q_1 + q_2 = q$, the total generated heat per unit area.

a. For case (6a) compare Equations 13 and 8 assuming a fast moving slider, i.e. $V\ell/2\chi_2 > 5$:

$$\alpha q \left(\frac{\ell}{2k_1 h} \right)^{1/2} = (1-\alpha) \frac{8q \, \chi_2 Pe^{1/2}}{3k_2 \, V \sqrt{\pi}} \quad . \tag{16}$$

where subscripts 1 and 2 refer to the slider and stationary surface respectively.

Solving for α:

$$\alpha = \left[1 + \frac{3\sqrt{2\pi}}{8} \left(\frac{k_2}{k_1} \right) \frac{\left(\frac{V\ell}{2\chi_2} \right)^{1/2}}{\left(\frac{h\ell}{k_1} \right)^{1/2}} \right]^{-1} \tag{17}$$

Substituting the partitioning coefficient, Equation 17, into the expression for frictional temperature given by Equation 16, and replacing the frictional heat flux with the equivalent expression given by Equation 3:

$$\bar{\theta} = \frac{\frac{\mu F_n V}{A_w}\left(\frac{\ell}{2k_1 h}\right)^{1/2}}{\left[1 + \frac{3\sqrt{2\pi}}{8}\left(\frac{k_2}{k_1}\right)\frac{\left(\frac{V\ell}{2\chi_2}\right)^{1/2}}{\left(\frac{h\ell}{k_1}\right)^{1/2}}\right]} \tag{18}$$

where $A_w = 4\ell^2$ is the area of contact. Equivalently:

$$\bar{\theta} = \frac{\frac{\mu F_n V}{A_w} \cdot \frac{\ell}{\sqrt{2}\, k_1}}{\left(\frac{h\ell}{k_1}\right)^{1/2} + \frac{3\sqrt{2\pi}}{8}\left(\frac{k_2}{k_1}\right)\left(\frac{V\ell}{2\chi_2}\right)^{1/2}} \tag{19}$$

$$\alpha q \left(\frac{\ell}{k_1 h}\right)^{1/2} = (1-\alpha)\frac{8q\,\chi_2\,Pe^{1/2}}{3\sqrt{\pi}\;k_2\;V}$$

b. For the two-dimensional slider of case (6b), again compare Equations 15 and 6, for $L > 5$:

$$\alpha = \left[1 + \frac{3\sqrt{\pi}}{4}\left(\frac{k_2}{k_1}\right)\frac{\left(\frac{V\ell}{2\chi_2}\right)^{1/2}}{\left(\frac{h\ell}{k_1}\right)^{1/2}}\right]^{-1} \tag{20}$$

$$\bar{\theta} = \frac{\frac{\mu F_n V}{A_w} \cdot \frac{\ell}{k_1}}{\left(\frac{h\ell}{k_1}\right)^{1/2} + \frac{3\sqrt{\pi}}{4}\left(\frac{k_2}{k_1}\right)\left(\frac{V\ell}{2\chi_2}\right)^{1/2}} \tag{21}$$

where

$$q = \frac{\mu F_n V}{A_w} \tag{22}$$

is the frictional heat flux rate at the contact area.

Equations 19 and 21 for the contact temperature of a three-dimensional and two-dimensional slider respectively are nearly identical except for constants. It is shown that the theoretical temperature over the contact surface is directly proportional to the frictional force μFn, and approximately proportional to $V^{1/2}$ for moderate cooling and high sliding

speeds. In addition the temperature varies inversely with a non-linear function of the convective cooling coefficient h.

It is enlightening to compare the temperatures for the two- and three-dimensional sliders by comparison of Equations 19 and 21. The ratio is:

$$\frac{\bar{\theta}_{2\text{-}D}}{\bar{\theta}_{3\text{-}D}} = \sqrt{2}\ \frac{\left[\left(\frac{h\ell}{k_1}\right)^{1/2} + \frac{3\sqrt{2\pi}}{8}\left(\frac{k_2}{k_1}\right)\left(\frac{V\ell}{2\chi_2}\right)^{1/2}\right]}{\left[\left(\frac{h\ell}{k_1}\right)^{1/2} + \frac{3\sqrt{\pi}}{4}\left(\frac{k_2}{k_1}\right)\left(\frac{V\ell}{2\chi_2}\right)^{1/2}\right]} \tag{23}$$

$$\cong 1.4\ \frac{\left[\left(\frac{h\ell}{k_1}\right)^{1/2} + 0.94\left(\frac{k_2}{k_1}\right)\left(\frac{V\ell}{2\chi_2}\right)^{1/2}\right]}{\left[\left(\frac{h\ell}{k_1}\right)^{1/2} + 1.33\left(\frac{k_2}{k_1}\right)\left(\frac{V\ell}{2\chi_2}\right)^{1/2}\right]}$$

From this it is shown that the two-dimensional slider model at most overpredicts the temperature by about 40%. Some results for a tungsten carbide slider sliding on rock are shown in Table 1 for these typical conditions.

$$\ell = \frac{d}{2} = 0.2 \text{ cm}$$

$$k_1 = k_{WC} = 0.42 \text{ W/cm-°C}$$

$$k_2 = k_{rock} = 0.02 \text{ W/cm-°C}$$

$$\chi_2 = \text{rock diffusivity} = 0.01 \text{ cm}^2/\text{s}$$

TABLE 1. NUMERICAL RESULTS FOR SIMPLIFIED SLIDERS

h (W/cm^2-°C)	V (cm/s)	$h\ell/K_1$	$V\ell/2\chi_2$	$\alpha_{2\text{-}D}$	$\alpha_{3\text{-}D}$	$\bar{\theta}_{2D}/\bar{\theta}_{3D}$
0.01	10.	0.005	105.	0.1027	0.1393	1.0425
0.01	50.	0.005	525.	0.0487	0.0675	1.0200
0.01	100.	0.005	1050.	0.0349	0.0487	1.0145
0.01	500.	0.005	5250.	0.0159	0.0224	1.0071
0.01	1000.	0.005	10500.	0.0113	0.0159	1.0041
1.00	10.	0.50	105.	0.5336	0.6181	1.2210
1.00	50.	0.50	525.	0.3385	0.4200	1.1400
1.00	100.	0.50	1050.	0.2657	0.3385	1.1100
1.00	500.	0.50	5250.	0.1393	0.1862	1.0577
1.00	1000.	0.50	10500.	0.1027	0.1393	1.0425

For this parameter range which spans the range of magnitudes which might be encountered for rotary drilling in rock, the energy partitioning fraction varies from 0.01 to about 0.6. Furthermore the greatest difference between calculated temperatures is about 20%. Realistically the comparison for h = 1.0 W/cm^2-°C is not valid since the implicit assumption of a one-dimensional temperature profile in the slider is violated. Nonetheless, it is interesting to note that for these physical properties the fraction of energy that is conducted into the slider is less than 10% for little cooling but up 60% for moderate cooling.

THE PDC CUTTER THERMAL RESPONSE

Computational Approach

As in the examples of the previous section it is possible to obtain approximate closed form expressions for the frictional temperature if convenient solutions can be derived for conduction in the sliding pair. Usually the geometry and boundary conditions either prohibit the derivation of analytic solutions or result in mathematical expressions which are not convenient to use. Ling [35] for example successfully applied integral transform techniques to obtain solutions for a number of different geometries. It is nearly impossible to obtain an analytic solution for the temperature response of an element given the multiple materials and relatively complicated three-dimensional geometry of a stud-mounted PDC cutter.

Referring again to Figure 4, it is seen that as a first approximation one can assume that the PDC cutter is two-dimensional and that the area of contact at the rock is a band. The boundary conditions of convection and conduction are applied at the lateral surfaces of the cutter as shown. The surface temperature response of the fixed rock is given by Equation 6 if no heat transfer is allowed at the non-contacted rock surface. The temperature response of the cutter can most conveniently be obtained with a numerical finite-difference model of the two-dimensional approximation, and the resulting expressions can then be combined as previously shown. This method will suffer from the inherent error in computing the thermal response in a three-dimensional element with a two-dimensional model, but it will be shown that within practical conditions the error does not nullify the usefulness of the results.

The typical polycrystalline diamond compact cutter design shown in Figure 5 was used to develop numerical finite-difference models representing three stages of wear. The three finite-difference meshes used are shown in Figure 7. Numerical solution of the differenced

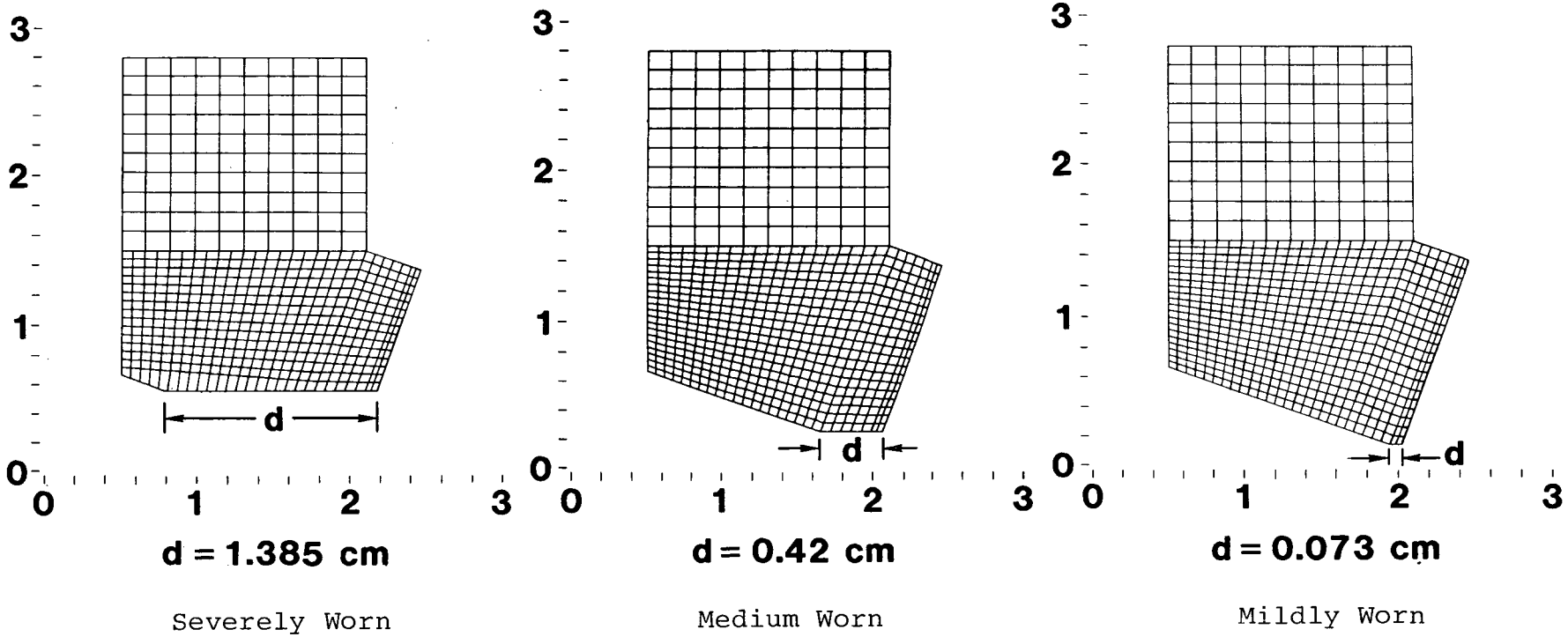

Figure 7. Two-Dimensional Cutter Finite Difference Meshes

form of the heat equation in two dimensions was accomplished with the simulator code CINDA [50]. Frictional heat was simulated as a line of heat sources applied at the wearflat surface elements. Constant convective cooling was allowed at the lateral surfaces. The upper surface which in practice would be in contact with the bit body was maintained at the fluid temperature, implying that the maximum amount of heat conduction possible is allowed into the bit body. This also implies that the bit body is modeled as being isothermal at the fluid temperature. Realistically, this condition could only be achieved under very high convective cooling rates. It is reasonable to expect, therefore, that for low cooling this constant temperature upper boundary condition will cause predicted temperatures to be lower than one would encounter in practice. For conditions of high cooling which are of greater significance in actual practice, the percentage of the heat removed by convection is greater than that removed by conduction into the bit body, and the underprediction of the frictional temperatures should then be less significant. In a subsequent section it will be shown that consideration of the cutter as a two-dimensional element tends to overpredict the temperatures compared to the full three-dimensional model. It is expected that these opposing features of the model will tend to negate each other; comparison of the final results with laboratory data generally verify that neither deficiency significantly affects the overall accuracy of the predicted temperatures.

Results for Various Degrees of Wear

Numerical simulation was performed for a range of wearflat heating rates from 250 W/cm^2 to 5000 W/cm^2 and heat transfer coefficients ranging from 0.001 W/cm^2-°C, representing negligible cooling, up to 10.0 W/cm^2-°C. The thermal properties of the tungsten carbide and sintered diamond components used for these simulations are shown in Table 2. The effects of temperature dependent properties were not investigated.

TABLE 2. PROPERTIES OF TUNGSTEN CARBIDE AND SINTERED DIAMOND AT APPROXIMATELY 100°C

Tungsten Carbide			Polycrystalline Sintered Diamond		
k (W/cm-°C)	ρ (gm/cm^3)	C (J/gm-°C)	k (W/cm-°C)	ρ (gm/cm^3)	C (J/gm-°C)
0.418	15.6	0.23	5.43	3.51	0.794

Temperature fields in the PDC cutters are shown in Figures A1 through A23 in Appendix A for a range of simulated conditions. It should be emphasized that the thermal response of the PDC is independent of the nature of the imposed wearflat heat flux as long as it can be modeled as a line of heat sources in the computational model. In this case the heating flux is frictionally induced. The magnitude of the surface flux used was calculated from Equation 22 for values of frictional force and velocity achievable in practice. A fluid temperature of 80°C was assumed.

For a mildly worn tool, Figures A1 through A5, only the sintered diamond component of the compact will be subject to heating as rubbing and cutting occurs. Because the frictional contact area is small and because the thermal conductivity of the diamond is much higher than that of the tungsten carbide, a mildly worn tool generally conducts and diffuses the wearflat heat well. Using a fluid temperature of 80°C it is noted from Figures A1 through A5 that the wearflat reaches a maximum of 280°C only under conditions of low cooling and high heating rates. Also because of its high conductivity, the sintered diamond layer sustains only small normal temperature gradients.

In a tool that is more severely dulled and worn as in Figures A6 through A11, where the wearflat dimension (d) is about 0.42 cm, both the tungsten carbide and sintered diamond components are directly exposed to frictional heat at the wearflat. It is important to note that the temperatures achieved in a worn PDC tool are high not only because the wearflat area (and the total friction heating) is greater, but also

because a tool with medium wear (Figures A6-A11) does not diffuse wearflat heat as well as a sharp tool (Figures A1-A5). This distinction has not been previously recognized. Because of the relatively low conductivity of the tungsten carbide, not only are the temperatures higher but the temperature gradients near the surface are much more severe as typified by Figures A9 and A11. These very high normal gradients probably contribute greatly to the heat checking and cracking observed at the wearflat of worn tools.

The tendency towards higher temperatures for increasing wearflat area is emphasized in the models shown in Figures A12 through A17. The tool is very severely worn with the wear flat dimension d of 1.385 cm. In this exaggerated case the tungsten carbide is the predominant material in contact at the wearflat. In all of the cases temperatures at the wearflat are considerably higher than for the lower wear cases. Temperatures above 1000°C are not physically reasonable for the cutter design. With moderate to high cooling rates, excessive temperatures are achieved for heat fluxes on the order of 1000 W/cm^2. Additionally, the near-surface temperature gradients at the wearflat can be enormous as shown in Figure A17. Note that the isotherms are 50°C apart.

One further set of runs was performed with the medium worn geometry and the sintered diamond layer replaced with tungsten carbide. The results for this all-metal tool are shown in Figures A18 through A23. In all cases temperatures of the all-metal tool were higher than the PDC cutter temperatures with the difference decreasing with increased cooling. The effectiveness of the high conductivity sintered diamond layer in decreasing frictional temperatures is clear from this comparison. A possible design improvement is suggested by this comparison. Increasing the total thickness of the diamond layer in comparison to the total compact thickness should reduce the risk of thermal deterioration by improving the thermal diffusion characteristics of the compact.

A PDC CUTTER FRICTIONAL TEMPERATURE MODEL

Numerical-Analytical Basis

As was suggested in the preceding section it is possible to derive approximate expressions for the temperatures produced by friction in sliding systems if the response of the sliding pair can be quantified. In the case of the numerically calculated data for the PDC models of the previous section, it would be preferable to obtain a more unified model of the thermal response with a minimum number of variables. The analytic expressions for the temperature elevation of the simplified sliders introduced in Figures 6a and 6b, i.e. Equations 13 and 15, suggest that the ratio of the difference in the average wearflat temperature and the fluid temperature, i.e. the temperature elevation of the contact surface, divided by the heat flux imposed on the slider end is a unique function of the geometry, the slider thermal conductivity and the degree of cooling or heat transfer coefficient. In equation form:

$$\frac{\bar{\theta}}{q_1} = \frac{T_W - T_f}{q_1} = f\{k_1, h, \text{geometry}\} \qquad (24)$$

where again q_1 is the heat flux conducted into the slider. Indeed it was found that to a good degree of accuracy the computed PDC average wearflat temperatures did collapse to discrete values of the ratio given by Equation 24 for given geometry and convection coefficient h. This is surprising only in that the PDC geometry is more complex and has two materials of enormously different conductivity in contact at the wearflat. Nonetheless, the resulting thermal response function f for the three cases considered in this study are well behaved functions as shown in Figure 8. As expected from the previous examination of the discrete cases run, it is found that the temperature response of the three geometries is distinct and as wearflat area increases so do the average wearflat temperatures for constant heating and cooling rates. As the strength of the convective cooling is increased, a demonstrable

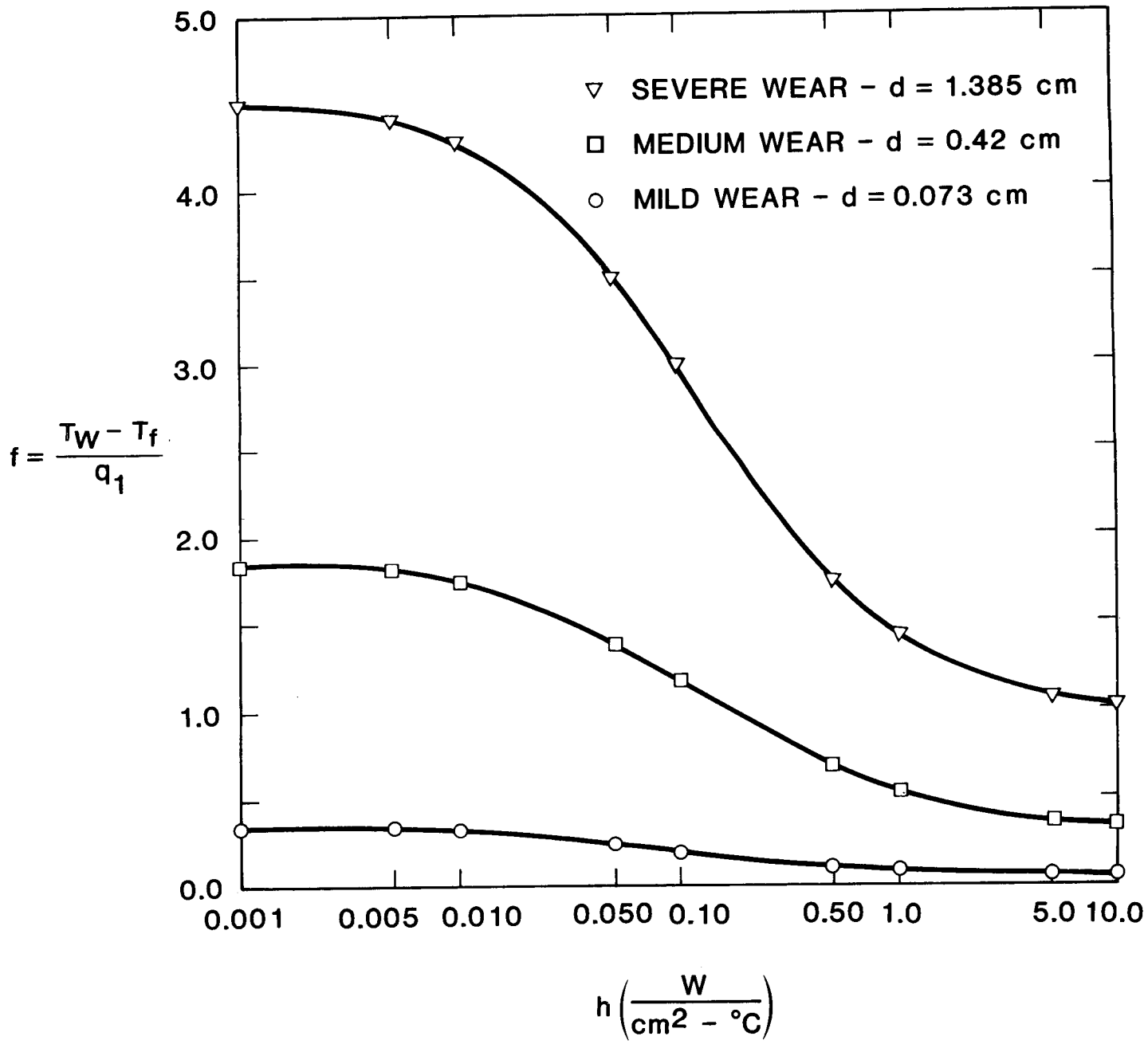

Figure 8. Thermal Response of PDC Cutters for Various Degrees of Wear

effect on the temperature at the wearflat is not noted below heat transfer coefficients of 0.01 W/cm^2-°C. More importantly it is seen that at cooling coefficients on the order of 5.0 to 10.0 W/cm^2-°C the wearflat temperatures are generally insensitive to further cooling.

In order to determine the reasonableness of the functions shown in Figure 8, a comparison is made with a simple slider model. Rather than comparing with results for a semi-infinite slider, consider the case of a two-dimensional slider of finite length L and thickness d. The upper surface is maintained at the fluid temperature T_f. The differential equation given by Equation 11 is still applicable, assuming a one-dimensional temperature profile, and the boundary conditions are:

$$\begin{aligned} z = 0 \quad & -k_1 \frac{d\theta}{dz} = q_1 \\ z = L \quad & \theta = 0 \end{aligned} \tag{25}$$

The solution to this system is given by:

$$\bar{\theta} = T_w - T_f = \frac{q_1}{(k_1/L)} \frac{\tanh\left[\left(\frac{2h}{k_1 d}\right)^{1/2} L\right]}{\left[\left(\frac{2h}{k_1 d}\right)^{1/2} L\right]} \tag{26}$$

which is slightly modified from the semi-infinite slider solutions used by Bowden and Tabor [28]. In order to compare the results for the PDC geometries with this solution the discrete computed temperatures are normalized as:

$$\frac{(T_w - T_f)(k_1/L)}{q_1} = F\left\{\left(\frac{2h}{k_1 d}\right)^{1/2} L\right\} \quad . \tag{27}$$

Since in the case of PDC cutter model both diamond and metal are exposed to heating, an approximate effective contact thermal conductivity is defined as:

$$k_1 \sim k_{WC} \frac{d_1}{d} + k_{PDC} \frac{d_2}{d} \tag{28}$$

where d_1 and d_2 are the linear dimensions of the carbide and diamond components. This weighting is merely convenient and by no means rigorous. The results of this comparison are shown in Figure 9. It is seen that qualitatively the numerical PDC calculations and the simple slider model, Equation 26, compare favorably, especially in maintaining the same monotonically decreasing behavior for increasing values of the cooling parameter, $(2h/k_1 d)^{1/2}$ L. For low values of the cooling parameter, the numerical PDC calculations diverge for different degrees of wear; for moderate and high values of the parameter the non-dimensional wearflat temperatures for the exact analytic solution are well below the PDC temperatures. There are enough simplifications such as the crude weighting of the thermal conductivity that better comparison than this cannot be expected. It is apparent that an analytic expression such as Equation 26 contains most of the physics to calculate frictional temperatures but is limited both by geometry and the assumption of a one-dimensional temperature profile. Even so, the calculated behavior of the PDC cutter model is seen to be quite reasonable.

Now that a convenient form of the response of the PDC cutter model has been obtained it is straightforward to combine this with the analytic results from the moving heat source theory to account for the energy partitioning between cutter and rock. The temperature elevation given by Equation 24 is equated to the temperature evaluation due to a moving band heat source on the rock given by Equations 5 and 6. The heat flux q is expressed in terms of the frictional equivalent. The result is:

$$\alpha \left(\frac{\mu F_n V}{A_w}\right) f = (1-\alpha) \left(\frac{\mu F_n V}{A_w}\right) \frac{8 \chi_2 Pe^{1/2}}{3 k_2 V \sqrt{\pi}} \qquad (29)$$

where here:

$$Pe = \frac{Vd}{4\chi_2} > 5 \quad . \qquad (30)$$

Solving for α:

$$\alpha = \left[1 + \frac{f}{\left(\frac{8 \chi_2 Pe^{1/2}}{3 k_2 V \sqrt{\pi}}\right)} \right]^{-1} \qquad (31)$$

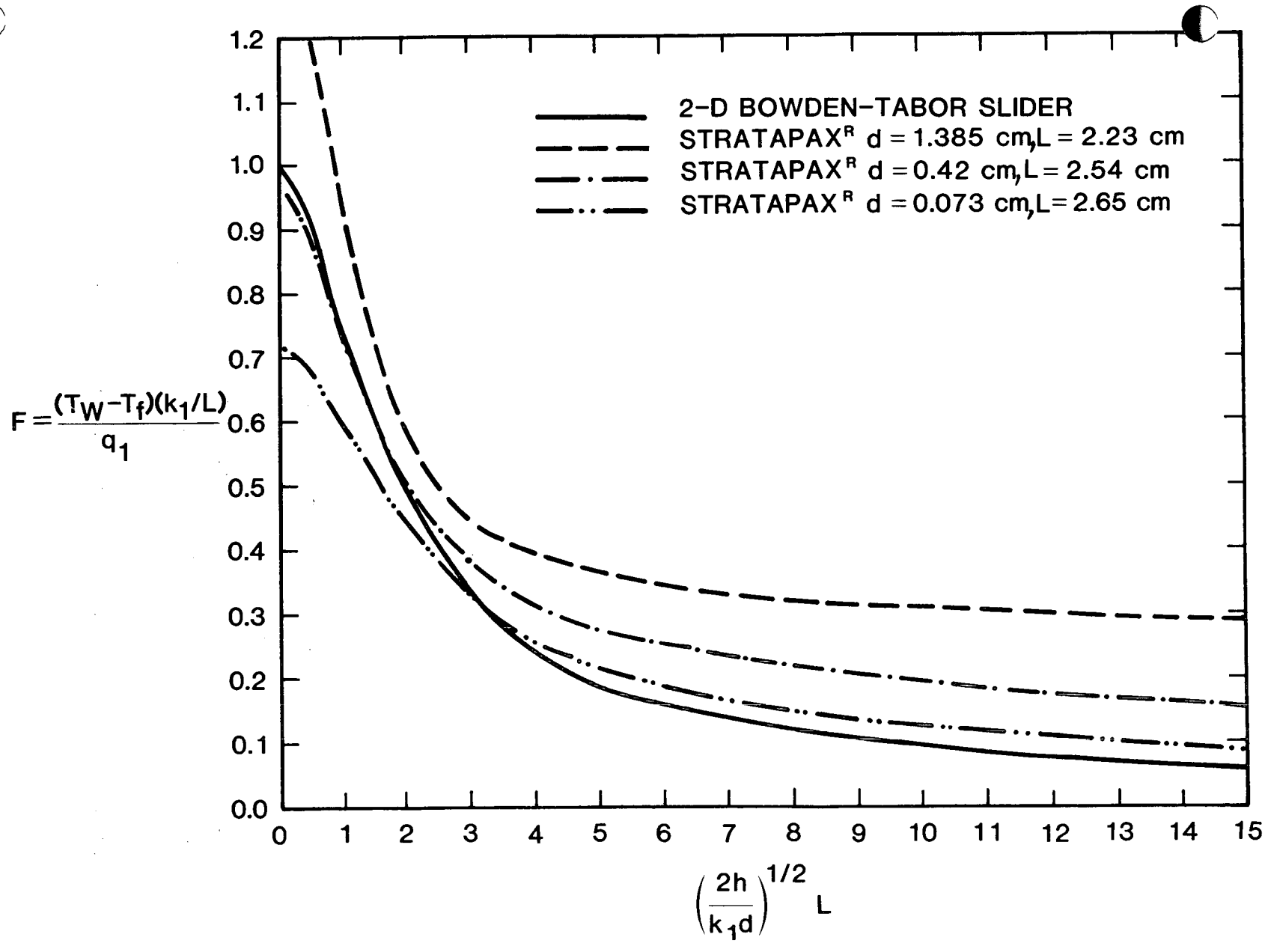

Figure 9. Comparison of Computed PDC Thermal Response to Simple Finite Length Slider

or simplifying:

$$\alpha = \left[1 + \frac{3\sqrt{\pi}}{2} \frac{k_2}{d} Pe^{1/2} f \right]^{-1} \tag{32}$$

The final form of the PDC frictional temperature is thus:

$$T_w - T_f = \frac{\left[\frac{\mu F_n V}{A_w} \right] f}{1 + \frac{3\sqrt{\pi}}{2} \frac{k_2}{d} \left(\frac{Vd}{4\chi_2} \right)^{1/2} f} \tag{33}$$

where the function $\underline{f}$ is given in Figure 8 as a function of the cooling parameter and degree of cutter wear. Equation 33 is clearly similar to the expressions derived for the simplified sliders given by Equations 19 and 21, except that the function $\underline{f}$ replaces the equivalent analytic function for the slider response. Some numerical evaluations of the partitioning fraction α, Equation 32, are given in Table 3 for common rock properties, and are plotted in Figure 10.

Appropriateness of Two-Dimensional Assumption

It has been shown that the numerically derived temperature response for cutter geometries shows reasonable similarity to theoretically derived results, the comparison being on a two-dimensional model. It is equally if not more important to ascertain the extent of the error introduced by neglecting the full three-dimensionality of the PDC cutter element. As before, it is more convenient to infer this consequence by comparison with tractable similar geometries than to attempt to solve a fully three-dimensional PDC geometry.

Referring to Figures 6c and 6d, the sliders shown are tapered sliders of finite length. Figure 6c represents a three-dimensional axisymmetric slider of circular cross-section. It is similar to a PDC cutter in that the area in frictional contact is smaller than the cross-sectional area of the majority of the element, and the upper surface is maintained at a fixed temperature. By comparing the results for these two- and three-dimensional elements of identical lateral cross-section, some inference can be made regarding the effects of three-dimensionality.

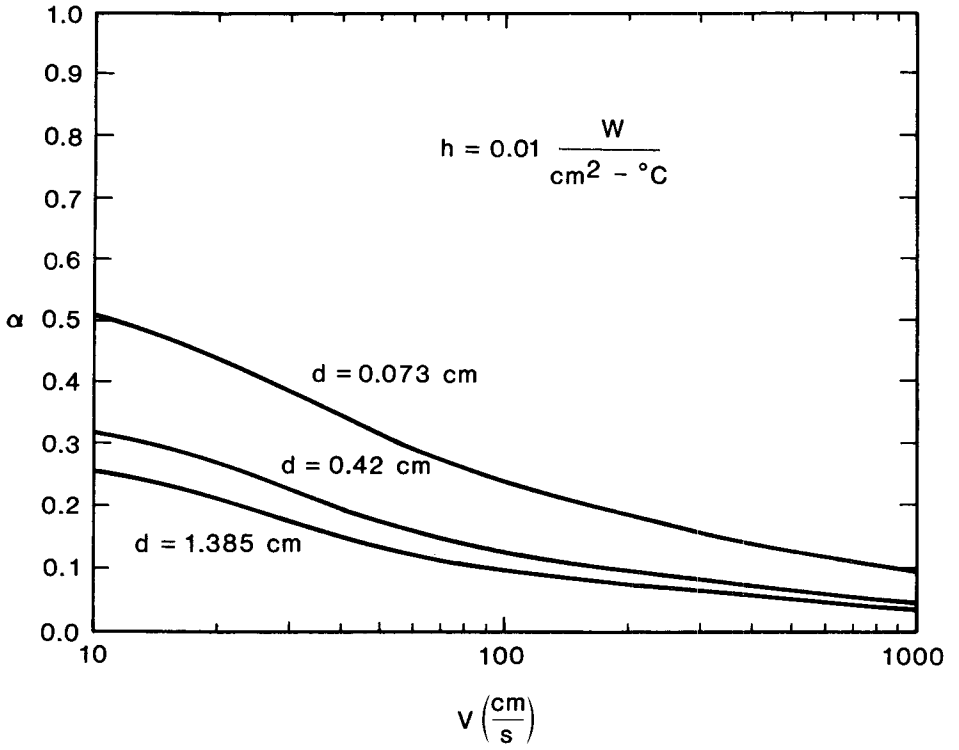

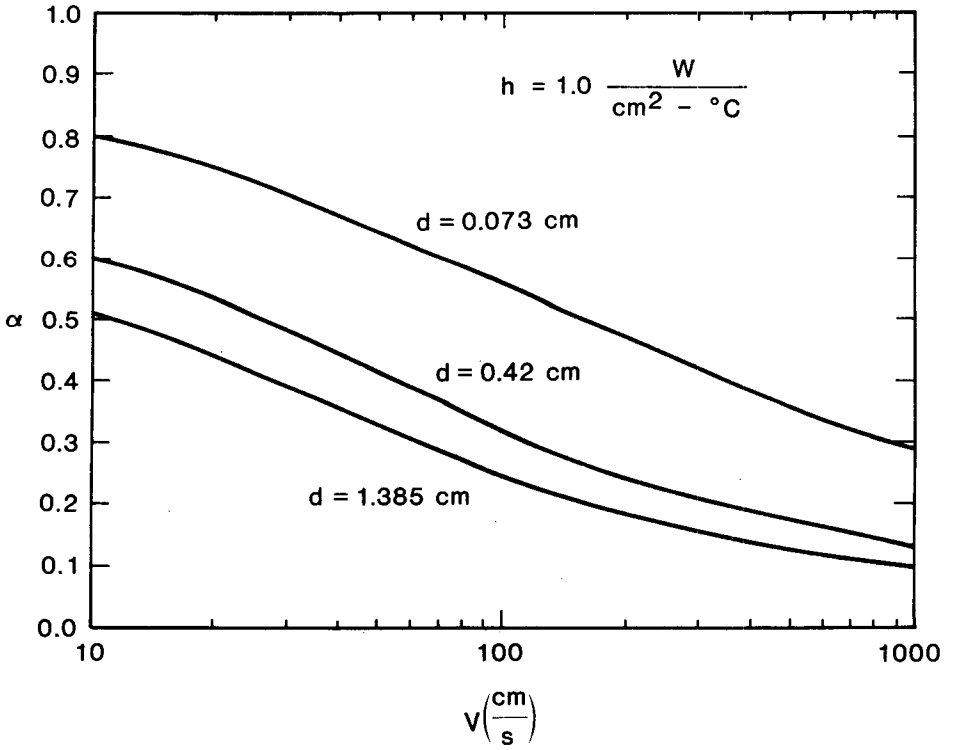

Figure 10. Partitioning Fraction for PDC Cutters

TABLE 3. ENERGY PARTITIONING FRACTION FOR PDC CUTTERS UNDER COMMON CONDITIONS

d (cm)	h (W/cm^2-°C)	V (cm/s)	α	Pe
0.073	0.01	10.	0.506	18.25
		50.	0.314	91.25
		100.	0.245	182.50
		500.	0.127	912.50
		1000.	0.093	1825.00
0.073	1.00	10.	0.799	18.25
		50.	0.640	91.25
		100.	0.557	182.50
		500.	0.360	912.50
		1000.	0.285	1825.00
0.420	0.01	10.	0.317	105.00
		50.	0.172	525.00
		100.	0.128	1050.00
		500.	0.062	5250.00
		1000.	0.044	10500.00
0.420	1.00	10.	0.600	105.0
		50.	0.402	525.0
		100.	0.322	1050.0
		500.	0.175	5250.0
		1000.	0.130	10500.0
1.385	0.01	10.	0.257	346.25
		50.	0.134	1731.25
		100.	0.098	3462.5
		500.	0.047	17312.5
		1000.	0.033	34625.0
1.385	1.00	10.	0.510	346.25
		50.	0.318	1731.25
		100.	0.248	3462.5
		500.	0.128	17312.5
		1000.	0.094	34625.0

Rock Properties: k_2 = 0.019 W/cm-°C χ_2 = 0.01 cm^2/s

The tapered slider geometries were also modeled with the finite-difference code CINDA, noting that the axisymmetry of the three-dimensional version made this calculation possible. In order to compare these calculations directly to a PDC cutter geometry, the following physical parameters were used: D = 1.6 cm, d = 0.34 cm, L_1 = 1.25 cm, L_2 = 2.54 cm. Thermal properties were taken to be those of tungsten carbide. The calculated temperatures for a two-dimensional PDC cutter

with only tungsten carbide properties are plotted for comparison in Figure 11.

It is seen in Figure 11 that the temperatures for the cutter geometry are consistently 10 to 20% higher than for the two-dimensional tapered slider. The two-dimensional tapered slider model overpredicts temperatures from 50 to 100% over the analogous 3-D axisymmetric case. Because of the remarkable similarity between the two-dimensional PDC cutter and tapered slider models, it is concluded that the error introduced by the two-dimensional PDC cutter model is of this same order and is clearly too high if the model is to be of any quantitative value. However, it is premature to conclude that the frictional temperature calculation is invalid until the effect of the partitioning coefficient has been accounted for.

As was done in the case of the Bowden-Tabor type sliders of Equations 13 and 15, an analytic comparison can be made of the two- and three-dimensional temperature response models for the tapered slider geometry using the notation of Equation 24. Thus the response is given by:

$$\frac{T_w - T_f}{q_1} = f_2 \quad ; \text{ two-dimensional} \tag{34}$$

and

$$\frac{T_w - T_f}{q_1} = f_3 \quad ; \text{ three-dimensional} \tag{35}$$

where the functions $\underline{f}$ are given by Figure 11. Now in order to form the partitioning fraction, an appropriate solution for the fixed rock response must be used. In the case of the two-dimensional tapered slider, the band-source solution given by Equation 6 is still valid. For the three-dimensional conical slider, the contact area is circular, and the rock sees a moving circular heat source. The solution for a circular source is given by Equation 9. Using the same technique as for previous derivations, the temperature for the two-dimensional slider

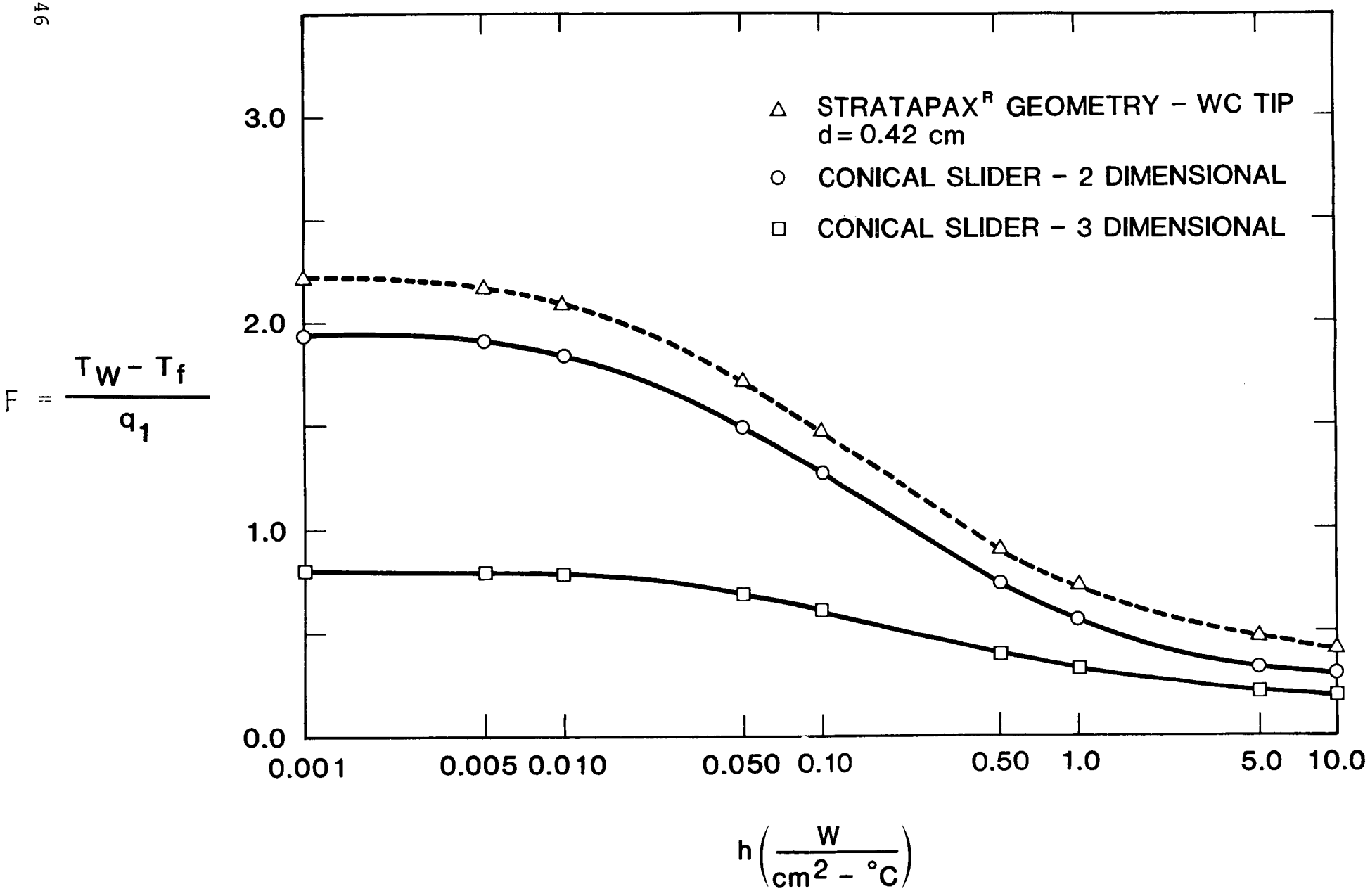

Figure 11. Comparison of Two- and Three-Dimensional Tapered Sliders

is given by:

$$T_w - T_f = \frac{\left[\frac{\mu F_n V}{A_w}\right] f_2}{1 + \frac{3\sqrt{\pi}}{2} \frac{k_2}{d} \left(\frac{Vd}{4\chi_2}\right)^{1/2} f_2} \tag{36}$$

and for the three-dimensional slider by:

$$T_w - T_f = \frac{\left[\frac{\mu F_n V}{A_w}\right] f_3}{1 + \frac{(3.25)2\sqrt{2}}{\pi} \frac{k_2}{d} \left(\frac{Vd}{4\chi_2}\right)^{1/2} f_3} \tag{37}$$

The ratio of the temperature elevations is:

$$\frac{\left(T_w - T_f\right)_{2\text{-}D}}{\left(T_w - T_f\right)_{3\text{-}D}} = \left[\frac{f_2}{f_3}\right] \cdot \frac{\left[1 + 2.93 \frac{k_2}{d} \left(\frac{Vd}{4\chi_2}\right)^{1/2} f_3\right]}{\left[1 + 2.66 \frac{k_2}{d} \left(\frac{Vd}{4\chi_2}\right)^{1/2} f_2\right]} \tag{38}$$

$$= \frac{\alpha_{2\text{-}D} f_2}{\alpha_{3\text{-}D} f_3} \cdot \tag{39}$$

By inspection one can note that in overpredicting the temperature response, the two-dimensional model also underpredicts the partitioning coefficient α so that the full frictional-temperature model is self-compensatory. To show the real effects of this result, the partitioning coefficients for the two- and three-dimensional tapered sliders have been calculated for the same properties as before. These results are given in Table 4.

The calculations show that at low velocities the two-dimensional assumption still produces prohibitively erroneous results in comparison to the full three-dimensional case. At velocities on the order of 100 cm/s, which are more nearly like those which would occur in a rotary drilling condition, the error is on the order of 30% or less. From these calculations it is obvious that the error in the calculation of frictional temperatures of PDC cutters which is due to the two-dimensional

TABLE 4. ENERGY PARTITIONING FRACTION FOR TWO- AND THREE-DIMENSIONAL TAPERED SLIDERS

h	V	Pe	$f_{2\text{-}D}$	$f_{3\text{-}D}$	$\alpha_{2\text{-}D}$	$\alpha_{3\text{-}D}$	$\theta_{2\text{-}D}$
W			°C	°C			$\theta_{3\text{-}D}$
cm^2-C	(cm/s)		W/cm^2	W/cm^2			
0.01	10	84.5	1.831	0.765	0.28446	0.46334	1.4694
	50	422.5	1.831	0.765	0.15095	0.27856	1.2970
	100	845.0	1.831	0.765	0.11167	0.21447	1.2462
	500	4225.0	1.831	0.765	0.05323	0.10881	1.1709
	1000	8450.0	1.831	0.765	0.03823	0.07948	1.15126
1.0	10	84.5	.570	0.325	0.56083	0.6702	1.4676
	50	422.5	.570	0.325	0.3635	0.47613	1.3389
	100	845.0	.570	0.325	0.28766	0.3912	1.2896
	500	4225.0	.570	0.325	0.15297	0.22325	1.2017
	1000	8450.0	.570	0.325	0.11324	0.16890	1.17588

Rock properties: k_2 = 0.019 W/cm-°C; χ_2 = 0.01 cm^2/s; d = 0.34 cm

effects is almost certainly of this same order. Since the prediction of true operating temperatures will require knowledge of the physical parameters such as heat transfer coefficient and frictional force which at best can be predicted to within 20 to 30%, it is satisfying to note that the predictive model is theoretically at least as accurate as the input parameters.

BIT HYDRAULICS AND CONVECTIVE COOLING OF PDC CUTTING ELEMENTS

Thus far, the analytical-numerical model for frictional temperatures in PDC cutters accounts for some of the more fundamental processes of frictional heating in PDC cutting elements by considering somewhat simplified versions of the full cutter geometry. As is the case in any physical system, prediction of temperatures is dependent on accurate knowledge of the physical parameters and/or variables which are contained in the model. In the case of Equation 33, it is necessary to know or compute the physical frictional heat dissipation, $\mu F_n V/A_w$, the thermal properties of the rock, and the thermal response function $\underline{f}$, which has been shown to be a function of the convective cooling coefficient $\underline{h}$. The magnitude of the convective cooling about a PDC cutting element in a real bit design is intimately related to the magnitude and character of the fluid flow around the element. This flow is complicated, geometry-dependent, and probably non-steady. Thus the idealization of a constant magnitude heat transfer coefficient at the cutter surface is simplistic, and the quantification of such a parameter can be accomplished only by experimental measurement.

The purpose of the experiments described in this section was to obtain basic measurements of local heat transfer coefficients for a PDC cutter placed in uniform, steady flow. Although this condition does not accurately describe the environment of a PDC cutter mounted on a bit downhole, it does provide a means of determining the order of magnitude of the convective cooling achievable with fluid mass flow rates on the order of those currently used in drilling. It was also deemed important to obtain the basic data and assess the accuracy of the measurement technique employed in order to properly design tests conducted in a downhole flow simulator [43]. Results from these tests augment the basic data by providing convective cooling rates for a bit in a downhole environment.

Flow Channel Design

The flow channel shown in Figure 12 was constructed for the purpose of obtaining basic heat transfer data for a PDC cutter. The channel was designed to provide uniform flow with minimal boundary layer thickness in the test section. To accomplish this objective, flow straightening vanes were inserted upstream of the ramp, and a honeycomb section was placed downstream of the ramp and immediately upstream of the test section to dissipate any large-scale transverse velocity components.

The width of the test section, 15.7 cm, was chosen to minimize, within practical limits, the effects of blockage caused by the presence of the PDC cutter on the test section velocity. The height of the test section, 1.9 cm, was chosen to simulate the standoff distance between the PDC bit body and the rock surface in the downhole environment.

Uniformity of flow in the test section was verified by measuring the local flow velocity, u_c, in the center of the test section and comparing these data with mean flow velocities, $\bar{u}$, computed from the corresponding volumetric flow rates. The centerline velocities were measured with a pitot-static tube and manometer. The volumetric flow rates were measured with a turbine flow meter.

A large difference in the centerline and mean velocities would indicate the development of large boundary layers on the channel walls and, hence, non-uniform flow in the test section. For instance, for a 15.7 cm by 1.9 cm rectangular duct, a fully developed flow (where the boundary layers extend to the center of the channel) would theoretically have the following characteristic, as shown in Appendix D

$$\frac{\bar{u}}{u_c} = 0.077 \quad . \tag{40}$$

The measured values of u_c and the computed values of $\bar{u}$ for the flow channel are plotted in Figure D1 as functions of volumetric flow rate. As seen in this figure, the minimum measured value of $\bar{u}/u_c$ is 0.93, indicating very little boundary layer development in the test section.

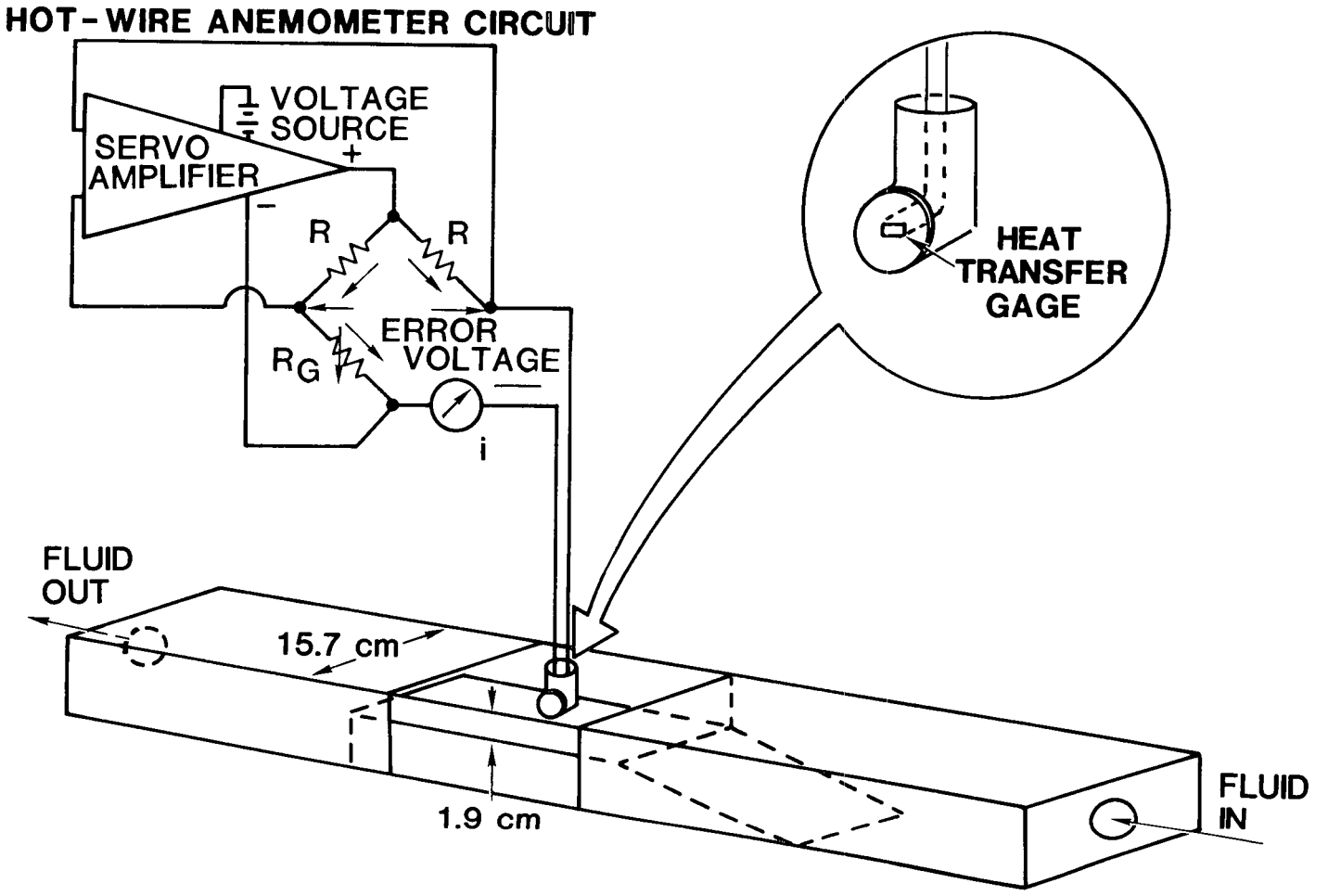

Figure 12. Single Cutter Convective Heat Transfer Measurement Apparatus (See Figure D1 for Details)

A large portion of the test section, and at least the center where the PDC cutter is located, thus has uniform flow.

Heat Transfer Coefficient Measurement Technique

The technique developed for measuring convective heat transfer coefficients is similar to that employed in hot-wire anemometry (see Figure 12). A thin film, temperature-dependent resistor is mounted to the surface for which heat transfer data is desired. This "heat transfer gage" consists of a thin foil grid of nickel, encapsulated in a phenolic matrix. The total thickness of the gage is only 0.0044 cm, and its sensing area, A, is 0.039 cm^2.

The gage is one arm of a four-arm bridge circuit which is used to supply current to the gage in a manner such that its temperature is maintained at a predetermined, fixed value. The electrical resistance corresponding to the desired gage temperature is determined (see Appendix D), and the variable resistor R_G in the bridge circuit is adjusted to this value. Electric current is supplied to the bridge and, when the bridge is balanced, is equally divided between two paths. If convective cooling of the gage changes, the temperature of the gage tends to change, resulting in a fractional change in gage resistance. This change causes the bridge to become unbalanced, resulting in an unequal division of current between the two paths. This results in an error voltage, the sign of which depends on the sign of the change in convective cooling. This error voltage is amplified, resulting in either an increase or decrease in bridge current. The electrical heating of the gage is thereby changed to bring the gage temperature and resistance back to their predetermined values, thus bringing the bridge back into balance. The response of the circuit is extremely fast, allowing only minute changes in gage temperature.

As shown in Appendix D, the following equation for the heat transfer coefficient h at the gage surface can be derived from a consideration of the thermal dissipation of electrical power supplied to the gage:

$$h = \frac{i^2 R_G - Q_\ell}{A(T_G - T_f) + (Q_\ell - i^2 R_G)/\kappa} \qquad (41)$$

All quantities on the right-hand side of this equation are either predetermined, measured, or computed. The gage temperature T_G is predetermined. Its value should be as high above the fluid temperature T_f as practical but below the boiling temperature of the fluid. Due to constraints on the current which the circuit employed in the present study could supply, the gage temperature was maintained at a nominal value of 60°C, whereas fluid temperature was measured in the range 21 to 27°C. The corresponding resistance R_G was determined from the calibration curve of Figure D3. The gage sensing area A is a known quantity, as is the specific thermal conductance κ of the phenolic layer between the gage grid and the surface in contact with the fluid.

The final parameter in Equation (41) is the electrical lead and mounting surface heat loss, Q_ℓ. To minimize the heat lost to the surface to which the gage is mounted, the following procedures were employed. When a gage was to be mounted at a location on the PDC stud, a pocket 0.8 cm in diameter and 0.16 cm deep was machined at the desired location and filled with thermally insulating epoxy. The epoxy fill was allowed to dry and was then sanded flush with the surface of the stud. The gage was then mounted to this epoxy surface. When a gage was to be located on the PDC element itself, a simulated PDC blank, consisting of a phenolic wafer of the same dimensions, was employed, and the gage was mounted to the blank.

The gage-electrical lead and gage-stud interfaces were numerically modeled with CINDA [50] to determine the lead and mounting surface heat losses. As shown in Figure D4, these losses are between 15 and 25% of the electrical power dissipated in the gage for heat transfer coefficients in the range 0.6 to 1.7 W/cm^2-°C.

Verification of Heat Transfer Measurement Technique

In order to verify the accuracy of the technique developed, it was

necessary to apply the technique to a geometry for which heat transfer coefficients are known. A right circular cylinder is one such geometry for which heat transfer coefficients have been measured with other techniques and reported in the literature [45-47]. These techniques consisted of uniformly heating the entire cylinder and measuring surface temperatures with thermocouples. These techniques, while applicable to simple geometries, are not applicable to complex geometries such as PDC cutters because it is not possible to heat complex geometries uniformly. The present technique, however, is applicable to both simple and complex geometries since only local heating of the gage is required.

A steel cylinder 1.6 cm in diameter and 1.9 cm in length was instrumented with a single heat transfer gage. The cylinder was mounted in the flow channel so that it could be rotated, thereby placing the gage at any desired angle ϕ from the leading edge of the cylinder. Heat transfer coefficients were measured at four different channel flow rates, using water as the working fluid, over the range ϕ = 0 to 180°.

To account for the effect of the cylinder on the local velocity in the test section, the velocity blockage correction method developed by Vliet and Leppert [48] and used for a cylinder in crossflow by Fand [46] was employed. This method assumes the corrected velocity u to be given by the equation

$$u = \frac{A_u}{A_m} u_u \quad , \tag{42}$$

where A_u is the unobstructed flow area, i.e., the test section flow area without the cylinder; A_m is the mean area for blocked flow; and u_u is the unobstructed flow velocity, i.e., the velocity in the center of the test section without the cylinder.

The unobstructed flow area is simply the cross-sectional area of the flow channel,

$$A_u = (15.7 \text{ cm})(1.9 \text{ cm}) = 29.8 \text{ cm}^2 \quad . \tag{43}$$

The mean area for blocked flow is defined as the area which, when multiplied by the test cylinder diameter D, is equal to the net volume

of fluid in the test section at the location of the test cylinder. Thus

$$A_m\ D = (15.7\ cm)(1.9\ cm)\ D - \frac{\pi}{4} D^2\ (1.9\ cm) \quad .$$

Using D = 1.6 cm gives the result

$$A_m = 27.4\ cm^2 \quad . \tag{44}$$

The unobstructed flow velocity is simply the measured centerline velocity,

$$u_u = u_c \quad . \tag{45}$$

Substituting Equations (43-45) into (42) gives the result

$$u = 1.088\ u_c \quad . \tag{46}$$

The corrected velocity thus differs from the unobstructed centerline velocity by only 8.8%.

The results of the cylinder heat transfer coefficient measurements are shown in Figure 13, where the four values of the corrected flow velocity are expressed in terms of the corresponding Reynolds numbers. For each Reynolds number, the heat transfer coefficient has a nominal value at the flow stagnation point, $\phi = 0$, increases to a maximum value near $\phi = 90°$, drops rapidly as the flow separates from the cylinder surface, and increases back to a nominal value at the trailing edge of the cylinder. As expected, the heat transfer coefficient increases with increasing Reynolds number. Qualitatively similar results have been obtained in air by Geidt [47], using a different measurement technique.

For verification purposes, the curves of Figure 13 were integrated to obtain the mean heat transfer coefficient as a function of Reynolds number. The results are plotted in Figure 14, together with a correlation of data reported in the literature [45,46]. Agreement between the data obtained with the present technique and that reported in the literature is seen to be quite good, with the maximum disparity being about 7%. It is, therefore, concluded that the present technique is at least as accurate as techniques developed for simpler geometries, with the advan-

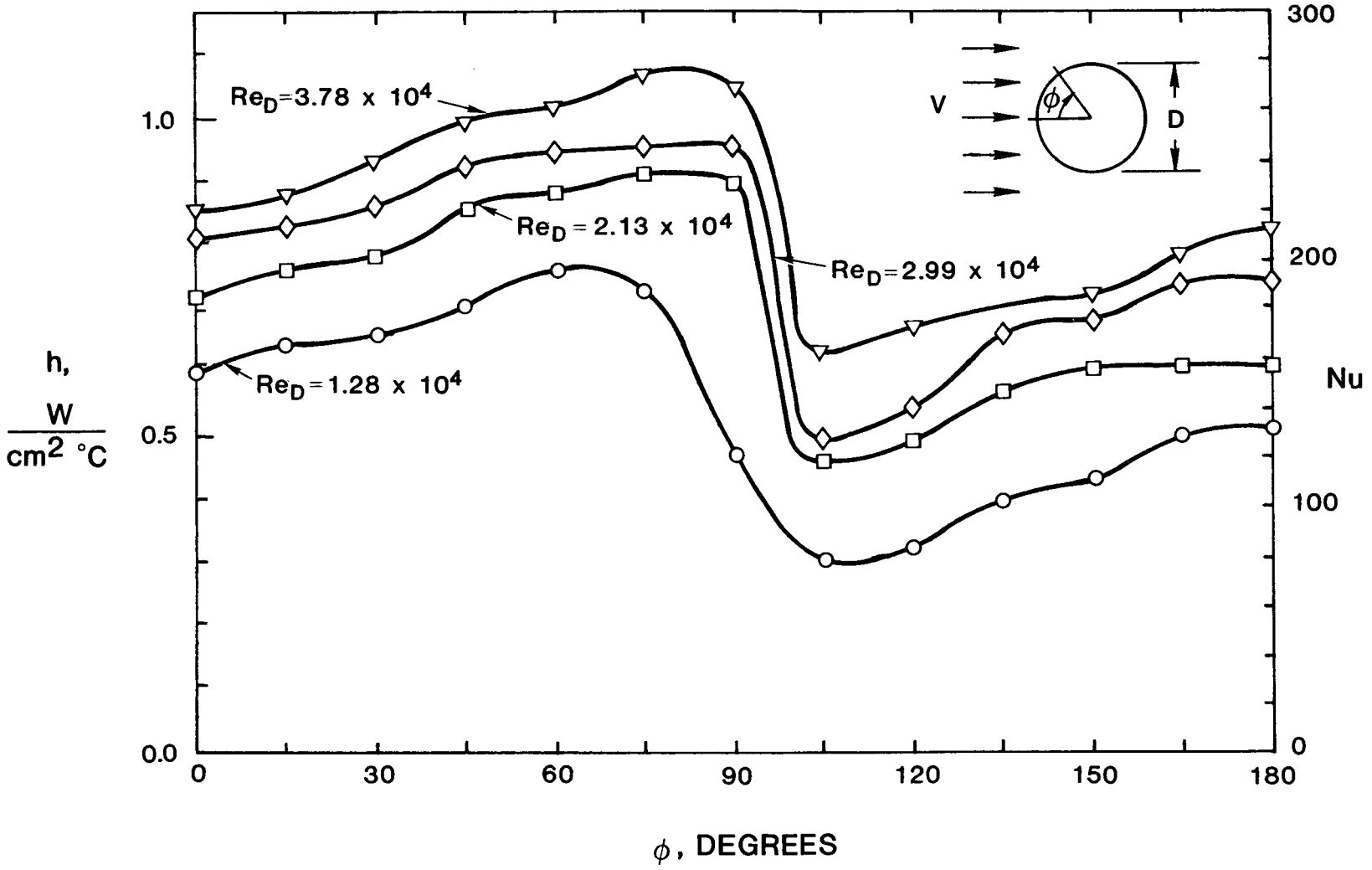

Figure 13. Local Convective Heat Transfer Coefficients for a Cylinder in Crossflow

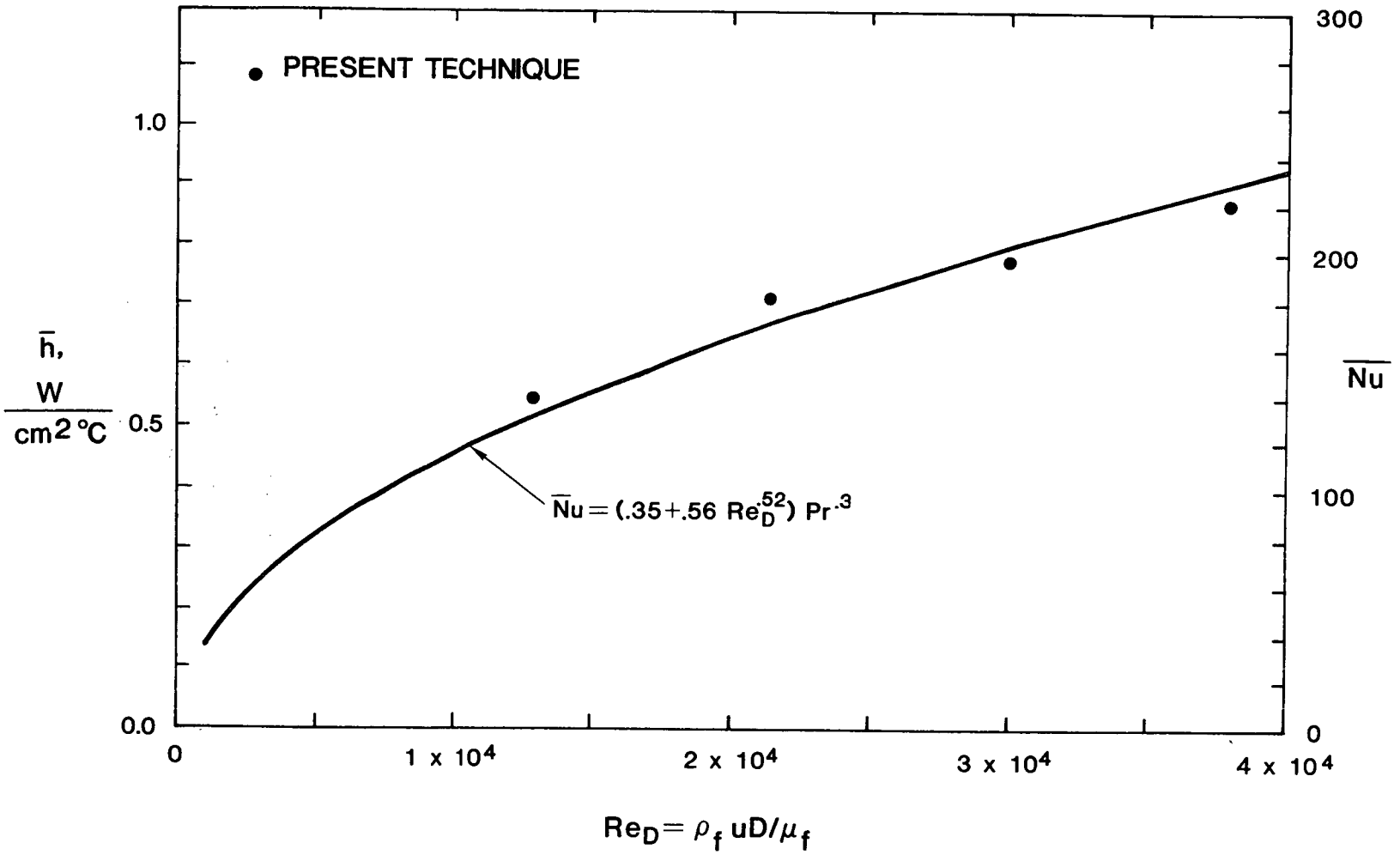

Figure 14. Mean Convective Heat Transfer Coefficients for a Cylinder in Crossflow

tage that the present technique can be used for more complex geometries such as PDC cutters.

Heat Transfer Coefficients for a PDC Cutter

A full-scale PDC cutter assembly, with a simulated PDC element of phenolic, was instrumented with four convective heat transfer gages. The locations of these gages, together with the results obtained in the flow channel with water, are shown in Figure 15. The position of the cutter relative to the oncoming flow was chosen to simulate the direction of flow most likely to be experienced by a cutter mounted to a bit in the downhole environment.

The correlations shown in Figure 15 were obtained through a simple least-squares fit of the data plotted in log-log space. Since only one fluid was tested, the Prandtl number dependency shown was inferred strictly from correlations reported in the literature for a cylinder and other geometries. Since the Prandtl number is not flow- or geometry-dependent, it is quite probable that the dependency shown is accurate.

It is interesting to note that this data is quite similar to the local cylinder data presented in Figure 13. The leading edge of the PDC cutter, gage location 1, has nominal values of $\underline{h}$. Gage location 2 has the highest values, being just upstream of the flow separation point. Gage location 3, at the trailing edge of the cutter, has relatively low values of heat transfer coefficient. Gage location 4 has no analogous location on the cylinder surface, but it has the lowest values of h, as expected, since it is in a low velocity portion of the flow.

Although not shown, superposition of Figures 14 and 15 reveals that mean heat transfer coefficients for the cylinder are bounded by the local data for the PDC cutter. It is thus concluded that mean heat transfer coefficients for a PDC cutter can be approximated from the mean correlation for a cylinder in crossflow.

The two-dimensional thermal numerical model of PDC cutters employed in the present study assumes equal convective cooling on three surfaces.

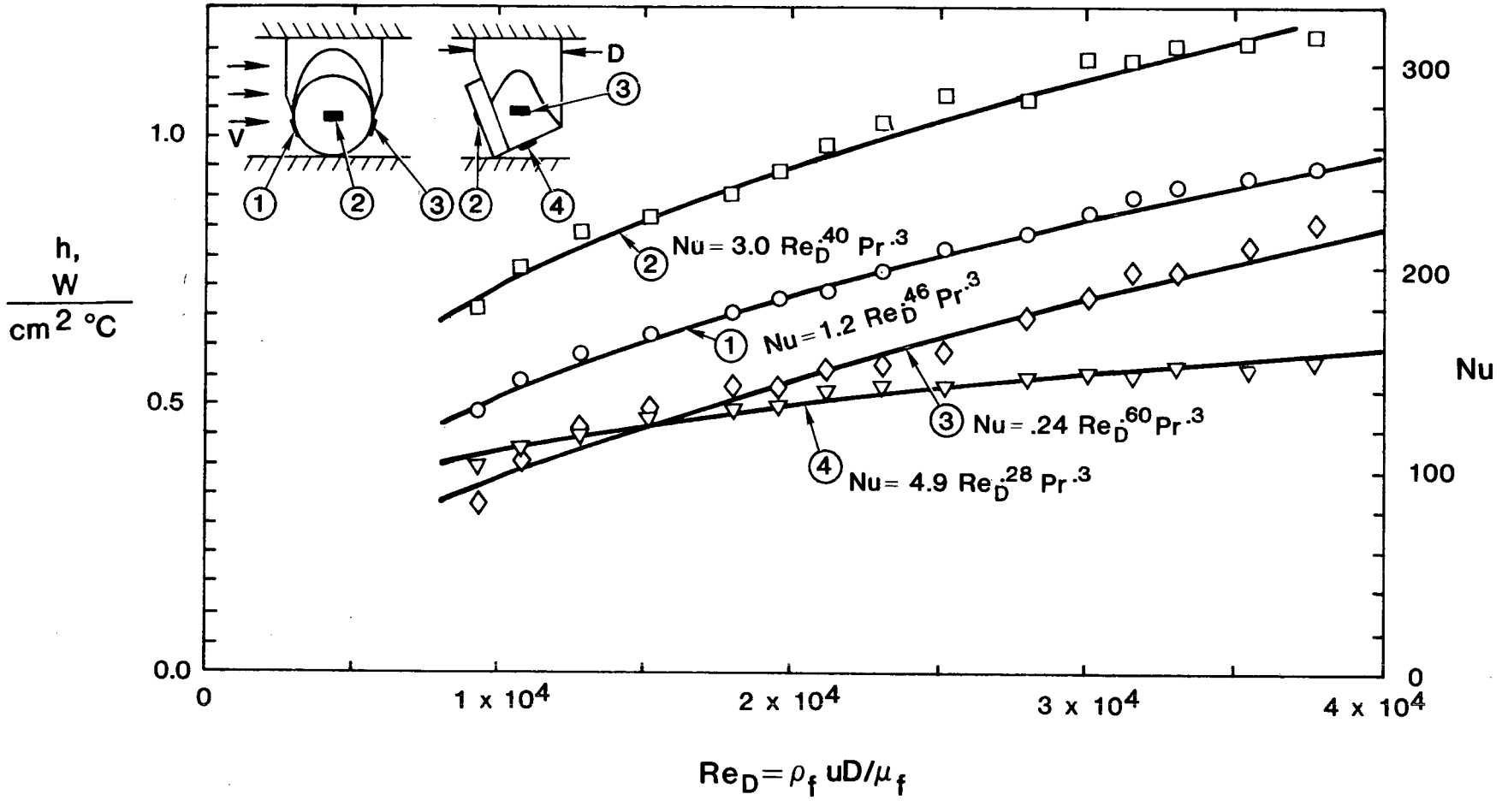

Figure 15. Local Convective Heat Transfer Coefficients for a PDC Stud in Crossflow

Two of these sufaces are those corresponding to gage locations 2 and 4. These locations have, respectively, the highest and lowest heat transfer coefficients of those measured. The third surface which is convectively cooled in the two-dimensional model is the backside of the cutter assembly opposite the PDC element. This surface has a location with respect to the assumed flow direction similar to that of gage location 2. Its heat transfer coefficients, while not measured, are therefore probably of the same magnitude as those of gage location 2. The use of an average heat transfer coefficient for all three surfaces, based on the mean correlation for a cylinder in crossflow, consequently seems justified, at least within the approximations and uncertainties of the two-dimensional model itself. The present measurements, however, do indicate the possible occurrence of hot spots on PDC cutters at locations where local heat transfer may be poor, as in location 4 of the element shown in Figure 15.

Interpretation of Data

The data of Figure 15 shows that heat transfer coefficients on the order of 1.0 W/cm^2-°C are achievable with the velocities employed in these tests. These velocities lie in the range 0.5 m/s ($Re_D = 9.25x10^3$) to 2.1 m/s ($Re_D = 3.78x10^4$). It is interesting to compare this range of velocities, which at first glance seems rather low, with the mean radial velocity past a PDC cutter mounted on a bit in the downhole environment.

Assuming a bit size of 22.2 cm (8-3/4 in), a typical flow rate would be 22 L/s (350 gal/min). Assuming all bit nozzles are located within a 10.2 cm (4 in) radius, a PDC cutter placed at this radius would experience a mean radial crossflow velocity of only 1.8 m/s, which lies within the range of velocities employed in the heat transfer coefficient measurements. This velocity assumes a bit body-rock clearance of 1.9 cm, a typical value for bits in which the PDC element is not recessed into the bit body. It is this relatively large clearance which results in the low crossflow velocity seen above. Some PDC bits are currently designed

with the elements recessed into the bit body, giving clearances of about one-half the non-recessed element clearance. The crossflow velocity at the assumed radius for such a bit would then be approximately 3.6 m/s ($Re_D = 6.6x10^4$). Extrapolation of the data of Figure 15 to this value reveals that the heat transfer coefficient would still be less than 2.0 $W/cm^2-°C$. It is thus apparent that higher heat transfer coefficients can be achieved only through means other than relying on mean radial flow, since clearance cannot be reduced much further and higher flow rates would tend to erode the sides of the borehole.

Examination of the correlations of Figure 15 show them to be of the form

$$Nu \propto Re_D^n \, Pr^m \quad , \tag{47}$$

where n and m are exponents between 0 and 1.0. Employing the definitions of Nu, Re_D and Pr produces the result

$$h \propto \frac{k_f}{D} \left(\frac{\rho_f \, u \, D}{\mu_f} \right)^n \left(\frac{c_f \, \mu_f}{k_f} \right)^m \tag{48}$$

This equation suggests two means whereby the heat transfer coefficient can be increased, employing a drilling fluid other than water and changing the hydraulic design to increase the local velocity $\underline{u}$ past the cutter.

The most common alternative drilling fluids are water-based drilling muds. These muds have the characteristic of having higher densities and viscosities compared to pure water. Due to the addition of weighting particles, it can be inferred that both the thermal conductivity, k_f, and the specific heat, c_f, are slightly lower for muds than for pure water. Densities are generally no greater than twice that of water, whereas viscosities can easily reach values ten times that of water. Most muds are highly thixotropic, meaning that viscosity decreases with increasing shear rate. Analysis shows, however, that shear rates for flows confined to the clearance area of a PDC bit are relatively low; therefore, viscosities of drilling muds are relatively high in the

region of interest for PDC convective cooling in the absence of any temperature effects. The result of these observations is that, since $n > m$ for most of the correlations of Figure 15, convective cooling could actually be decreased somewhat by the use of conventional drilling muds as opposed to pure water. The addition of polymers to water-based muds may improve their convective cooling capabilities by increasing their thixotropic behavior, thereby lowering viscosities at the predominate shear rates of interest; however, the improvement is expected to be low.

Similarly, the use of air is expected to result in a decrease in convective cooling. The major cause in this instance is the very low density, specific heat and thermal conductivity. An example serves to illustrate this point. A typical air flow rate for an air drilling operation employing a 22.2 cm (8-3/4 in.) bit would be approximately 1200 L/s (2600 SCFM) [52]. The bottom-hole Reynolds number corresponding to this flow rate is approximately 1.0×10^5. Although the curves of Figure 15 have not been validated for air, it is assumed for purposes of analysis that they apply in this situation. Using these correlations gives the result that heat transfer coefficients for a typical air drilling operation are on the order of only 0.05 $W/cm^2-°C$. As shown in Figure 8, the computed thermal response of a PDC cutter to this level of cooling is similar to the response obtained with no cooling whatsoever. It is, therefore, concluded that air drilling provides essentially no cooling to PDC cutters. Although further testing is required to confirm these results, it appears unlikely that PDC cutter temperatures can be kept subcritical in cases where air drilling is employed.

Other low density fluids, such as foam or mist, are expected to produce convective heat transfer coefficients which lie somewhere between the values for pure air and pure water. The exact values would depend on the density and thermal properties of the fluid employed. In any event, it is doubtful that such low density fluids could ever yield

cooling rates which are greater than or even equal to those presently achieved with pure water.

Short of the development of an inexpensive, low viscosity, high density drilling fluid, which would not be particularly attractive from the chip removal or borehole pressure control standpoints, the only apparent means whereby convective cooling can be increased is through modification of the hydraulic design to provide greater local velocities past the cutter. Since bit body clearance cannot be reduced much further, the only practical means for accomplishing this goal is to design the bit nozzles so that the jets are directed at the PDC cutters. Since jet velocities are much higher for a given flow rate than the mean radial velocity, the convective cooling would be greatly enhanced by such a design. Chip removal and lubrication would also be improved by enhanced hydraulics.

For instance, ten 0.64 cm (0.25 in.) nozzles, each directed at a PDC cutter, would provide cutter cooling (using water) on the order of 5.0 W/cm^2-°C at 22 L/s (350 gal/min). The corresponding jet velocity and bit pressure drop would be 70 m/s and 2.4 MPa (350 psi), respectively. Cooling rates for cutters not directly in the jet paths would be closer to the value for mean radial flow, on the order of 1.0 W/cm^2-°C. Since there would not be enough flow to provide direct cooling for all cutters (typically 25 to 40 cutters for a 22.2 cm bit), it would be necessary to optimize the design to provide direct cooling to those cutters which generate the most frictional heat and indirect cooling to those with less severe work loads.

From the available data, it appears that convective cooling rates on the order of 10 W/cm^2-°C cannot be practically achieved. Such high cooling rates would require water jet velocities on the order of 300 m/s and bit pressure drops on the order of 46 MPa (6700 psi). Not only are such high pressures not routinely available in drilling, but such high velocities could cause problems with erosion of the PDC studs

and bit body. With respect to the predicted effects of convective cooling on the wearflat temperatures, it was previously noted that cutter temperatures are generally insensitive to cooling beyond heat transfer coefficient magnitudes of 1.0 to 10.0 W/cm^2-°C. The conclusion is that efforts to increase convective cooling of the entire cutter assembly beyond currently achievable levels are not worthwhile where cutter heating is a problem. Enhanced hydraulics may, however, significantly reduce frictional heating by other means, such as direct cooling of the wearflat, improved lubrication at the wearflat and reduction of the necessary cutter forces by more efficient chip removal. These considerations will be discussed in more detail in a subsequent section.

PREDICTED FRICTIONAL TEMPERATURES UNDER OPERATING CONDITIONS

Some Comments on Rock Friction

In order to evaluate the frictional force which produces the heating during cutter sliding, it is necessary to know the rock surface conditions which may affect the microscopic phenomena that result in friction. It is intuitively obvious that a wetted rock surface should create less friction than a dry rock surface and that the friction should also depend on the fluid properties, i.e. the degree of lubricity provided by the fluid. For the purposes of calculating macroscopic surface temperatures, the frictional conditions are described by the dynamic friction coefficient,

$$\mu = \frac{F_f}{F_n} \quad . \tag{49}$$

Referring to the force balance given by Equations 1 and 2, the friction component F_f can be no greater than the total cutting force F_c, and the wearflat normal force, F_n, can be no greater than the total tool thrust force F_{th}. The ratio of cutting to thrust force,

$$\mu_c = \frac{F_c}{F_{th}} \tag{50}$$

has been referred to in the literature as the cutting coefficient of friction and it is dependent not only on the friction at the wearflat but also on the penetration rate or depth of cut, and the condition of the cutter, since the rock reaction force on the leading edge is dependent on these quantities. Although the ratio given by Equation 41 is not a true friction coefficient it is a useful quantity nonetheless if used in the proper context. If it is assumed that the cutting force is approximately the wearflat friction force for a dull tool, i.e.:

$$F_c \sim F_f \tag{51}$$

which is a fairly good approximation for small depths of cut, then since $F_{th} > F_n$,

$$\mu_c \sim \frac{F_f}{F_{th}} < \mu \quad . \tag{52}$$

The following rules of thumb are suggested by Equations 49 through 52 for cutting at small depths of cut:

1. If the horizontal cutting force is measured in a cutting experiment it is probably reasonable to assume that it is equal to the friction force F_f in order to obtain an upper bound on the friction heating.
2. If only the total normal thrust force per cutter, F_{th}, is known or can be approximated, the frictional force can be approximated as $\mu_c F_{th}$ using the best available data for the cutting coefficient of friction for a cutter with similar wear, at the same depth of cut, and of course under the same lubrication conditions.
3. If only the total normal thrust force per cutter, F_{th}, is known or can be approximated, an upper limit on the friction force F_f can be calculated as μF_{th} using the best available data for the sliding dynamic friction coefficient μ taken under similar sliding (not cutting) conditions.

The reader is referred to the work of Kenny and Johnson [21] for a description of techniques to deduce the friction on cutters at large depths of cut.

Unfortunately, available data for the dynamic and cutting coefficients of friction between a PDC cutter and rock are sparse. Some recent measurements in single point cutting tests with PDC cutters in Tennessee marble are available [15] and are shown in Table 5. From these few data points the cutting coefficients of friction for cutting with two flow rates of water impinging on the cutter leading edge vary from 0.25 to 0.32 for a depth of cut of 0.006 in/rev and from 0.16 to 0.22 for a depth of cut of 0.002 in/rev. Since both the tool thrust force and cutting force increase with an increasing depth of cut, it is not obvious from these few data that the cutting friction coefficient

would continue to decrease with decreasing depth of cut.

The imaginatively designed experiments of Kenny and Johnson [21] provide some valuable data for friction coefficients between tungsten carbide and Darley Dale sandstone. Flat ended carbide specimens were rubbed against Darley Dale sandstone at various downward thrusts from 35 MN/m^2 to 75 MN/m^2. Some rock removal was unavoidable but for the most part the specimens were in sliding contact with the sandstone. By measuring the simultaneous mean cutting and thrust forces on their specimens they measured apparent dynamic friction coefficients, μ, from 0.5 to 0.7. The coefficient of friction was alternatively calculated from numerous measurements made on various carbide-tipped cutters. From inspection of Equations 1 and 2 for tools with positive rake angles, they determined that in plotting the cutting and thrust forces versus depth of cut for a tool at a given degree of wear, the intercept of the cutting force plot to zero depth of cut should be the friction force on the wearflat, and the intercept of the thrust forces versus depth of cut, should be the normal force. By plotting the cutting force intercept versus the thrust force intercept for three stages of tool wear, the indicated value of μ was 0.72 for the mean force data. A similar analysis of the results from ten tungsten-carbide tipped tools with various rake and clearance angles cutting in Portland limestone gave average values of μ of 0.72 for the mean force data. These data were consistent with the friction rubbing tests.

Finally, measurements of the dynamic coefficients of steel sliding on rock were made by Gaffney [24] at sliding speeds from 10 to 30 m/s. At speeds on the order of 10 m/s which is above any present operating speed for PDC bits, μ was measured to be 0.4 for dry Tuff, 0.34 for wet sandstone and 0.39 for dry sandstone. Although not many measurement were taken at speeds below 10 m/s, data for Tuff show coefficients to be more on the order of 0.6 for speeds around 1.0 m/s. It was concluded

that the dynamic friction coefficients decreased for increasing sliding velocity. The results of these groups of tests are summarized in Table 5 for reference.

TABLE 5. FRICTION COEFFICIENTS FOR SOME PERTINENT SLIDING PAIRS

Reference	Friction Pair	μ	μ_c	Comments
[15]	PDC on Tennessee Marble	--	0.16-0.32	See Table 8 for details of cutting conditions.
[21]	WC on Darley Dale Sandstone	0.72		Both friction sliding tests and cutting tests.
	WC on Portland Limestone	0.72		Dry, nominal cutting speeds.
[24]	Steel on Dry Tuff	0.40 0.60		10.0 m/s 1.0 m/s
	Steel on Wet Sandstone	0.34		10.0 m/s
	Steel on Dry Sandstone	0.39		10.0 m/s

Results for Varying Wear

Perhaps the most meaningful way in which to assess the potential severity of frictional heating is to predict temperature under typical operating conditions using best estimates of the physical parameters, and compare these temperatures with known damage thresholds. It was shown that heat transfer coefficients on the order of 1.0 W/cm^2-°C can be easily achieved and probably represent the order of magnitude of cooling achieved in practice. Dynamic friction coefficients of 0.6 for dry rock and 0.2 for wet or lubricated rock are reasonable from the data available. If a typical PDC cutting element is assumed to be placed at a 10.2 cm (4 inch) radius on a bit, the linear velocities for rotational speeds of 10, 100 and 1000 rpm are approximately 0.10, 1.0 and 10.0 m/s, respectively. It would be ideal to compare the resulting temperatures under conditions of constant penetration rate for various degrees of wear, however the applied cutter forces and thus the resulting frictional

force would vary between cases. Since precise data of this sort is not presently available, the PDC cutter temperatures are compared under conditions of equal normal loading and indirectly under equal heat flux conditions. The results of these parameter runs are summarized in Tables 6, 7 and 8 for mildly worn, medium worn and severely worn tools, respectively.

It is seen from comparison of the results that under conditions of equal normal load the temperature decreases for increasing wear since the wearflat area over which the heat is distributed increases. Comparison of the heat flux, $\mu F_n V/A_w$, shows the large decrease clearly. This does not however always imply that worn tools run cooler than sharp tools. On the contrary, to achieve a constant penetration rate the bit thrust must be increased as wear progresses. The relative increase or decrease in a worn tool as compared to a sharp tool thus depends largely on the relative increase of the tool thrust as the wearflat grows. To emphasize this in another way, suppose that as the wearflat area increases the tool thrust force is increased such as to maintain a constant contact pressure, F_n/A_w, at the wearflat. Under these conditions the heat generation per unit area is also constant, all other parameters being equal. It is possible then under conditions of equal heat flux to compare the relative increase or decrease in temperatures by comparison of the product $\underline{\alpha f}$. It is seen from the tables that as wear increases the wearflat temperatures increase as well for equal contact pressure. For example for moderate cooling, h = 1.0 W/cm^2-°C, the temperature elevation in a medium worn tool is 3.7 times higher that that for a mildly worn tool at 100 rpm and 2.9 times higher at 1000 rpm. For a severely worn tool, Table 8, the temperature elevations are 7.5 and 5.5 times higher at 100 and 1000 rpm, respectively. Even though contact pressure is probably not maintained constant for constant penetration rate with progressive wear, it is probable that the increase in normal loading with increasing wear is such that wearflat temperatures increase.

TABLE 6

PREDICTED FRICTIONAL TEMPERATURES FOR A MILDLY WORN PDC DRAG TOOL

d	h	F_n		V	μ	$\frac{\mu F_n V}{Aw}$	α	f	$T_w - T_f$	αf
(cm)	$\frac{W}{cm^2\ C}$	(N)	(lb_f)	(m/s)		$\frac{W}{cm^2}$		$\frac{°C}{W/cm^2}$	°C	
.073	.01	1112	250	0.10	0.6	914.0	.506	.33	152.6	.167
				1.00		9139.7	.245	.33	738.9	.081
				10.00		91397.3	.093	.33	2805.0	.031
.073	.01	1112	250	0.10	0.2	304.7	.506	.33	50.9	.167
				1.00		3046.6	.245	.33	246.3	.081
				10.00		30465.7	.093	.33	935.0	.031
.073	.01	2224	500	0.10	0.6	1827.9	.506	.33	305.2	.167
				1.00		18279.5	.245	.33	1477.9	.081
				10.00		182794.5	.093	.33	5610.0	.031
.073	.01	2224	500	0.10	0.2	609.3	.506	.33	101.7	.167
				1.00		6093.2	.245	.33	492.6	.081
				10.00		60931.5	.093	.33	1870.0	.031
.073	1.0	1112	250	0.10	0.6	914.0	.799	.085	62.1	.068
				1.00		9139.7	.557	.085	432.7	.047
				10.00		91397.3	.285	.085	2214.1	.024
.073	1.0	1112	250	0.10	0.2	304.7	.799	.085	20.7	.068
				1.00		3046.6	.557	.085	144.2	.047
				10.00		30465.7	.285	.085	738.0	.024
.073	1.0	2224	500	0.10	0.6	1827.9	.799	.085	124.1	.068
				1.00		18279.5	.557	.085	865.4	.047
				10.00		182794.5	.285	.085	4428.2	.024
.073	1.0	2224	500	0.10	0.2	609.3	.799	.085	41.4	.068
				1.00		6093.2	.557	.085	288.4	.047
				10.00		60931.5	.285	.085	1476.0	.024

TABLE 7

PREDICTED FRICTIONAL TEMPERATURES FOR A MEDIUM WORN PDC DRAG TOOL

d	h	F_n		V	μ	$\frac{\mu F_n V}{Aw}$	α	f	$T_w - T_f$	αf
(cm)	$\frac{W}{cm^2 C}$	(N)	(lb_f)	(m/s)		$\frac{W}{cm^2}$		$\frac{°C}{W/cm^2}$	°C	
.42	.01	1112	250	0.1	0.6	158.9	.317	1.746	87.9	.553
				1.0		1588.6	.128	1.746	355.0	.223
				10.0		15885.7	.044	1.746	1218.1	.077
.42	.01	1112	250	0.1	0.2	52.95	.317	1.746	29.3	.553
				1.0		529.5	.128	1.746	118.3	.223
				10.0		5295.2	.044	1.746	406.8	.077
.42	.01	2224	500	0.1	0.6	317.7	.317	1.746	175.8	.553
				1.0		3177.1	.128	1.746	710.0	.223
				10.0		31771.4	.044	1.746	2440.8	.077
.42	.01	2224	500	0.1	0.2	105.9	.317	1.746	58.6	.553
				1.0		1059.0	.128	1.746	236.7	.223
				10.0		10590.5	.044	1.746	813.6	.077
.42	1.0	1112	250	0.1	0.6	158.9	.600	.54	51.5	.324
				1.0		1588.6	.322	.54	276.2	.174
				10.0		15885.7	.130	.54	1115.2	.070
.42	1.0	1112	250	0.1	0.2	52.95	.600	.54	17.2	.324
				1.0		529.5	.322	.54	92.1	.974
				10.0		5295.2	.130	.54	371.7	.070
.42	1.0	2224	500	0.1	0.6	317.7	.600	.54	102.9	.324
				1.0		3177.1	.322	.54	552.4	.974
				10.0		31771.4	.130	.54	2230.4	.070
.42	1.0	2224	500	0.1	0.2	105.9	.600	.54	34.4	.324
				1.0		1059.0	.322	.54	184.2	.974
				10.0		10590.5	.130	.54	743.4	.070

TABLE 8

PREDICTED FRICTIONAL TEMPERATURES FOR A SEVERELY WORN PDC DRAG TOOL

d	h	F_n		V	μ	$\frac{\mu F_n V}{Aw}$	α	f	$T_w - T_f$	αf
(cm)	$\frac{W}{cm^2 C}$	(N)	(lb_f)	(m/s)		$\frac{W}{cm^2}$		$\frac{°C}{W/cm^2}$	°C	
1.385	.01	1112	250	0.1	0.6	48.2	.257	4.261	52.8	1.095
				1.0		481.7	.098	4.261	201.1	0.418
				10.0		4817.3	.033	4.261	677.4	0.141
1.385	.01	1112	250	0.1	0.2	16.1	.257	4.261	17.6	1.095
				1.0		160.6	.098	4.261	67.1	0.418
				10.0		1605.8	.033	4.261	225.8	0.141
1.385	.01	2224	500	0.1	0.6	96.3	.257	4.261	105.5	1.095
				1.0		963.5	.098	4.261	402.3	0.418
				10.0		9634.7	.033	4.261	1354.8	0.141
1.385	.01	2224	500	0.1	0.2	32.1	.257	4.261	35.2	1.095
				1.0		321.2	.098	4.261	134.1	0.418
				10.0		3211.6	.033	4.261	451.6	0.141
1.385	1.0	1112	250	0.1	0.6	48.2	.510	1.415	34.8	.722
				1.0		481.7	.248	1.415	169.0	.351
				10.0		4817.3	.094	1.415	640.7	.133
1.385	1.0	1112	250	0.1	0.2	16.1	.510	1.415	11.6	.722
				1.0		160.6	.248	1.415	56.4	.351
				10.0		1605.8	.094	1.415	213.6	.133
1.385	1.0	2224	500	0.1	0.6	96.3	.510	1.415	69.5	.722
				1.0		963.5	.248	1.415	388.1	.351
				10.0		9634.7	.094	1.415	1281.5	.133
1.385	1.0	2224	500	0.1	0.2	32.1	.510	1.415	23.2	.722
				1.0		321.2	.248	1.415	217.9	.351
				10.0		3211.6	.094	1.415	427.2	.133

This subject is one that can be clarified only by carefully instrumented cutting tests.

Effectiveness of Convective Cooling

The drilling fluid which flows vigorously about an individual cutting element may affect wearflat temperatures by influencing convective heat removal from the lateral surfaces, by lubricating the contact between wearflat and the rock, and by removing rock chips and obstructions which influence the cutting efficiency. In addition, it has been noted that in real bit operation there exists a likelihood that the individual cutters are not always in contact with the rock, so that a fourth mode of temperature reduction is by direct convective heat transfer at the wearflat in those instances where flow may exist underneath the cutter. In this study only the first two of these processes have been investigated. Recent experiments in flow visualization over full prototype PDC bits [43] should provide clues regarding the importance of the remaining two processes.

It was shown in Figure 8 that substantial decreases in wearflat temperatures can be achieved with convective cooling coefficients on the order of 1.0 W/cm^2-°C over lateral surfaces but that temperatures are generally insensitive to further increases in convective cooling. The experimental measurements of the heat transfer coefficients on PDC cutting elements in water showed that magnitudes on the order of 1.0 W/cm^2-°C are commonly achievable in crossflow, and it is not likely that magnitudes on the order of 10.0 W/cm^2-°C can be achieved with high mud or water flow rates in bit operations presently. For the three wear stages investigated here, the following trends are noted. For a mildly worn tool, temperatures decrease by 42% in increasing the cooling coefficient from 0.01 W/cm^2-°C to 1.0 W/cm^2-°C. Further increases from 1.0 W/cm^2-°C to 10.0 W/cm^2-°C decreased the temperatures only an additional 9%. For a medium worn tool the comparable decreases are 22% from 0.01 W/cm^2-°C to 1.0 W/cm^2-°C and an additional 4% from

1.0 to 10.0. Finally for a severely worn tool, the corresponding decreases are 10% and 2.5%. These calculations are performed for a speed of 100 rpm.

The reader is cautioned that whereas consideration of only the thermal response functions given by Figure 8 would indicate much higher percentage decreases in temperature for increases in heat transfer coefficient h, consideration must also be given to the effect on the partitioning coefficient α. Comparisons must not be made on the function f, but rather on the product αf. The conclusion from Tables 6 through 8 is that significant cooling of mildly worn tools can be achieved by convective cooling up to a heat transfer coefficient of 1.0 W/cm^2-°C, and little reduction can be effected for further cooling. This cooling effectiveness decreases for increasing velocity. For medium worn and severely worn tools a moderate decrease in temperatures can be obtained by convective cooling for sliding velocities on the order of 1.0 m/s (100 rpm) and less than 10% decrease in temperatures can be achieved when sliding at velocities on the order of 10.0 m/s (1000 rpm).

Effectiveness of Wearflat Lubrication

It is straightforward to analyze the effect of lubrication at the sliding interface on the generation of macroscopic wearflat temperatures since the dynamic friction coefficient does not enter into the calculation of energy partitioning. The wearflat temperatures vary directly with the parameter μ. In Tables 6 through 8 a value of 0.6 represents dry sliding and 0.2 sliding with some lubrication. For this decrease in μ, decrease in temperatures in all cases is 66%, which is greater than the decrease practically achievable with convective cooling of tool lateral surfaces. The data are insufficient to indicate the degree that friction can be reduced by use of oil-base muds or additives, but it is clear that even wetting the rock provides some degree of lubrication. Decreasing the source of frictional heat by lubrication is a more efficient means of reducing wearflat temperatures than cooling the tool

lateral surfaces, but is insufficient by itself at high sliding speeds. The combination of convective cooling and lubrication may be an effective measure except at very high sliding speeds.

Effect of Cutting Speed

For speeds on the order of 1.0 m/s and higher, the frictional temperatures vary approximately as $V^{1/2}$ as shown by Equation 33. From Table 6 one can see that even for moderate cooling, h = 1.0 W/cm^2-°C, and low friction, μ = 0.2, temperatures on a sharp tool are prohibitive with sliding speeds on the order of 10.0 m/s (1000 rpm). They will be even higher for worn tools. For speeds which are anticipated to be common operating speeds for PDC bits (1.0 and 10.0 m/s, i.e. 100 to 1000 rpm) temperatures could approach 1000°C for conditions of high friction and poor cooling.

One further note should be made. The temperatures shown in Tables 6 through 8 are the average wearflat temperatures above the fluid temperature. In geothermal applications fluid temperatures could easily be as high as 200°C; thus the allowable margin for frictional temperatures to achieve destructive magnitudes is conservatively 500 to 600°C. The reader is referred to the tables for further details.

Design Curves For Predicting Temperatures

The analytical model of the PDC tool frictional temperature response given by equation 33 and Figures 8 and 10 has been used to develop design curves for PDC cutters of the geometry used in this study. These are given in Appendix B. Equation 32 or Figure 10 can be used to compute probable values of the energy partitioning coefficient α. Estimates of the heat transfer coefficient can be derived from Figure 15, and the frictional heat flux can be calculated from known cutting parameters using the rules reviewed in a previous section. The wearflat area A_w should be taken to be equal to the wearflat dimension d, since the model is two dimensional.

EXPERIMENTAL MEASUREMENT OF PDC CUTTER FRICTIONAL TEMPERATURES

Experimental Technique

Single point cutting tests have recently been performed by Hibbs [15] on a vertical turret lathe using preground Stratapax® cutters with measurable wearflat areas. The cutters have been instrumented with miniature thermocouples at locations very near the wearflat surface, at the compact-stud braze joint, and in the stud. Precise locations of the thermocouple junctions are shown in Figure 16. In order to provide cutting at constant velocity along the 3 ft. by 3 ft. block of the rock specimen, cutting was performed on a standing circular ridge on the rock prepared beforehand so that problems encountered when cutting in the same groove would be avoided. A water-soluble oil (40:1 water to oil) coolant jet was directed so as to impinge squarely on the leading circular face of the cutter, and measurements were made for flow rates of 6.3 and 1.4 gpm. Each test was run long enough for the measured temperatures to attain their equilibrium, and the three mutually perpendicular forces acting on the cutter were simultaneously measured. Measurements were made for cutting at speeds of 1.12 m/s (221.0 ft/min) and 0.44 m/s (87.1 ft/min), and at penetration rates of 0.002 and 0.006 in/rev. The results of the tests are summarized in Table 9.

Comparison With Analytical Results

The cutter used for this series of tests had a preground wearflat area of 0.030 in^2 (.194 cm^2) and a dimension d of 0.145 in (0.37 cm). This degree of wear is approximately the medium worn condition examined in this study in which the dimension d is 0.42 cm. The temperature measurements at locations A and B in Figure 16 were intended to approach the macroscopic average surface temperature; however, some inherent experimental error should be expected because of the finite distance from the surface at which the junctions are placed. In some cases the measured temperatures at A and B were considerably different and the average of the two was taken as the average measured wearflat temperature.

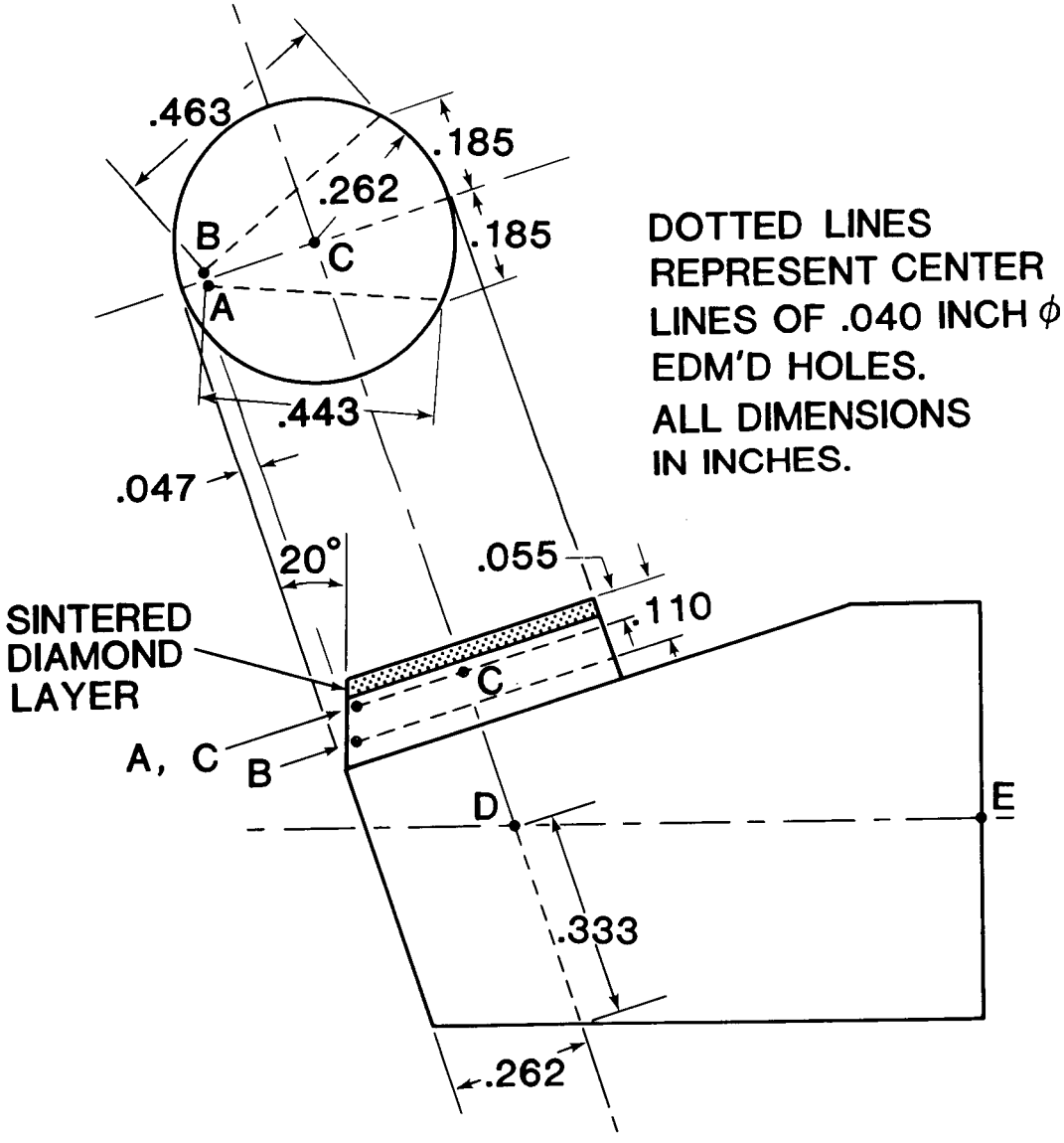

Figure 16. Thermocouple Locations in PDC Cutter Instrumented for Temperature Measurements

TABLE 9 [Reference 15]

EXPERIMENTAL WEARFLAT TEMPERATURES FOR CUTTING IN TENNESSEE MARBLE - RAW DATA

Test #	Flow Rate (gal/min)	V (m/s)	V (ft/m)	F_{thrust} (lb_f)	F_{thrust} (N)	F_{cut} (lb_f)	F_{cut} (N)	F_c/F_{th}	F_cV/Aw ** (W/cm^2)	T_A (°C)	T_B (°C)	T_w * (°C)	Down Feed (in/rev)
45	6.5	1.123	221.0	323	1436.7	104	462.6	.320	2684.1	-	129	-	.006
59	6.5	1.123	221.0	363	1614.6	110	489.28	.303	2838.9	233	163	198.0	.006
46	6.5	1.123	221.0	323	1436.7	73	324.7	.226	1883.9	105	101	103.0	.002
57	1.4	1.123	221.0	334	1485.6	100	444.8	.299	2580.8	253	181	217.0	.006
54	1.4	1.123	221.0	305	1356.6	63	280.2	.206	1625.8	212	154	183.0	.002
48	6.5	.443	87.1	360	1601.3	91	404.8	.253	926.5	86	75	80.5	.006
47	6.5	.443	87.1	284	1263.2	46	204.6	.162	468.3	69	62	65.5	.002
58	1.4	.443	87.1	308	1369.9	83	369.18	.269	844.9	104	87	95.5	.006
60	1.4	.443	87.1	310	1378.9	82	364.74	.264	834.8	102	88	95.0	.006
53	1.4	.443	87.1	306	1361.1	55	244.6	.179	559.85	95	73	84.0	.002

* $T_w = (T_A + T_B)/2$

** $A_w = .030\ in^2 = .1935\ cm^2$

By using the measured values of the cutting force F_c as a reasonable magnitude for the friction force F_f on the wearflat, it was not necessary to make any assumptions regarding the coefficient of friction and it was possible to make an order estimate of the convective heat transfer coefficients with knowledge of the coolant jet velocity, the fluid properties and the data of Figure 15. The best available thermal properties for Tennessee marble were used in evaluating the energy partitioning fraction. The reduced data and the predicted wearflat temperatures from the analytical model are shown in Table 10. Sample calculations of the wearflat temperatures using Equation (33) are given in Appendix C.

In Figure 17 the measured wearflat temperature elevations have been plotted versus the ratio $\alpha F_c V/A_w$ which represents the fraction of the maximum frictional heat flux attainable at the wearflat which is transferred to the tool. Since two different flow rates were used, the data should plot as two families in these coordinates. It is seen that even with the difficulty in accurately measuring the true wearflat frictional temperatures, the theoretical predictions are quite close to the measured data. The temperatures indeed increase linearly with increased frictional heating, and the rate of increase is greater for the lower flow rate as predicted because of the decreased cooling. Furthermore, the predicted temperatures are generally higher than the measured values, probably because the true friction force F_f is somewhat less than the cutting force F_c used in calculating the heating rate. Even though the amount of data available for comparison is as of yet small, the comparison with the general theory developed for PDC cutting elements is extremely encouraging for the use of the analytical model as a predictive tool. A more extended comparison with experimental data will be presented in work currently in preparation [51].

Observed Effects of Coolant

Because of the relatively low temperatures developed and the non-

TABLE 10

COMPARISON OF WEARFLAT TEMPERATURES TO THEORY FOR CUTTING IN TENNESSEE MARBLE

Test #	(gpm)	Downfeed (in/rev)	V (m/s)	F_{thrust} (N)	F_{cut} (N)	$F_c V/A_w$ * (W/cm^2)	α	$\alpha F_c V/A_w$ (W/cm^2)	$^{\circ}C_f$ ($\sqrt{W/cm^2}$)	$[T_w-T_f]$ ** Calculated	$[T_w-T_f]$ *** Measured
59	6.5	.006	1.123	1614.6	489.3	1308.3	.31	405.6	.54	219.0	178
46	6.5	.002	1.123	1436.7	324.7	868.2	.31	269.1	.54	145.3	83
57	1.4	.006	1.123	1485.6	444.8	1189.3	.26	309.2	.68	210.3	197
54	1.4	.002	1.123	1356.6	280.2	749.2	.26	194.8	.68	132.4	163
48	6.5	.006	.443	1601.3	404.8	427.0	.42	179.3	.54	96.8	60.5
47	6.5	.002	.443	1263.2	204.6	215.8	.42	90.6	.54	48.9	45.5
58	1.4	.006	.443	1370.0	370.0	390.3	.36	140.5	.68	95.5	75.5
60	1.4	.006	.443	1378.9	364.7	384.7	.36	138.5	.68	94.2	75
53	1.4	.002	.443	1361.1	244.6	258.0	.36	92.9	.68	63.2	64

* $A_w = (d)(1.0)$ to correspond to 2-D

** Calculated using 2-D theory

*** $T_w = (T_A+T_B)/2$ $T_f = 20°C$

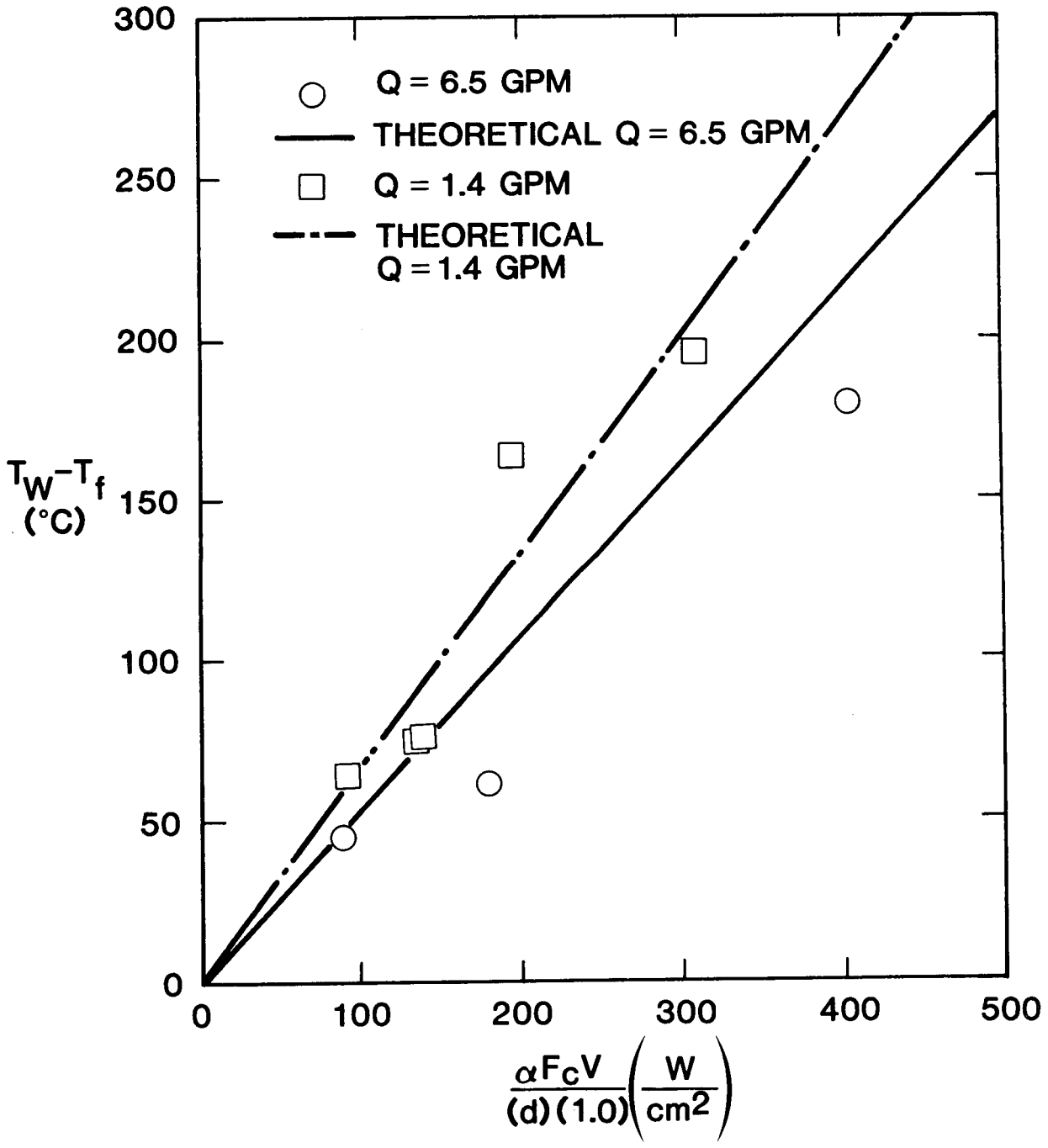

Figure 17. Measured Frictional Temperatures in PDC Cutter in Comparison to Predictive Theory

abrasive character of the Tennessee marble, very little wear was observed on the Stratapax® cutter for the frictional temperature tests. Wear tests have been carried out, however, in Nugget Sandstone with a water-soluble oil coolant and with no coolant [15].

For the cutters run with coolant (6.3 gpm), microscopic examination of the wear scars showed no evidence of accelerated wear due to thermal effects, probably because temperatures achieved were low as in the tests on marble. The predominant wear mode was microchipping of individual diamond crystallites [15].

The wear rate for dry cutting was much greater than that obtained with coolant. Wear was observed to be caused by microchipping and by thermally induced failure. In a test run at a speed of 443 ft/min (2.25 m/s) which would represent a typical cutter speed at 200 rpm bit rotation, gross thermal degradation of the sintered diamond edge was observed along with evidence of diamond crystal pullout. At a speed of 104 ft/min (0.53 m/s) or roughly 50 rpm in a bit, diamond grains were worn flat but there was no evidence of pullout [15].

It is clear that the coolant reduces the rate of wear by reducing the cutter temperatures at the cutting zone and at the rock-cutter rubbing interface. The predominant reason for this beneficial reduction, however, is not clear. In this series of experiments the coolant jet impinged directly on the sintered diamond cutting face; hence the convective heat removal was greatest on this surface. Since for a sharp tool only the sintered diamond component of the compact is in rubbing contact and receives frictional heat, the low thermal resistance diamond layer provides an efficient path for heat dissipation to the convecting surface. It has been previously noted that when the wearflat area increases and the tungsten carbide component is also in frictional contact, the effective surface thermal resistance increases, and the ability to dissipate the heat to the convecting surface also decreases. A sharp tool thus benefits most from convective cooling.

Additional benefit is gained from use of coolant in that the cutter forces were markedly lower for the tests run with coolant compared to those run dry. Since the Nugget sandstone has some porosity, it has been suggested that the fluid can penetrate the rock pores and provide lubrication at the rock-cutter rubbing interface. Much more work needs to be done in this area to further understand the relative contributions of convective cooling and lubrication.

DISCUSSION AND CONCLUSIONS

The numerical-analytical model that was developed to analyze frictional temperatures in polycrystalline diamond compact drag cutters was found to be in reasonable agreement with experimentally measured wearflat temperatures during controlled laboratory single point cutting tests. Even though more data is necessary to fully test the predictive model, it is felt that temperatures can be predicted to an accuracy of 20 to 30%, which is at least as good as the uncertainty in the physical parameters which must be estimated to predict cutter thermal behavior.

Based on the analysis and the available data, it is found that cutter temperatures vary directly with the friction force on the wearflat and approximately as the one-half power of the sliding velocity. Temperatures also vary inversely with a non-linear function of the convective heat transfer coefficient. The degree of wear on a tool has a significant influence on the ability to dissipate frictional heat from the wearflat surface. Because a sharp tool rubs only on the high thermal conductivity diamond leading edge, the frictional heat is dissipated efficiently to the convecting surfaces cooled by the fluid, and convection cooling can thus significantly lower frictional temperatures. As the wearflat area increases for progressive wear, the ability to dissipate the frictional heat is reduced principally because the lower thermal conductivity tungsten carbide or steel mounting materials begin to occupy the majority of the wearflat area compared to the diamond. Since the ability to conduct heat from the wearflat to the lateral surfaces being cooled by convection is impaired, frictional temperatures in severely worn tools cannot be reduced to levels comparable to those of midly worn tools by convective cooling at any level.

The effect of coolant flow about PDC cutting tools is to reduce frictional temperatures by convective cooling at the lateral surfaces and by reducing frictional heating at the wearflat by lubrication. Analytically it is shown that the temperatures are more sensitive to the friction at the wearflat, i.e. the magnitude of the dynamic friction

coefficient between the tool and rock, than to the magnitude of convection cooling at the lateral surfaces. In addition it is found that tool temperatures are generally insensitive to increases in the heat transfer coefficients from 5.0 to 10.0 W/cm^2-°C. Experimental determination of the heat transfer coefficients on polycrystalline diamond compact cutting elements showed that heat transfer coefficients on the order of 1.0 W/cm^2-°C are easily achievable in laboratory flow conditions, but it is very unlikely that cooling coefficients on the order of 10.0 W/cm^2-°C can be achieved in bit flows under conventional drilling conditions.

Analysis shows that the use of weighted drilling fluids can actually decrease convective cooling rates below those achieved with pure water due to the increase in viscosity which occurs when conventional weighting materials are added to water. It is further determined that air drilling provides essentially no cooling to PDC cutters. It is, therefore, unlikely that PDC cutter temperatures can be kept subcritical, even at low speeds and low bit weights, when air is employed as the drilling fluid. Other low density fluids, such as foam and mist, provide greater cooling than air but lower cooling than pure water. Further analysis is required to determine whether such fluids can keep PDC cutter temperatures subcritical under a variety of operating conditions.

The conclusion of the foregoing results is that the maximum beneficial convective cooling of PDC cutter assemblies is already achieved in present bit designs when water is employed as the drilling fluid. Any further reduction in frictional temperatures must, therefore, be achieved either by increasing the effectiveness of the fluid lubrication of the rock-cutter contact zone, or by increasing the probability of direct convective cooling of the wearflat itself. It has been suggested that individual cutters on bits are not in continuous contact with the rock during bit rotation because of drill stem flexing and cutter

interaction. From the standpoint of cutter wear this operating mode is beneficial because it will allow direct forced cooling of the cutter wearflat and lubrication of the rock.

The frictional heating rate of a PDC cutter depends on the wearflat area, the dynamic friction coefficient, the bit thrust (or weight on bit), the translation speed of the cutter relative to the rock, and the convective cooling rates on lateral surfaces. The latter dependency is a result of the division of thermal energy between the cutter and the rock. A larger percentage of this energy flows into the cutter when higher cooling rates are achieved. For the range of operating conditions considered in this study, between 3% and 80% of the total energy dissipated at the rock-cutter interface flows into the cutter as heat.

On the basis of the present study, it is concluded that the rate of wear of polycrystalline diamond compact drag cutters can be reduced substantially by reduction of the wearflat frictional temperatures with drilling fluid. For cutter normal loads on the order of 500 lb_f, cutter temperatures can be kept subcritical in rock cutting for speeds on the order of 1.0 m/s (which is commonly achieved with bit rotation on the order of 100 rpm) and perhaps higher with presently used drilling flow rates, especially if rock lubrication and forced wearflat cooling enhance the convective cooling of the exposed tool surfaces. At cutting speeds on the order of 10.0 m/s (approximately 1000 rpm), it is doubtful that temperatures can be kept subcritical except under conditions of very good lubrication at the rock-wearflat contact zone and with forced cooling of the wearflat itself. It is recommended therefore that the design of high speed PDC bits should incorporate measures to enhance the probability of direct forced cooling of the wearflat and that the associated fluid system should provide maximum interface lubrication where feasible.

ACKNOWLEDGMENTS

The authors would like to acknowledge and thank Samuel G. Varnado* for his patient and enthusiastic support of basic studies while manager of the DOE/DGE Geothermal Drilling and Completions Technology Program and Don L. Wesenberg* for recommending the study and making intelligent decisions that affected it. We would also like to acknowledge the contributions of Lou E. Hibbs, Jr. of the General Electric Corporate Research and Development Laboratories who was solely responsible for the experimental frictional temperature measurements described in this report. We would finally like to thank Donna Wilkinson for her typing and editing of this report.

* Present position with NL Petroleum Services, Houston, Texas.

REFERENCES

1. Yarrington, P., "Proposed Areas of Research in Support of Drag Bit Development", Sandia National Laboratories Internal Memorandum RS5533/79/22, May 1979.

2. Fairhurst, C. and Lacabanne, W. D., "Hard Rock Drilling Techniques", Mine and Quarry Engineering, April 1957.

3. Clark, George B., "Principles of Rock Drilling", Colorado School of Mines Quarterly, V74, No. 2, April 1979.

4. Maurer, W. C., "The State of Rock Mechanics Knowledge in Drilling", Proc. 8th Symp. on Rock Mechs., Univ. Minnesota, 1966.

5. Huff, C. F. and Varnado, S. G., "Recent Developments in Polycrystalline Diamond Compact Drill Bit Design", Sandia National Laboratories Report SAND79-1592C, May 1980.

6. Varnado, S. G., Huff, C. F. and Yarrington, P., "The Design and Use of Polycrystalline Diamond Compact Drag Bits in the Geothermal Environment", 54th Annual Fall Technical Conference and Exhibition of SPE/AIME, Las Vegas, Nevada, September 1979.

7. Hibbs, L. E., Jr., Dunn, K. J., Komanduri, R. and Flom, D. G., "Geothermal Compax Drill Bit Development", G. E. Report DGE-2360-Z, 1978.

8. Nishimatsu, Y., "The Mechanics of Rock Cutting, "Int. J. of Rock Mech and Min. Science, V9, 1972.

9. Goodrich, R. H., "High Pressure Rotary Drilling Machines", 2nd Symposium on Mining Research, Univ. Missouri, 1956.

10. Hood, M., "A Study of Methods to Improve the Performance of Drag Bits Used to Cut Hard Rock", Chamber of Mines of S. Africa, Mining Tech. Lab., Project GT2 NO2, Report No. 35/77, August 1977.

11. Swenson, D. V., "Finite Element Analysis of Rock Material Model Tests and Drag Tool Cutting", Sandia National Laboratories Internal Memorandum 5521/81/1, February 1981.

12. Larsen-Basse, G., "Wear of Hard Metals in Rock Drilling: A Survey of the Literature", Powder Metallurgy, V16, No. 31, 1973.

13. Hibbs, L. E., Jr. and Lee, M., "Some Aspects of the Wear of Polycrystalline Diamond Tools in Rock Removal Processes", Wear, V46, 1978.

14. Lee, M. and Hibbs, L. E., Jr., "Role of Deformation Twin Bands in the Wear Processes of Polycrystalline Diamond Tools", Wear of Materials, ed. Ludema, K. C., Glaeser, W. A., and Rhee, S. K., ASME Pub., 1979.

15. Hibbs, L. E., Jr., Unpublished Research, General Electric Corporate Research and Development, Schenectady, New York, Contract No. Sandia 13-9406, April 1981.

16. Cortes, J. and Besson, A., "Behavior of Polycrystalline Diamond Compact Cutters While Drilling in Bottomhole Conditions-Field Applications", Proc. Int. Conf. on Geothermal Drilling and Completion Technology, Albuquerque, New Mexico, January 21-23, 1981, Sandia National Laboratories Report SAND81-0036C.

17. Hoover, E. R., private communication, Sandia National Laboratories Division 4741, June 1981.

18. Rae, D., S.M.R.E. Research Rep., 223, 1964.

19. Nevill, H. F. C. and Crone, J. G. D., "Wear of Rotary Drag Drill Bits in Granitic Rock", Instu. of Min. and Met. Trans., 71, Part 5, 1961-62.

20. Osburn, H. G., "Wear of Rock Cutting Tools", Powder Metallurgy, V12, 24, 1969.

21. Kenny, P. and Johnson, S. N., "An Investigation of the Abrasive Wear of Mineral Cutting Tools", Wear, 36, 1976.

22. Rubenstein, C., "An Analysis of Tool Life Based on Flank Face Wear", Trans. ASME - J. Eng. for Ind., February 1976.

23. Pope, L. E., private communication, Sandia National Laboratories Division 5833, June 1981.

24. Gaffney, E. S., "Rock/Steel Dynamic Friction Measurements", System, Science, and Software Report No. SSS-R-75-2686, Defense Nuclear Agency Contract No. DNA 001-75-C-0183, August 1975.

25. Whitbread, J. E., "Bit Temperatures in Rotary Drilling", Colliery Engineering, V37, January 1960.

26. Fish, B. G., Mine and Quarry Engineering, V23, 1957.

27. Fish, B. G., "The Basic Variables in Rotary Drilling", Mine and Quarry Engineering, Part 1, January 1961, Part 2, February 1961.

28. Bowden, F. P. and Tabor, D., The Friction and Lubrication of Solids, Oxford University Press, London, 1953.

29. Kragelskii, I. V., Friction and Wear, Butterworths, Washington, 1965.

30. Blok, H., "The Flash Temperature Concept", Wear, 6, 1963.

31. Jaeger, J. C., "Moving Sources of Heat and the Temperature at Sliding Contacts", Proc. Royal Soc. New S. Wales, 76, 1942, p. 203.

32. Blok, H., "Theoretical Study of Temperature Rise at Surfaces of Actual Contact Under Oiliness Lubricated Conditions", Proc. Instu. Mech. Engrs., General Discussion on Lubrication and Lubricants, 2, 1937.

33. Archard, J. F., "The Temperature of Rubbing Surfaces", Wear, 2, 1958-59, p. 438.

34. Ling, F. F. and Pu, S. L., "Probable Interface Temperatures of Solids in Sliding Contact", Wear, 7, 1964.

35. Ling, F. F., Surface Mechanics, John Wiley and Sons, New York, 1973.

36. Ling, F. F. and Simkins, T. E., "Measurements of Pointwise Juncture Condition of Temperature at the Interface of Two Bodies in Sliding Contact", Trans. ASME J. Basic Eng., Dec. 1963.

37. Ling, F. F. and Ng, C. W., "On Temperatures at the Interface of Bodies in Sliding Contact", Proc. 4th U.S. Nat. Congress of Applied Mechs., V2, 1962.

38. Dayson, C., "Surface Temperatures at Unlubricated Sliding Contacts", ASLE Trans., V10, 1967.

39. Furey, M. J., "Surface Temperatures in Sliding Contact", ASLE Trans., V7, 1964.

40. Kennedy, F. E., Jr., "Surface Temperatures in Sliding Systems - A Finite Element Analysis", Trans. ASME-ASLE Lubrication Conf., San Francisco, California, August 18-21, 1980.

41. Kounas, P. S., Dimarogonas, A. D. and Sandor, G. N., "The Distribution of Friction Heat Between A Stationary Pin and A Rotating Cylinder", Wear, 19, 1972.

42. Burgemeister, E. A., "Syndite® - Its Thermal Conductivity Above Room Temperature", Industrial Diamond Review, March 1980.

43. Glowka, D. A., "Optimization of Bit Hydraulic Configurations", SPE Paper 10240, Presented at 56th Annual Fall Tech. Conf. and Exhibition of the SPE/AIME, San Anotnio, Texas, October 1981.

44. Goodman, M. A., "Temperature Histories in Geothermal Wells - Survey of Rock Thermomechanical Properties and Drilling, Production, and Injection Case Studies", Sandia National Laboratories Report to be published, Contract No. 13-8769, March 1981.

45. McAdams, W. H., Heat Transmission, Third Ed., McGraw-Hill, New York, 1954.

46. Fand, R. M., "Heat Transfer by Forced Convection From a Cylinder to Water in Crossflow", Int. J. Heat & Mass Transfer, Vol. 8, pp. 995-1010, 1965.

47. Giedt, W. H., "Investigation of Variation of Point Unit Heat-Transfer Coefficient Around a Cylinder Normal to an Air Stream", Trans. ASME, Vol. 71, pp. 375-381, 1949.

48. Vliet, G. C. and Leppert, G., "Forced Convection Heat Transfer from an Isothermal Sphere to Water", Journal of Heat Transfer, Trans. ASME, pp. 163-175, May 1961.

49. White, F. M., Viscous Fluid Flow, McGraw-Hill, New York, 1974, p. 123.

50. Chrysler Improved Numerical Differencing Analyzer (CINDA), Technical Note TN-AP-67-287 Chrysler Corporation Space Division, New Orleans, Louisiana.

51. Ortega, A., Glowka, D. A. and Hibbs, L. E., "Frictional Heating, Convective Cooling and Lubrication of Polycrystalline Diamond Drag Tools During Rock Cutting", In preparation.

52. Hook, R. A. and Cooper, L. W., "Air Drilling", Oil and Gas Journal, June 27, 1977, p. 100.

APPENDIX A

ISOTHERM PLOTS FOR NUMERICAL CUTTER MODELS AT VARIOUS CONDITIONS

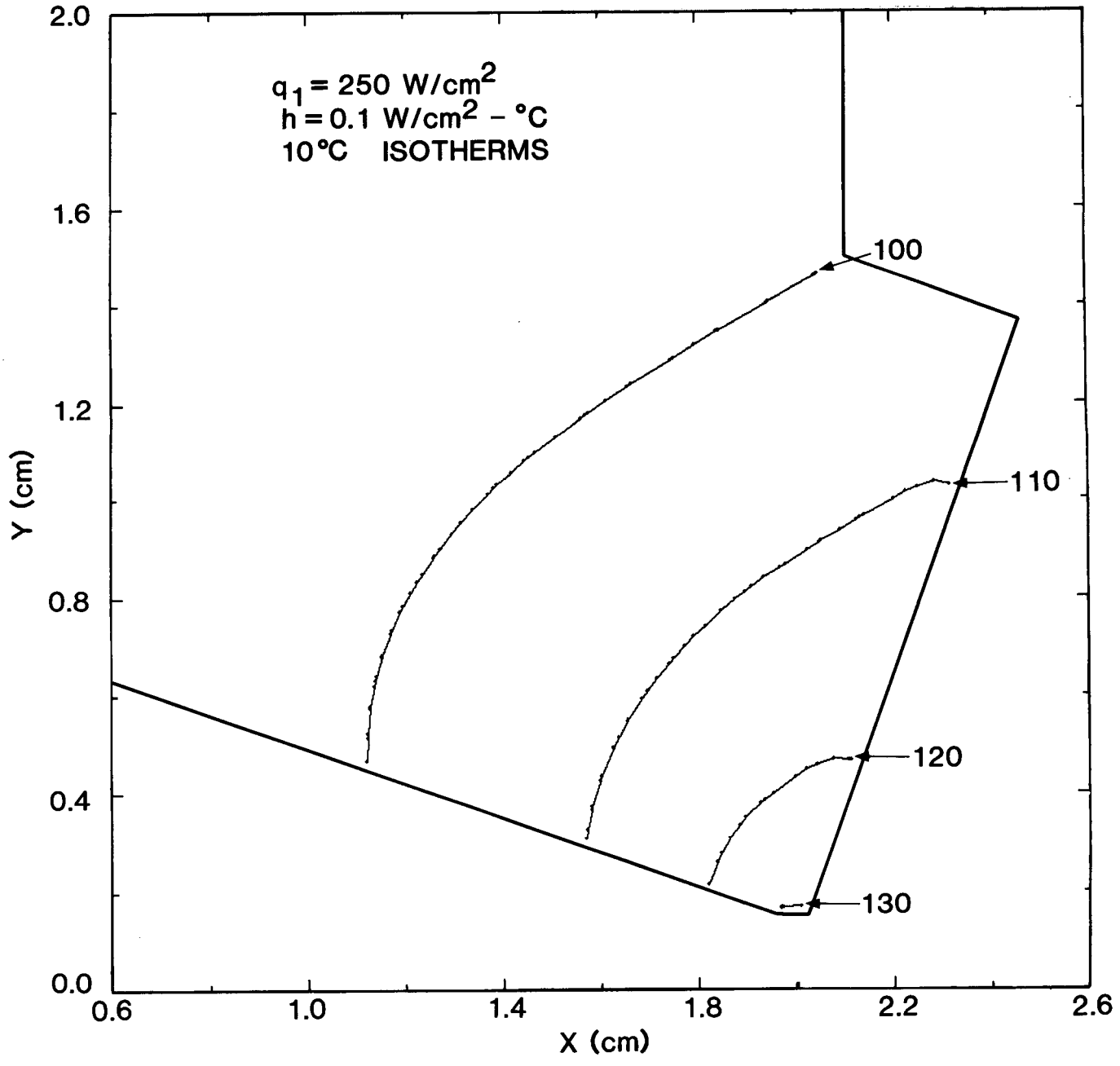

Figure A1. Isotherm Plot for Mildly Worn Tool

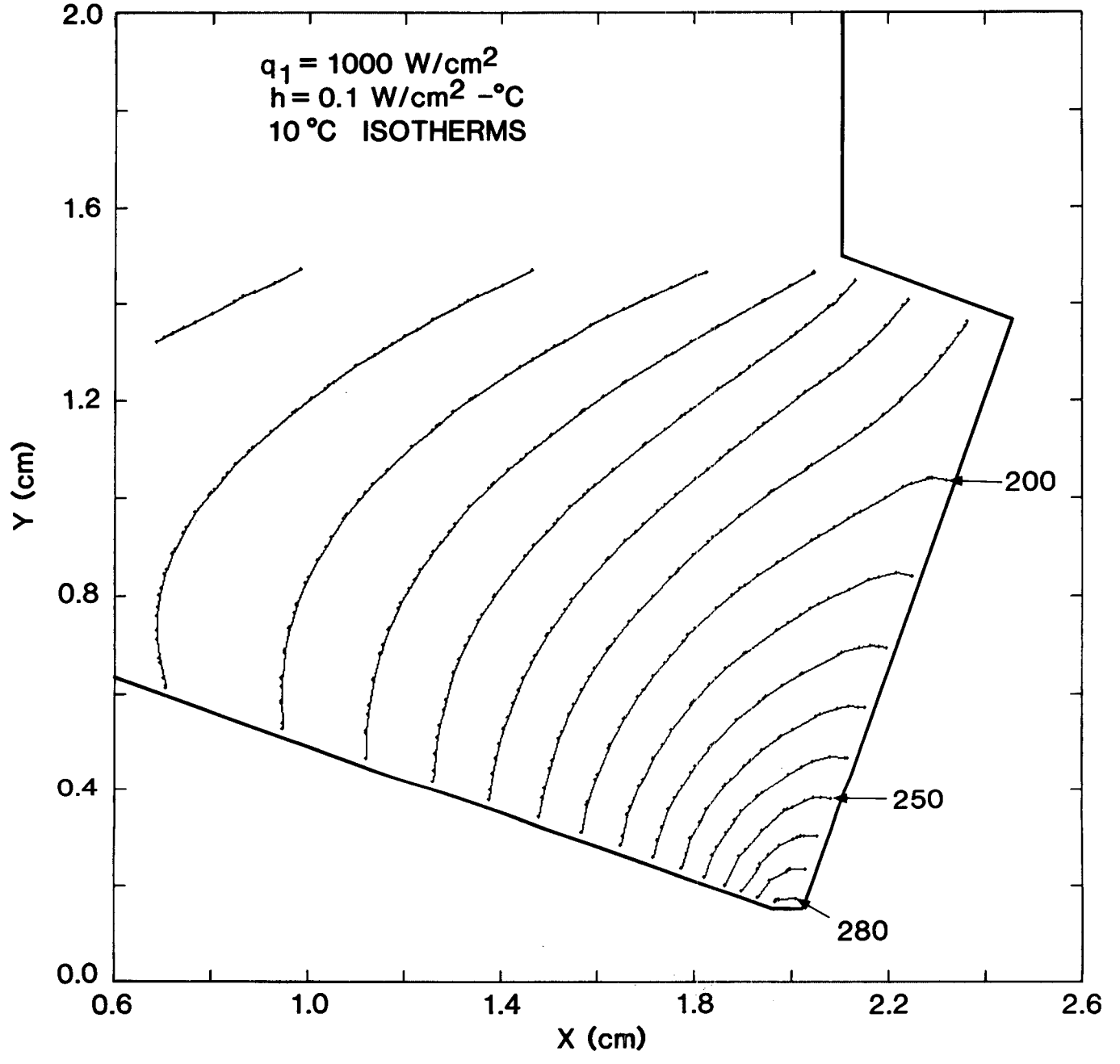

Figure A2. Isotherm Plot for Mildly Worn Tool

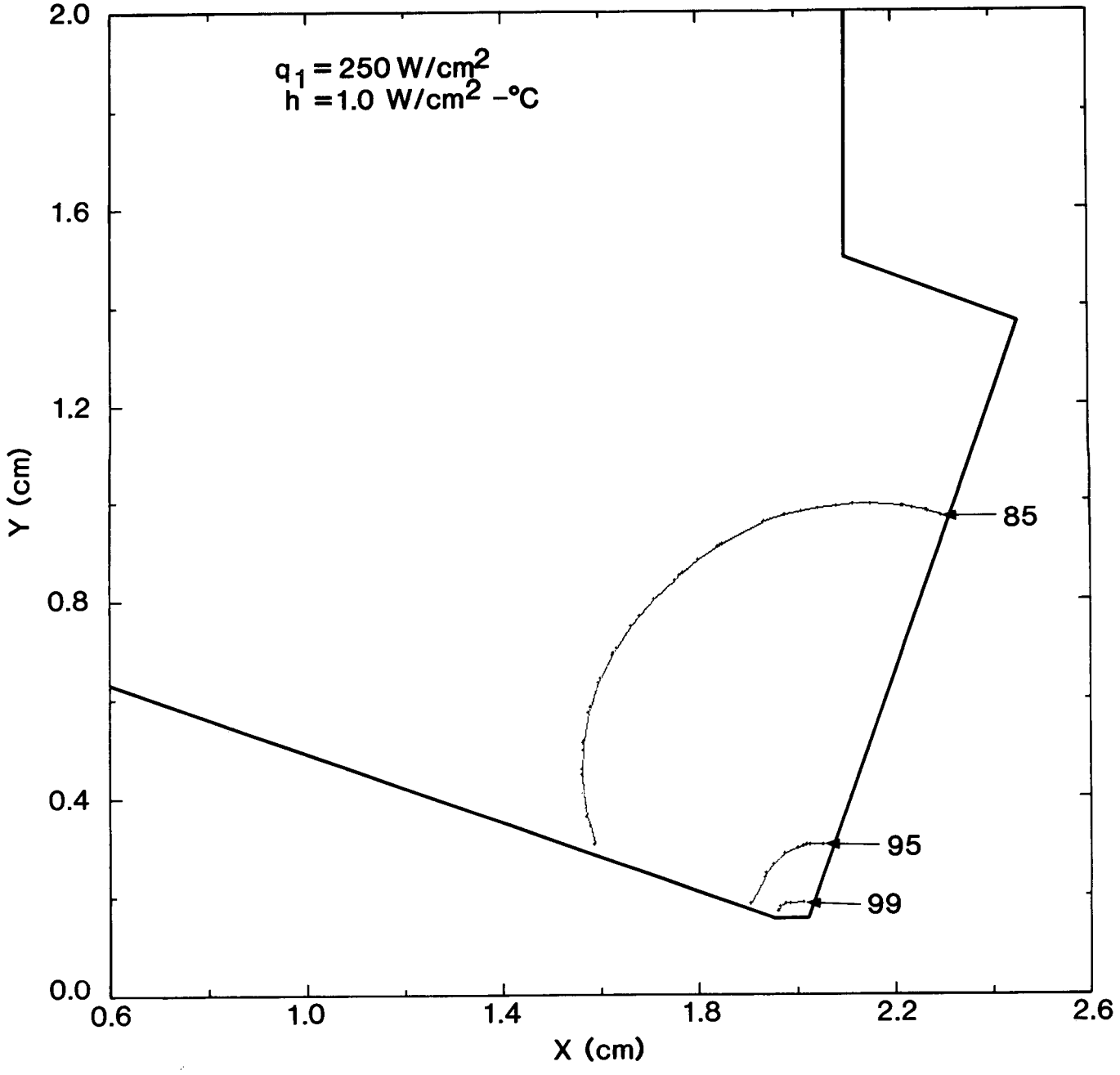

Figure A3. Isotherm Plot for Mildly Worn Tool

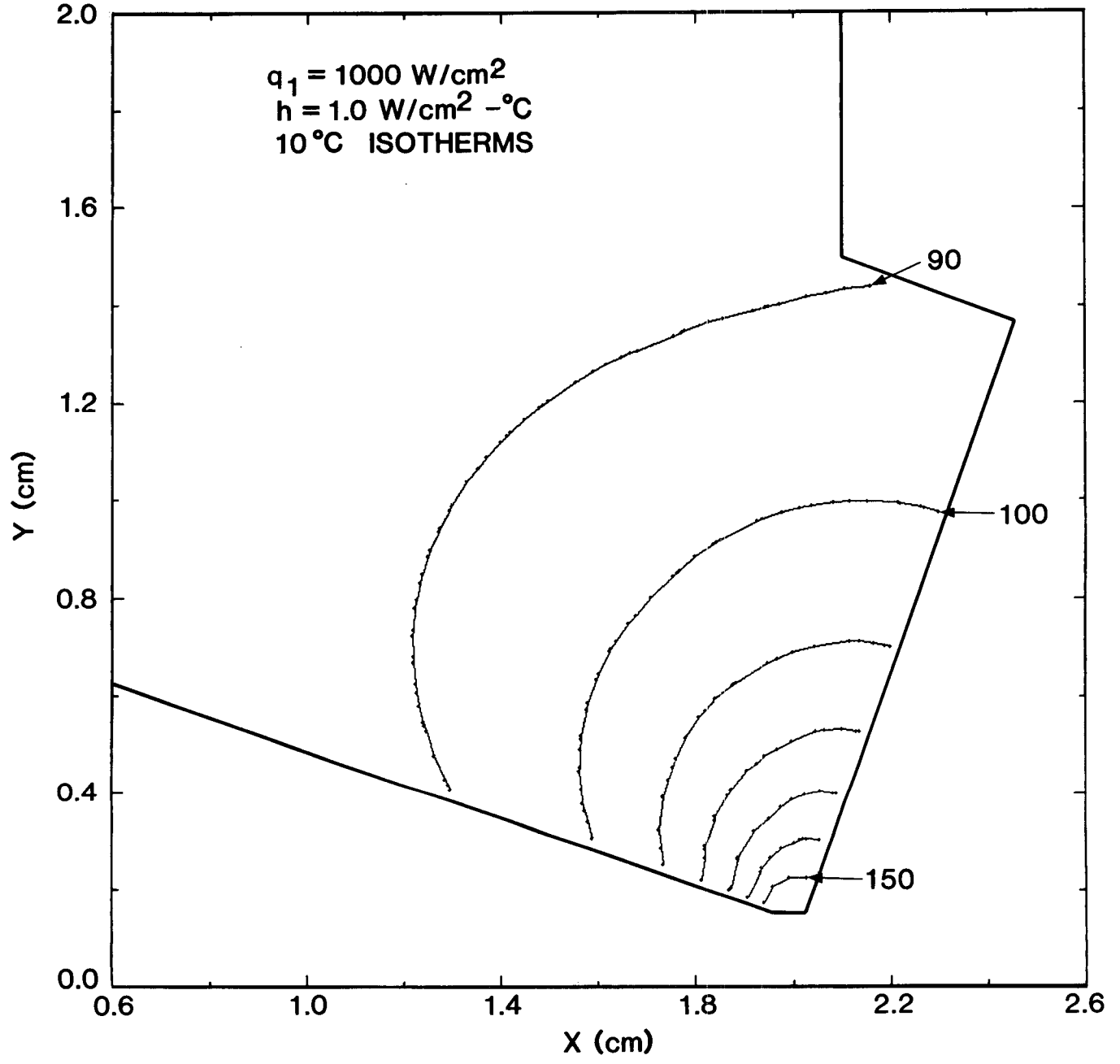

Figure A4. Isotherm Plot for Mildly Worn Tool

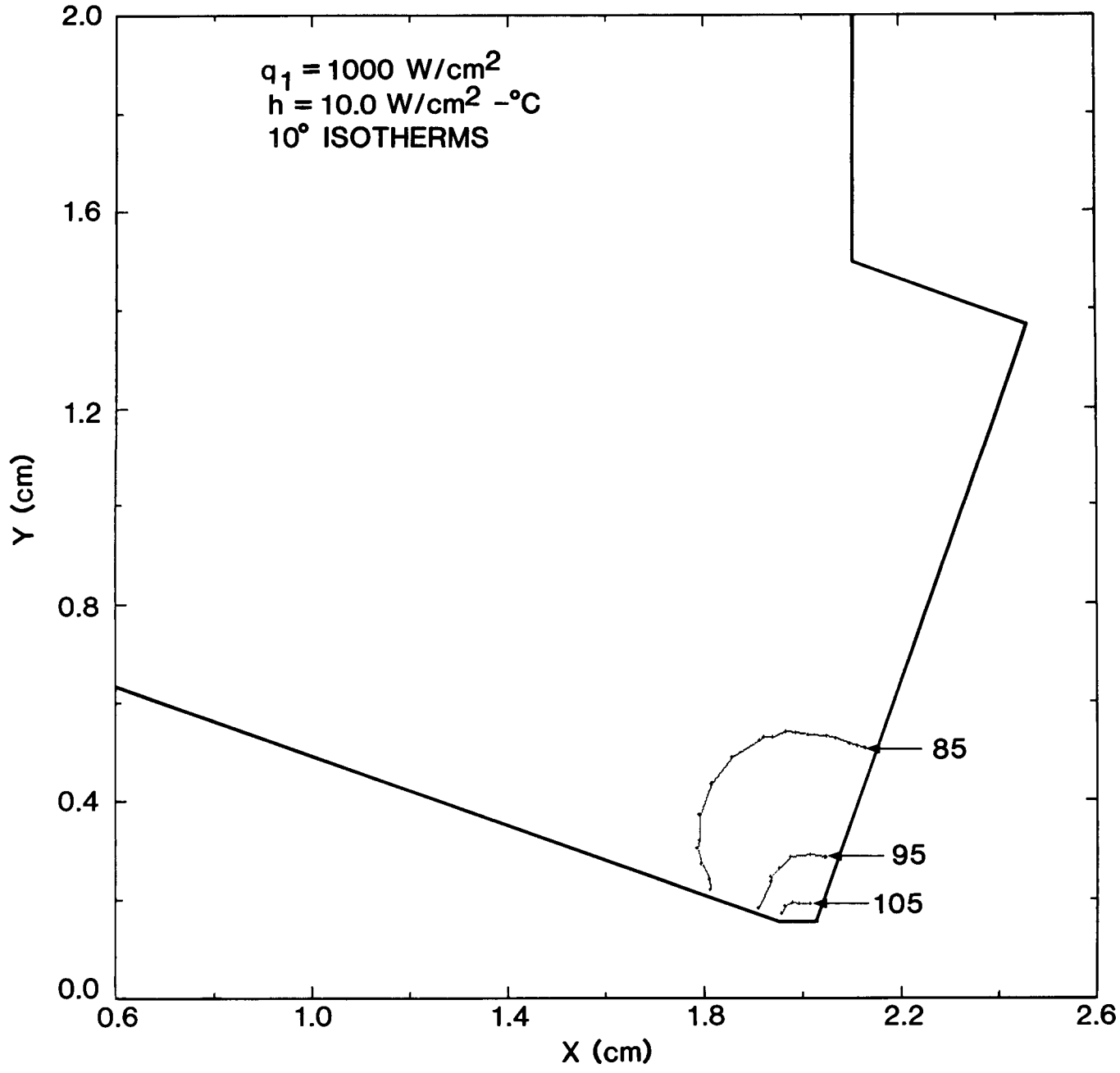

Figure A5. Isotherm Plot for Mildly Worn Tool

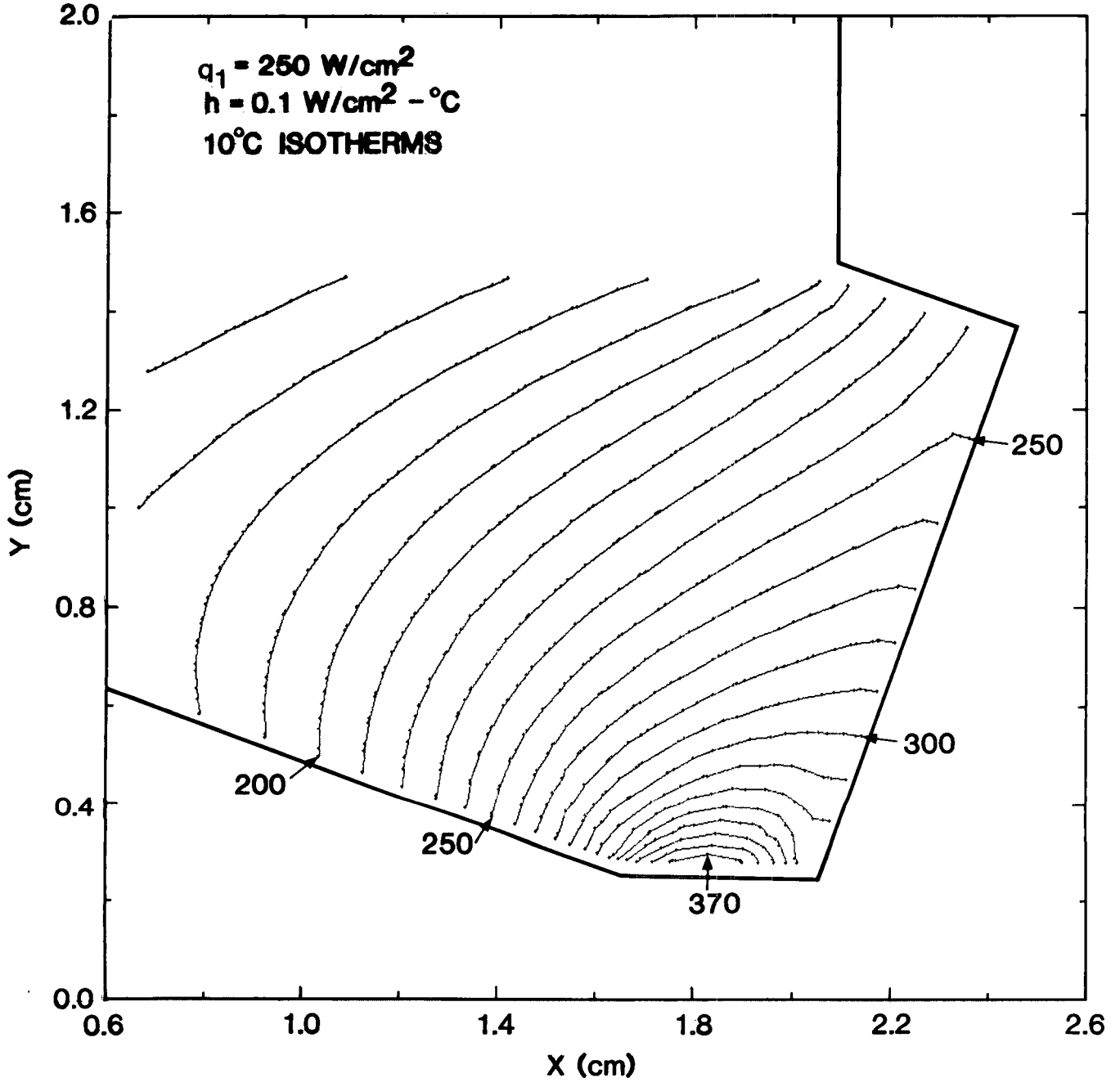

Figure A6. Isotherm Plot for Medium Worn Tool

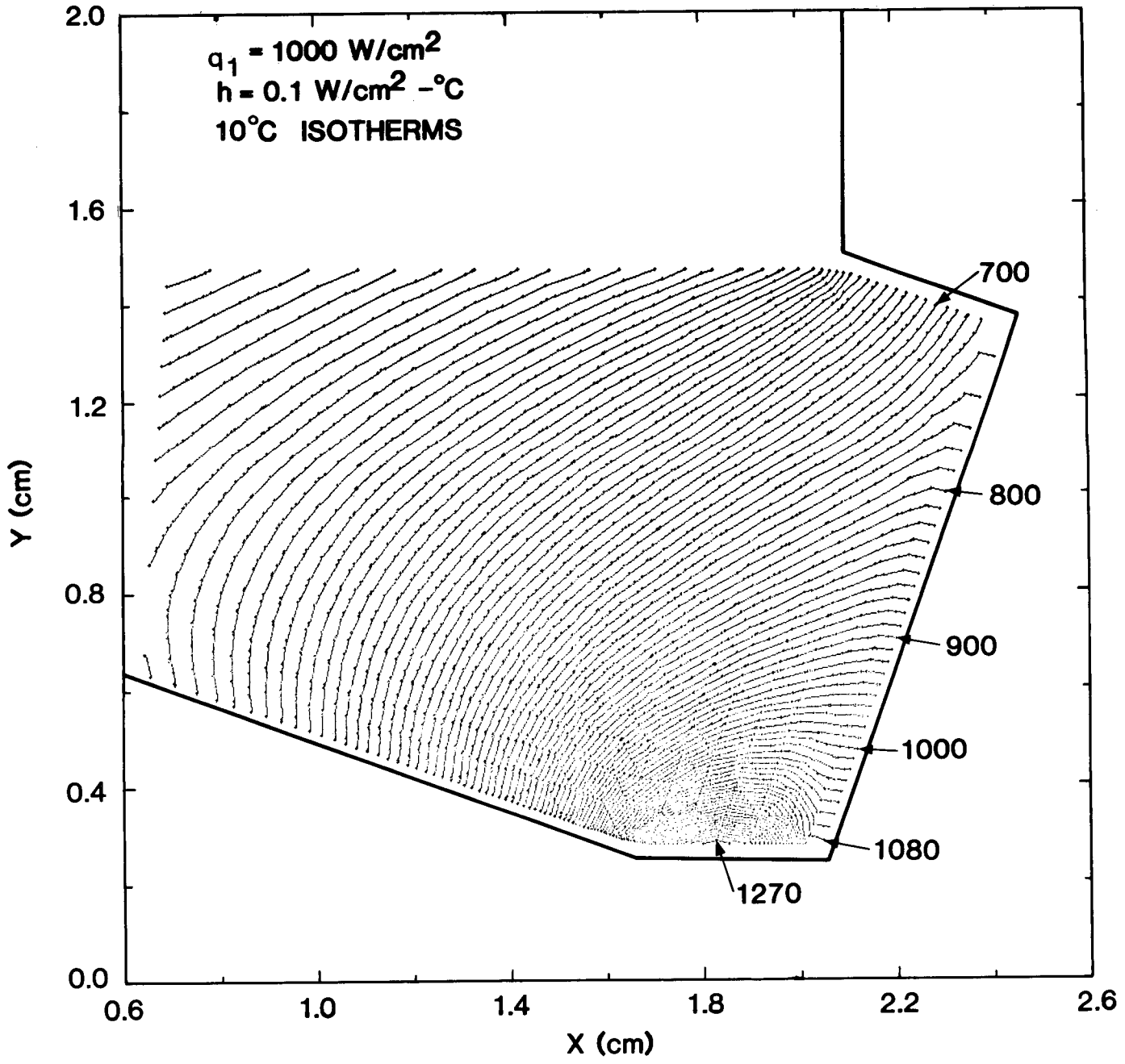

Figure A7. Isotherm Plot for Medium Worn Tool

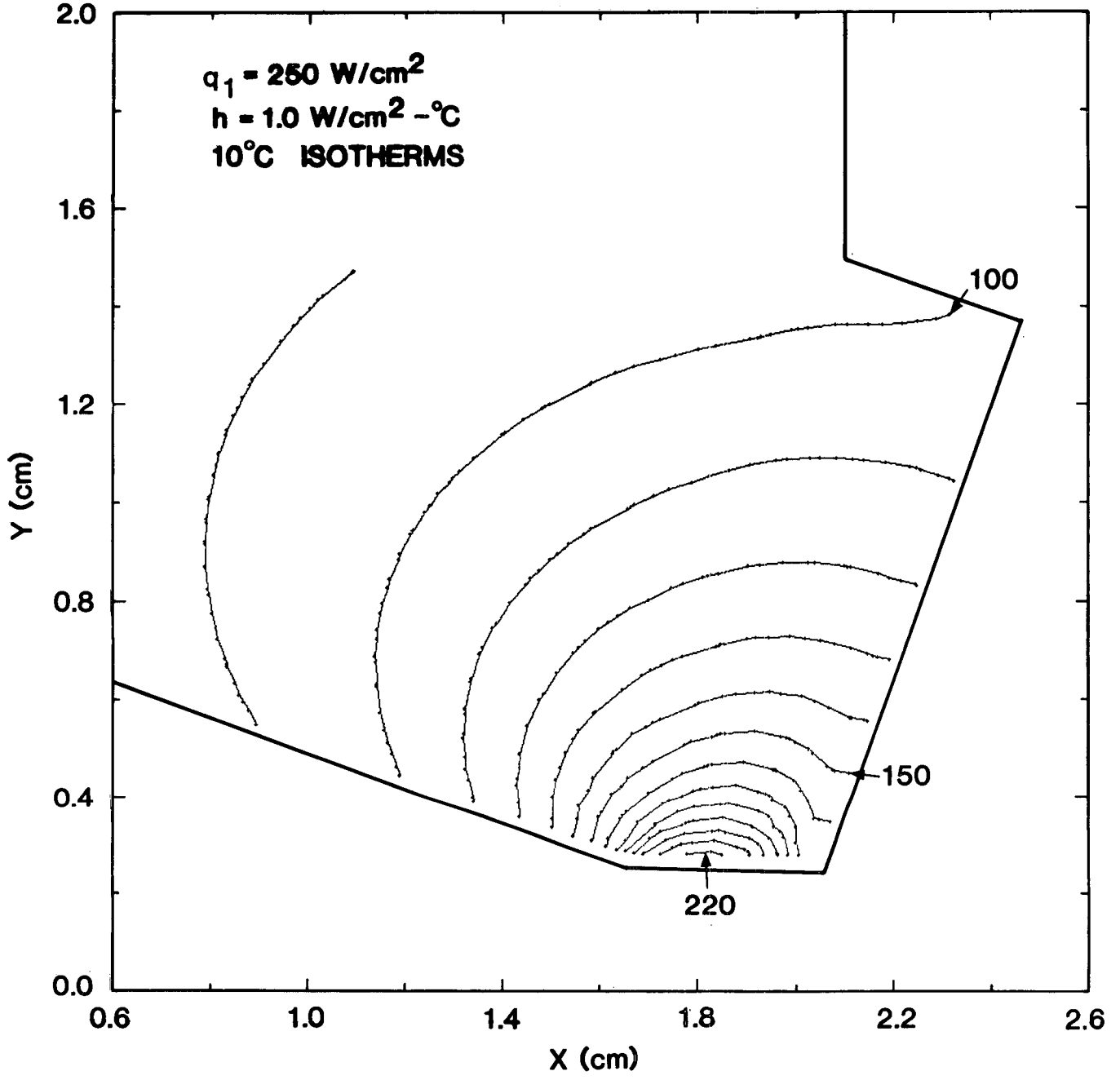

Figure A8. Isotherm Plot for Medium Worn Tool

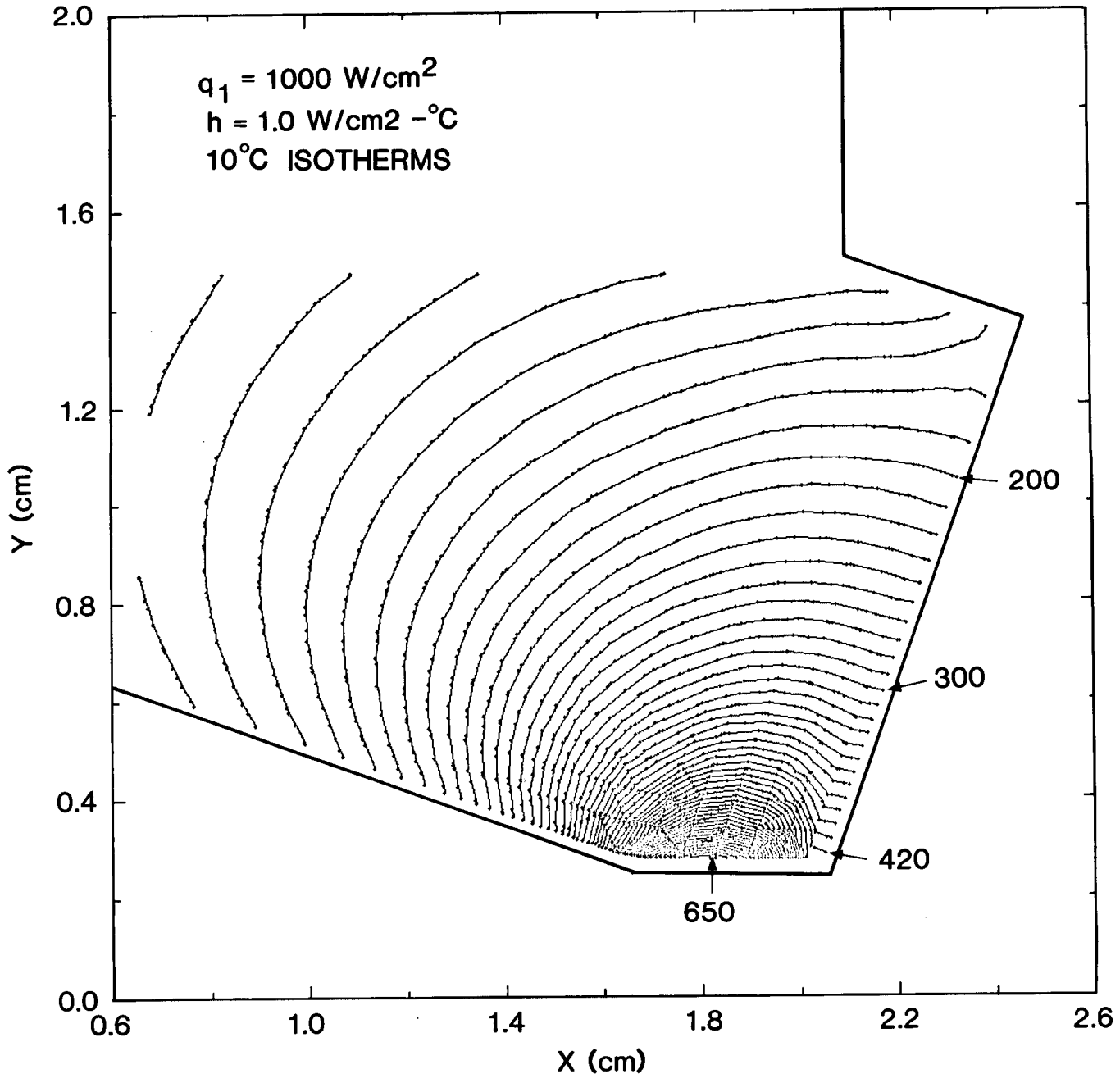

Figure A9. Isotherm Plot for Medium Worn Tool

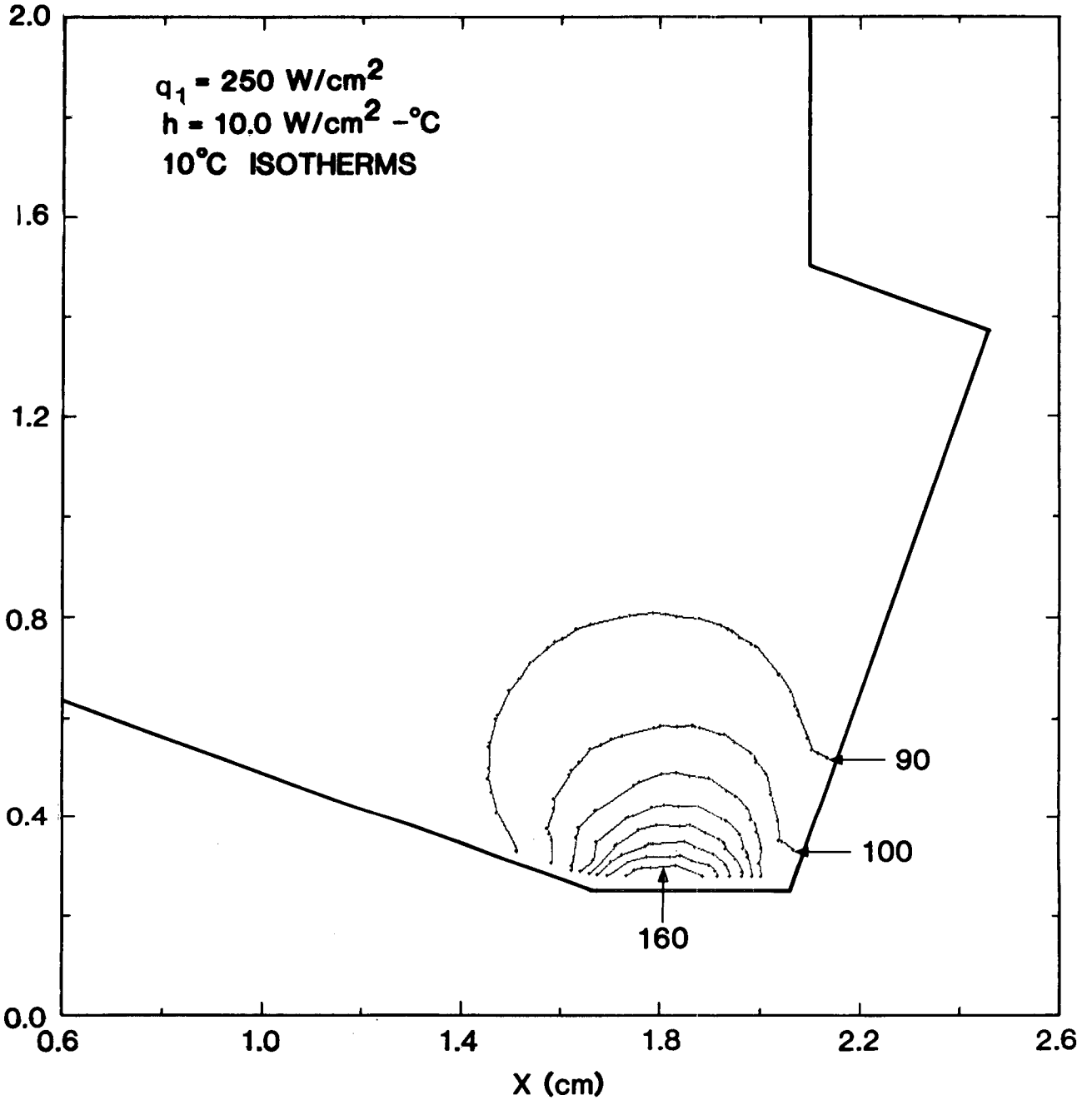

Figure A10. Isotherm Plot for Medium Worn Tool

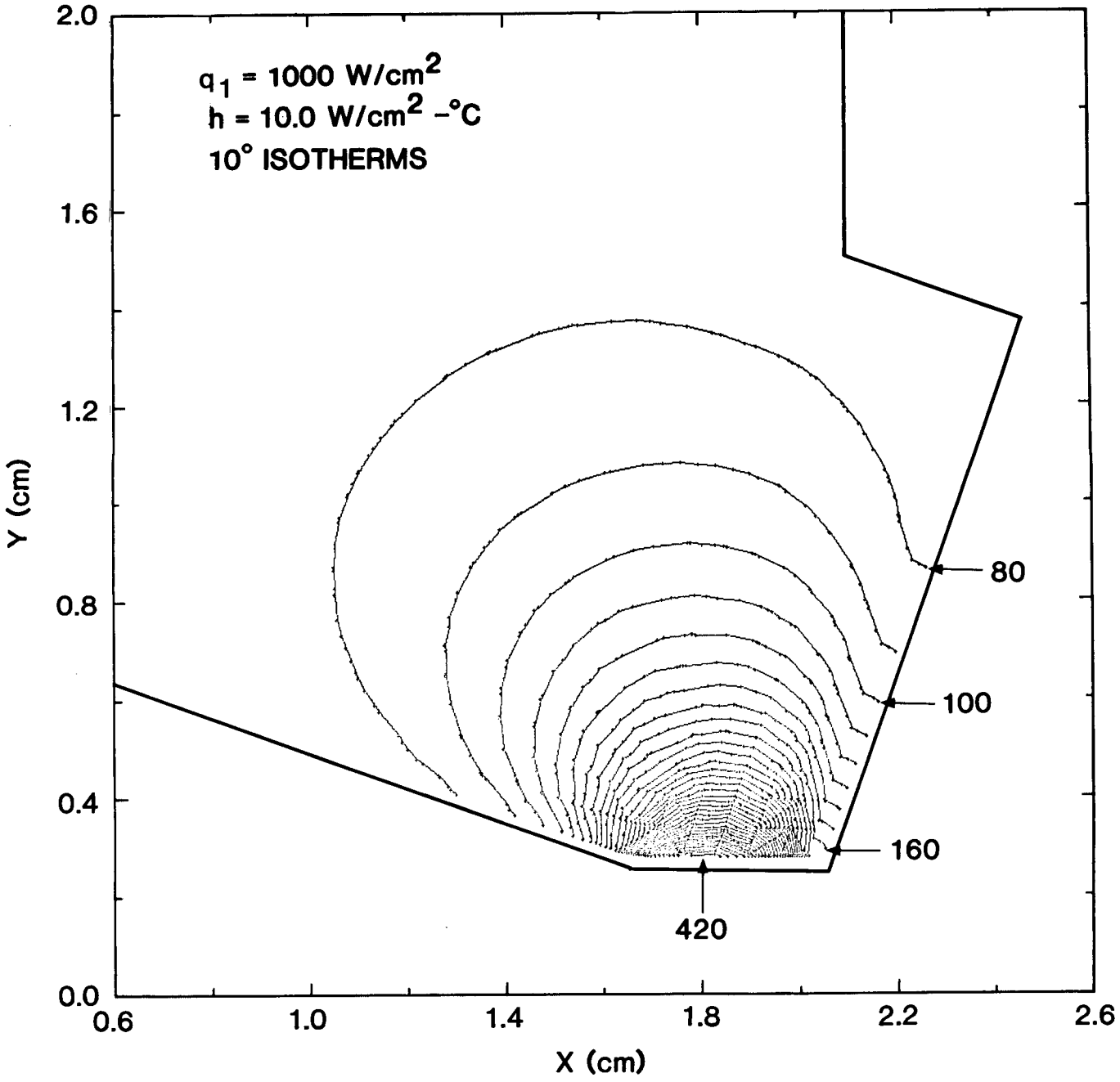

Figure All. Isotherm Plot for Medium Worn Tool

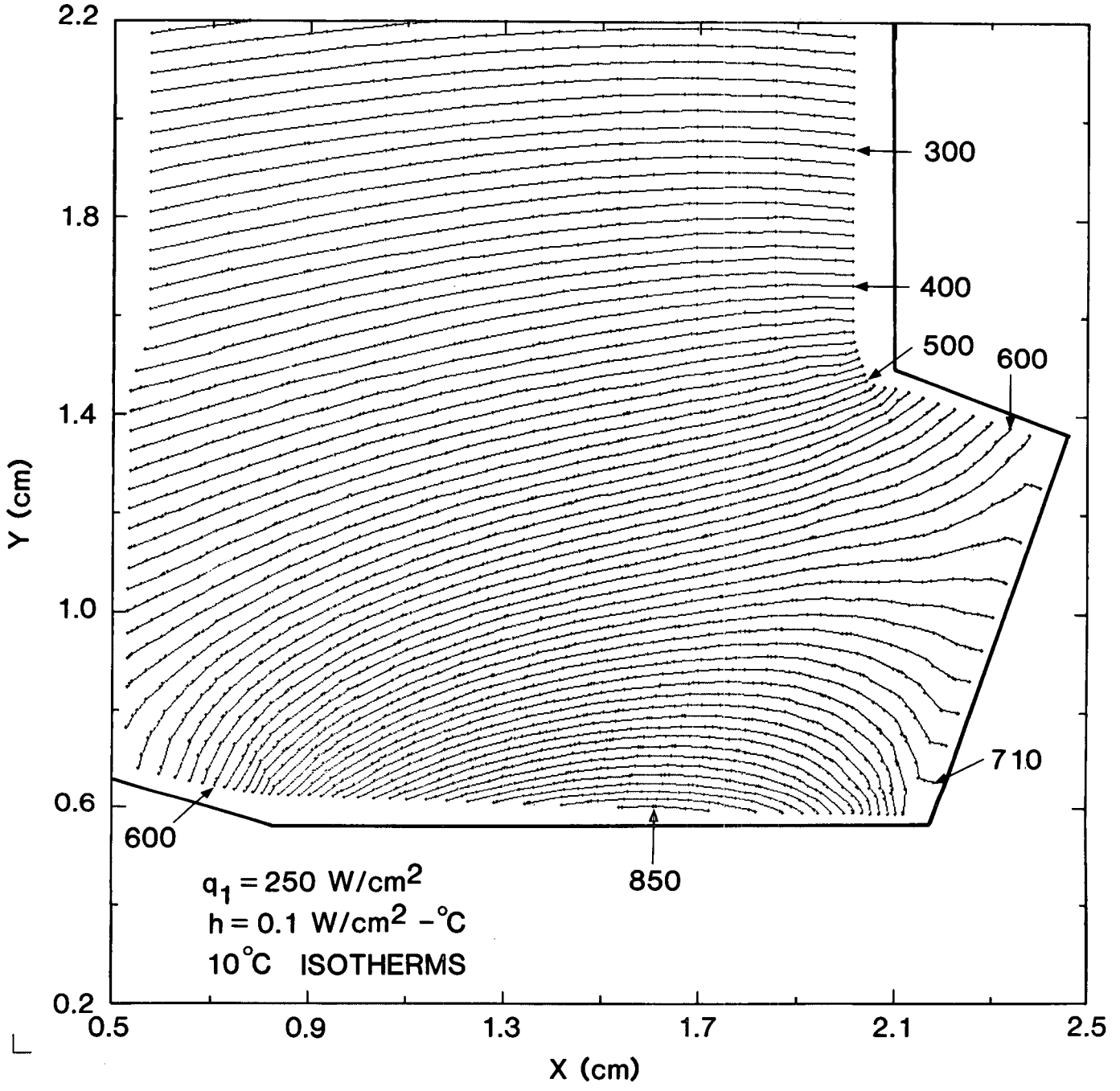

Figure A12. Isotherm Plot for Severely Worn Tool

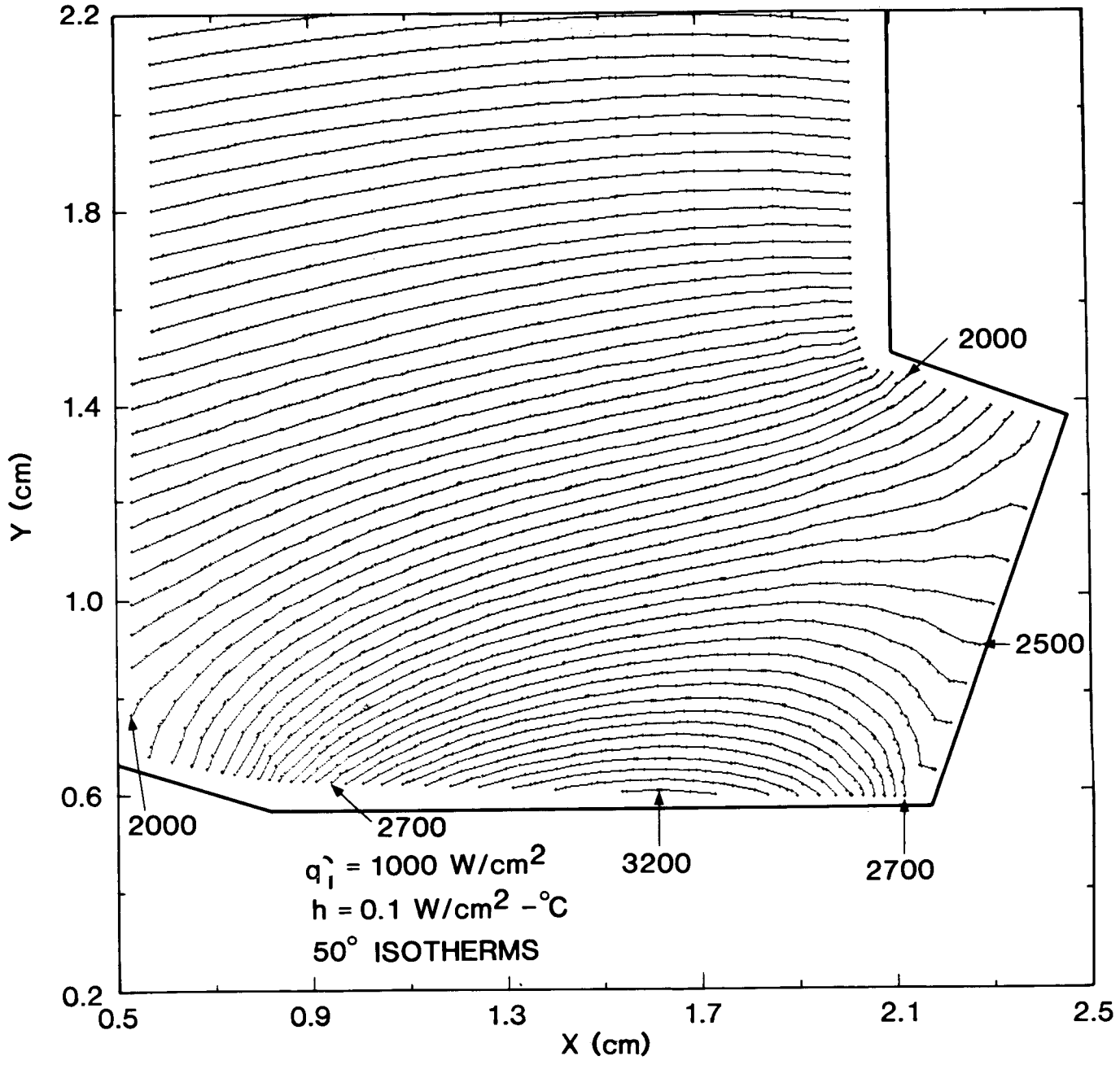

Figure A13. Isotherm Plot for Severely Worn Tool

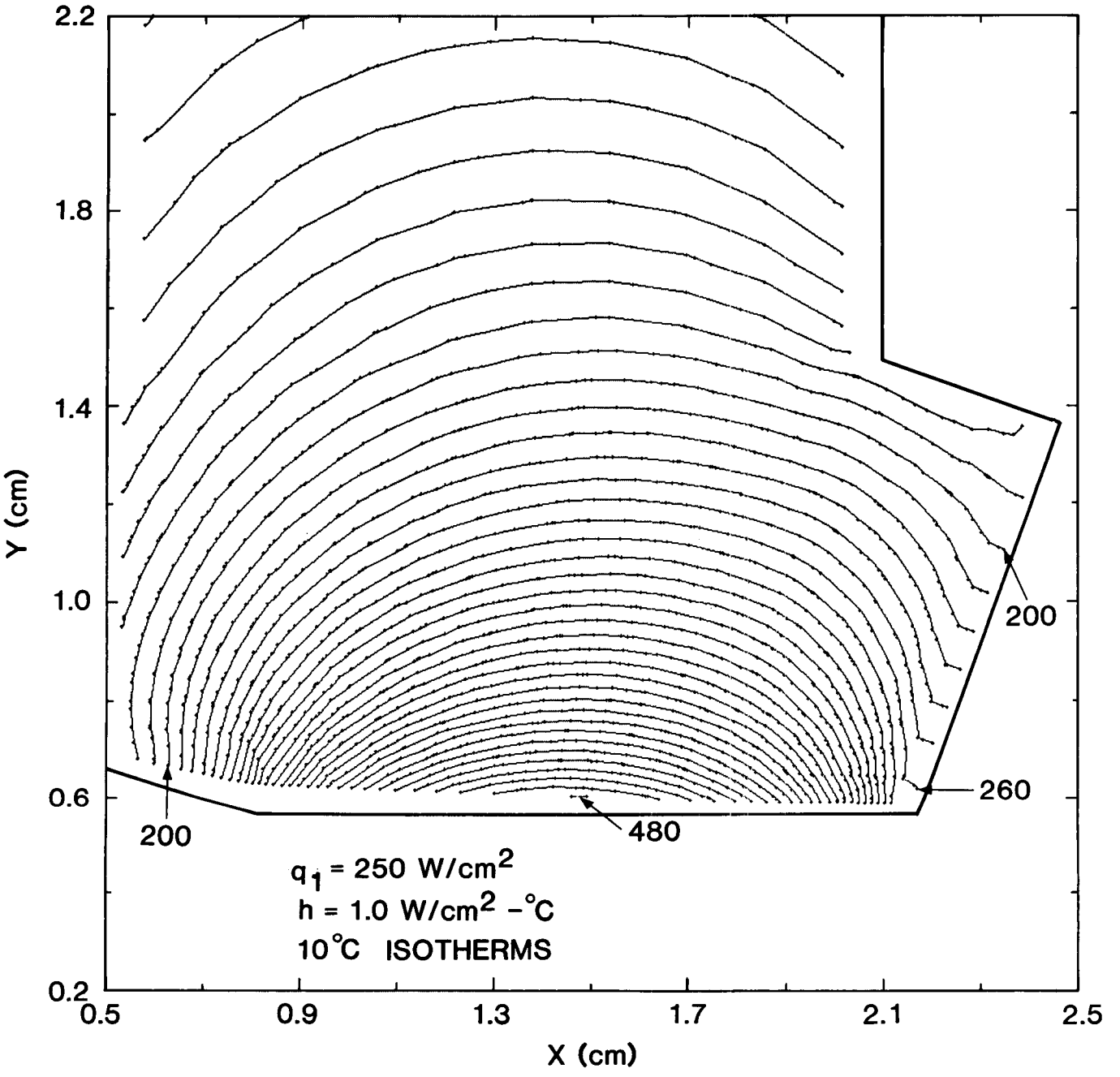

Figure A14. Isotherm Plot for Severely Worn Tool

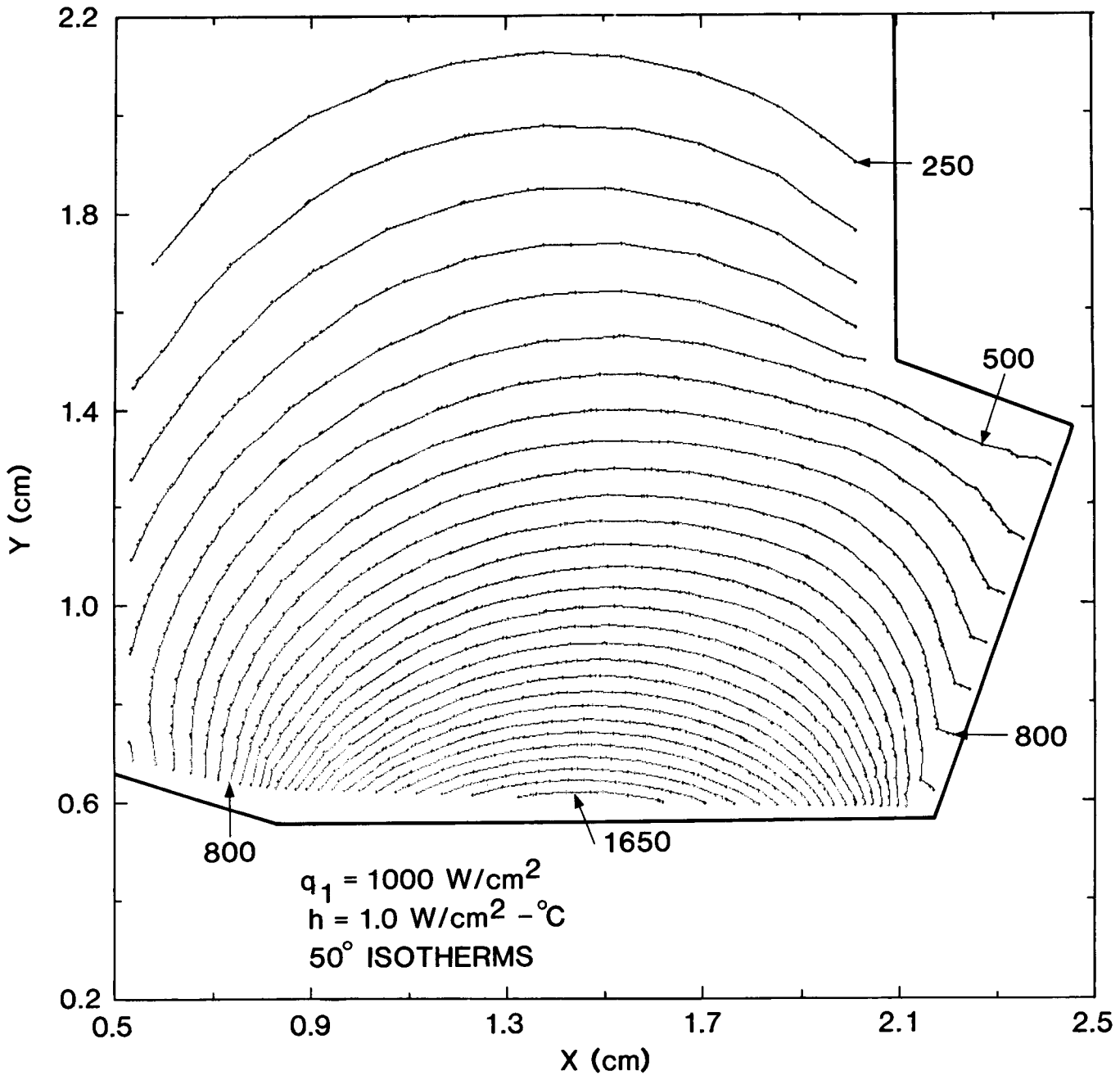

Figure A15. Isotherm Plot for Severely Worn Tool

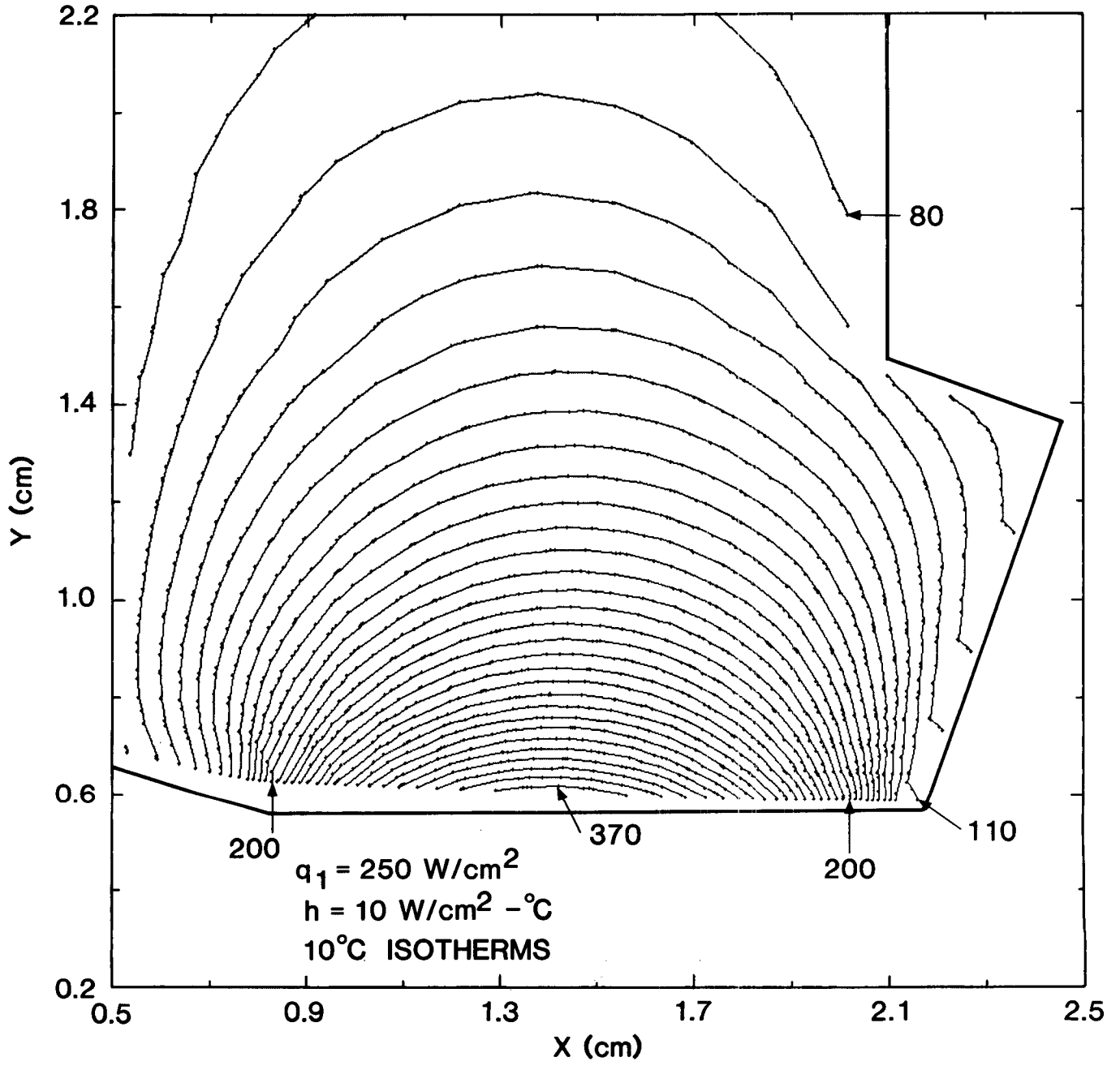

Figure A16. Isotherm Plot for Severely Worn Tool

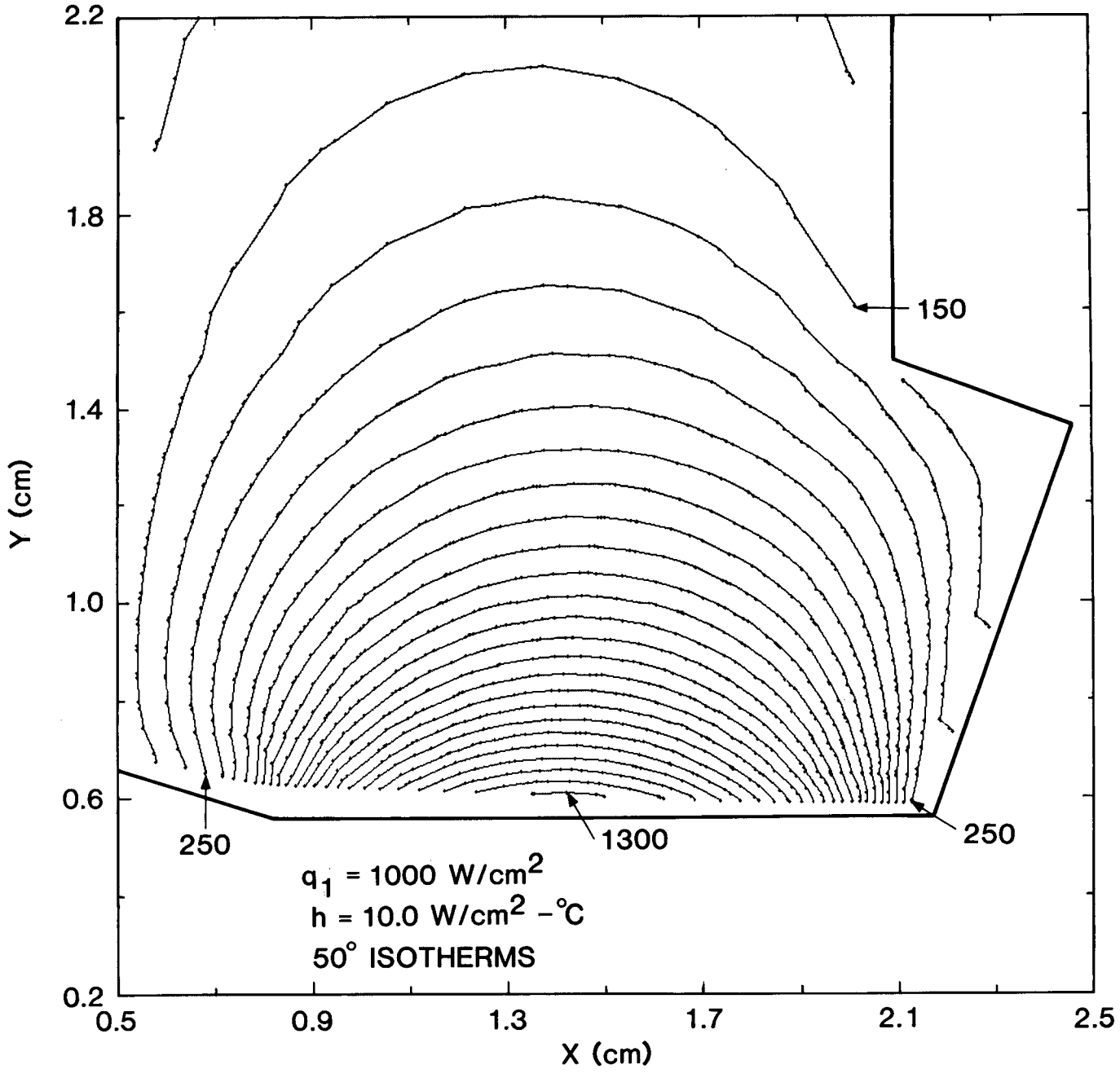

Figure A17. Isotherm Plot for Severely Worn Tool

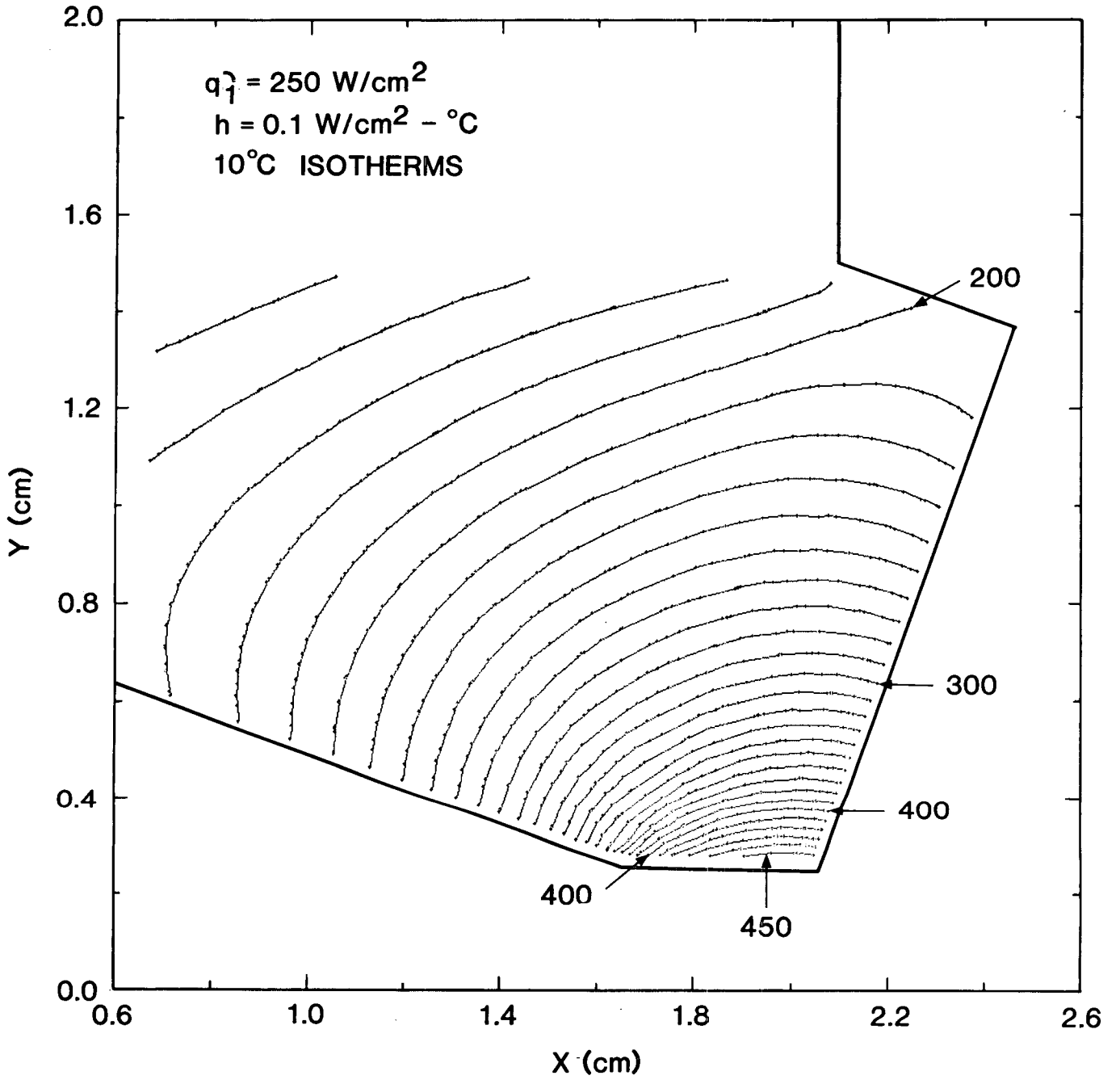

Figure A18. Isotherm Plot for Moderately Worn All WC Tool

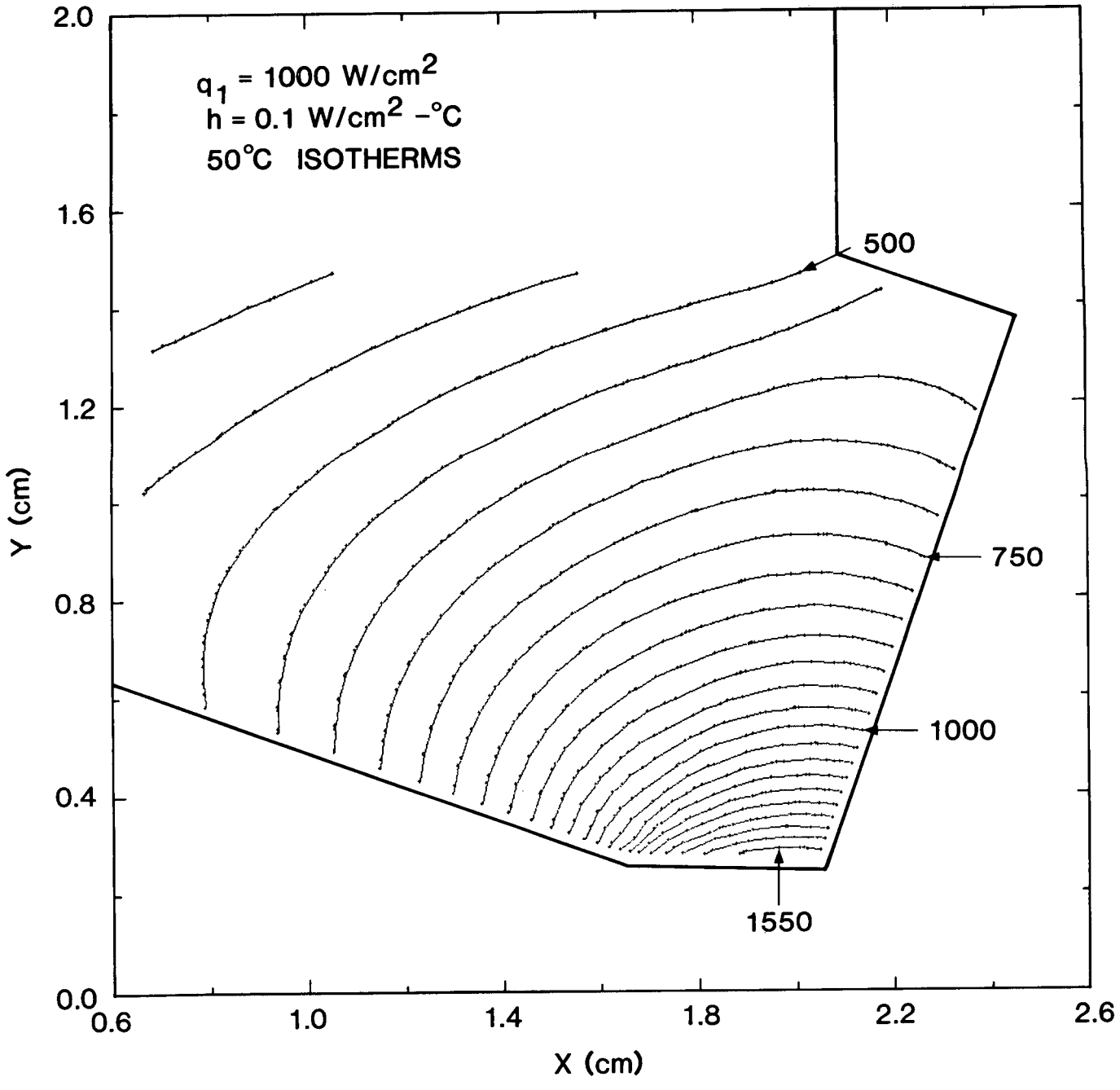

Figure A19. Isotherm Plot for Moderately Worn All WC Tool

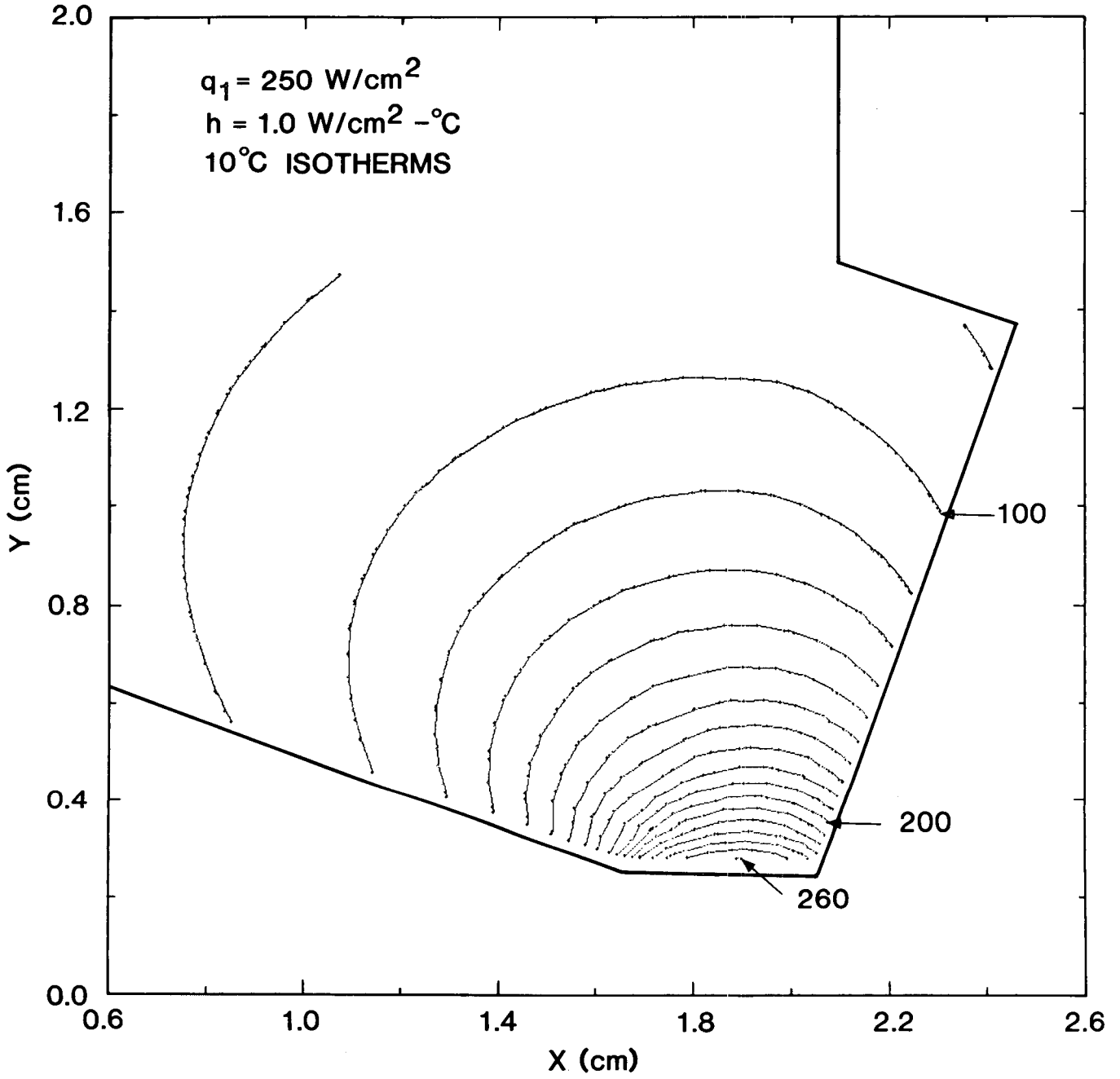

Figure A20. Isotherm Plot for Moderately Worn All WC Tool

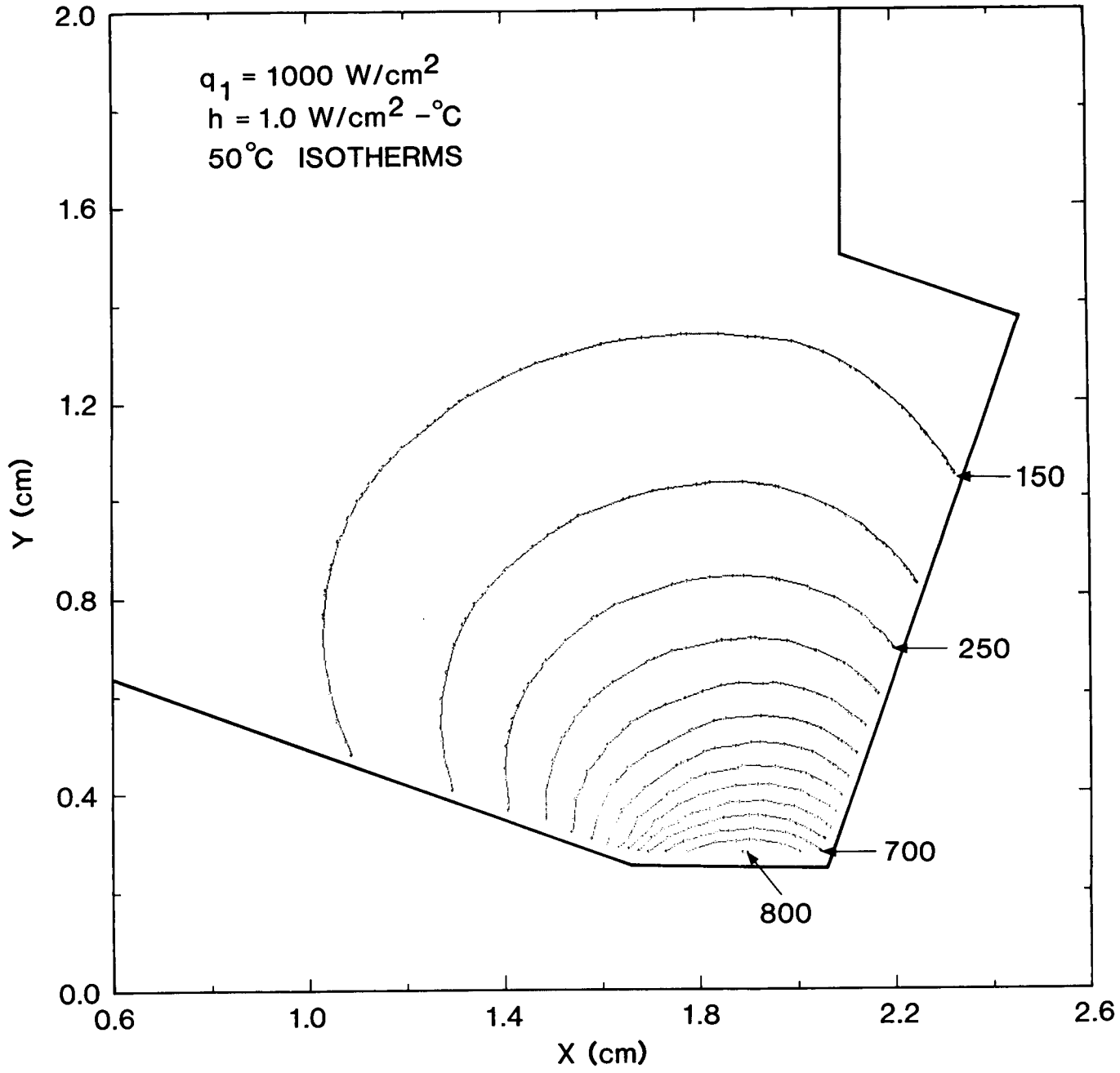

Figure A21. Isotherm Plot for Moderately Worn All WC Tool

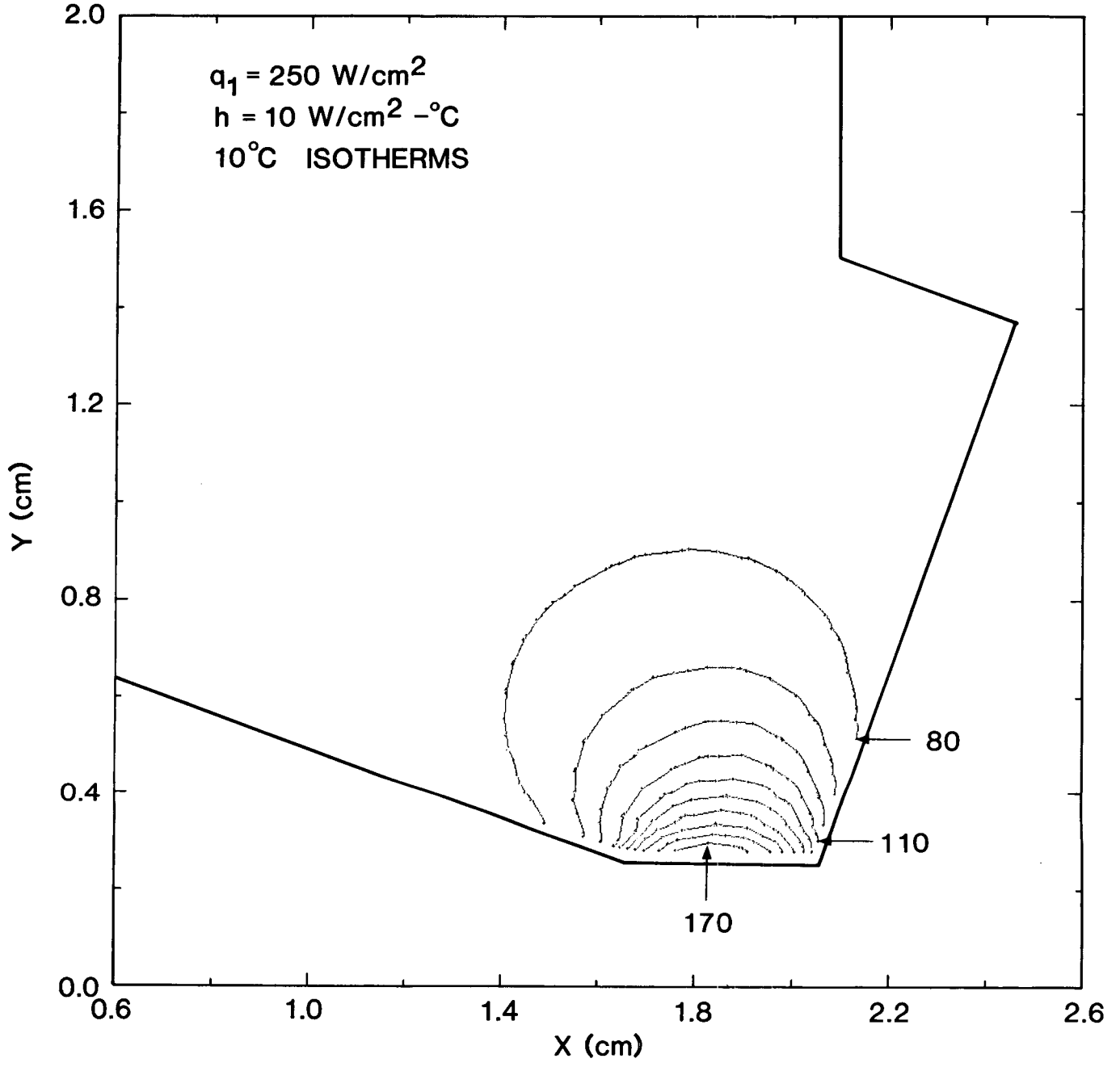

Figure A22. Isotherm Plot for Moderately Worn All WC Tool

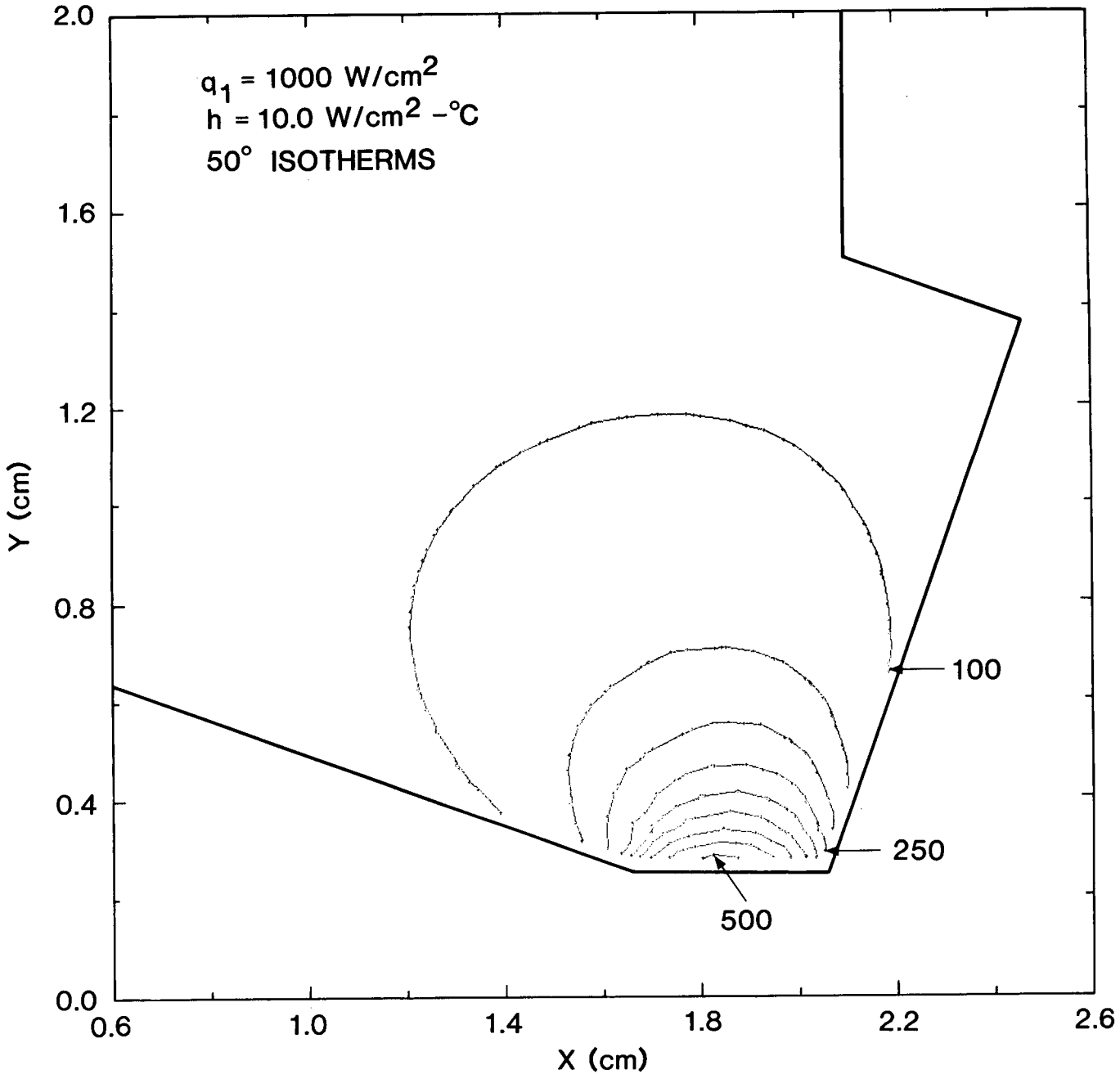

Figure A23. Isotherm Plot for Moderately Worn All WC Tool

APPENDIX B

DESIGN CURVES* FOR PREDICTION OF TEMPERATURES IN PDC CUTTERS

* Refer to explanation (p. 56) for use of these curves.

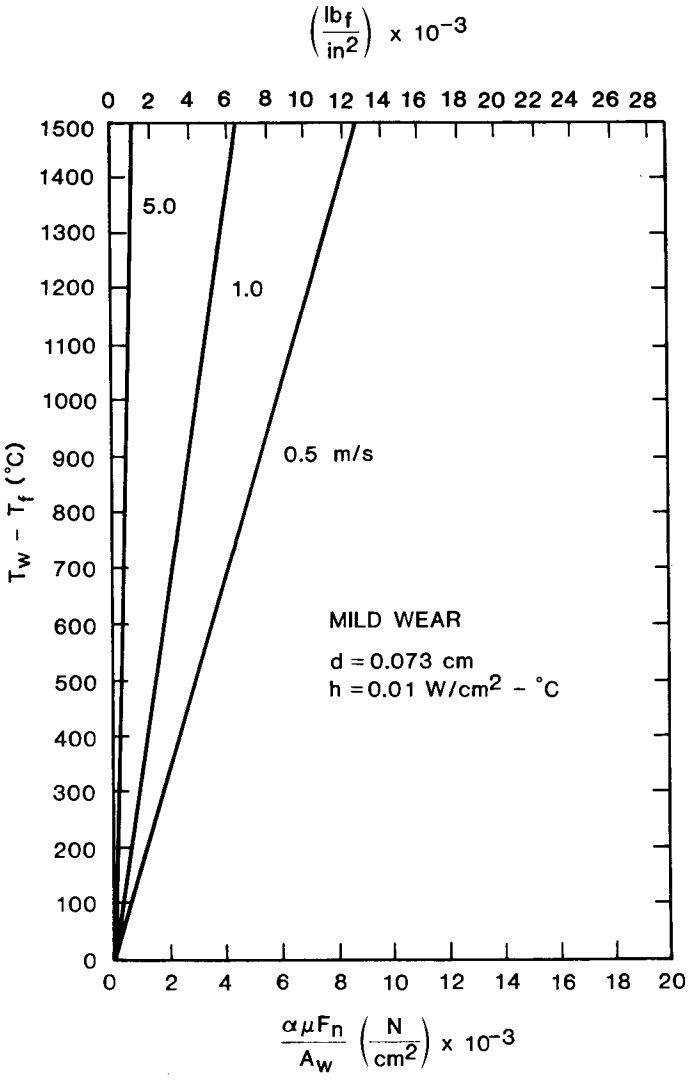

Figure B1

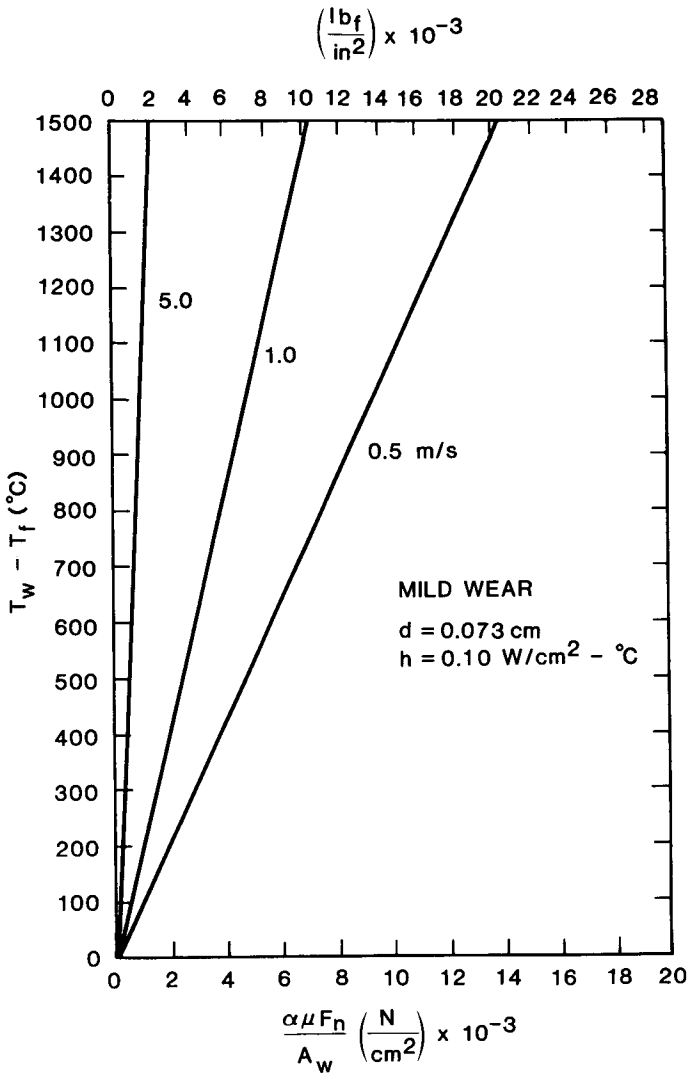

Figure B2

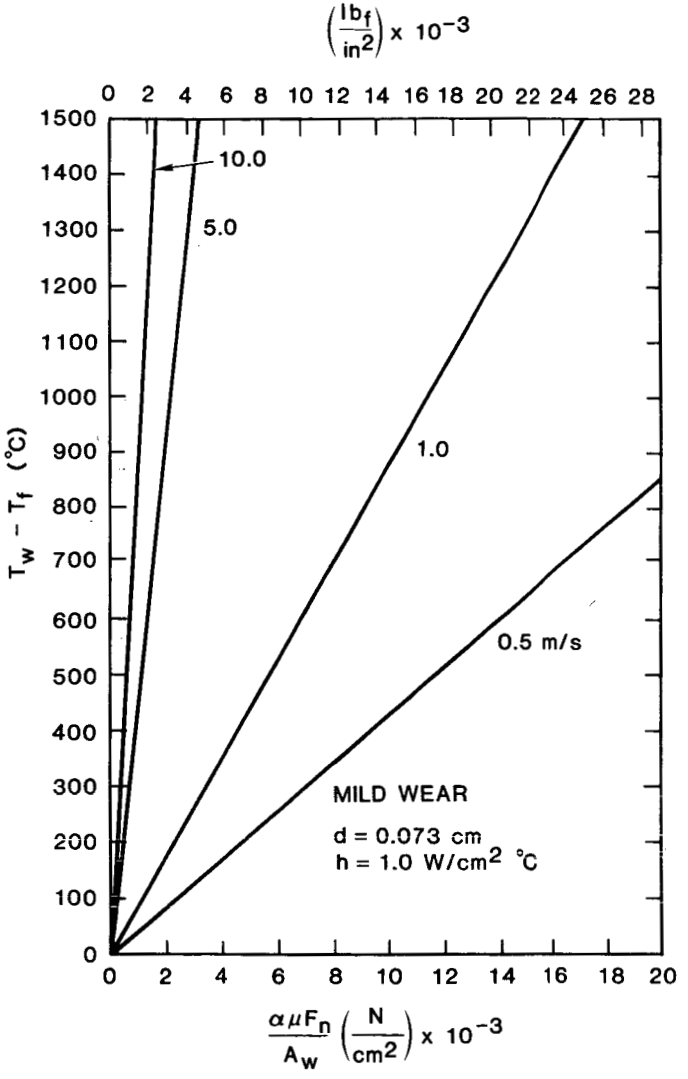

Figure B3

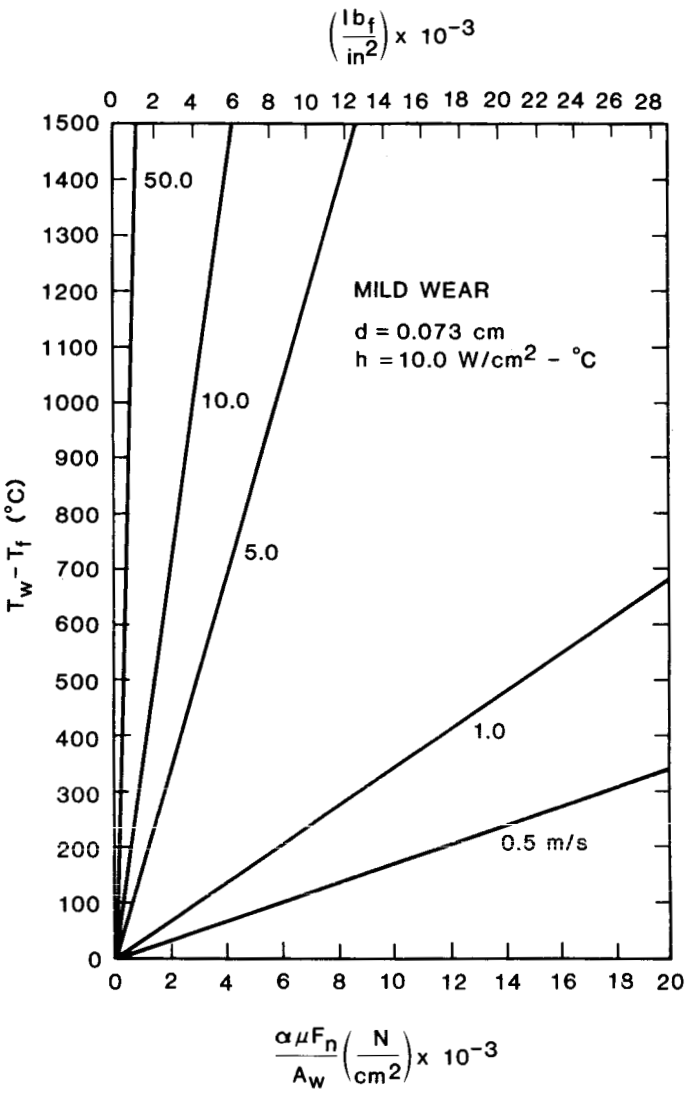

Figure B4

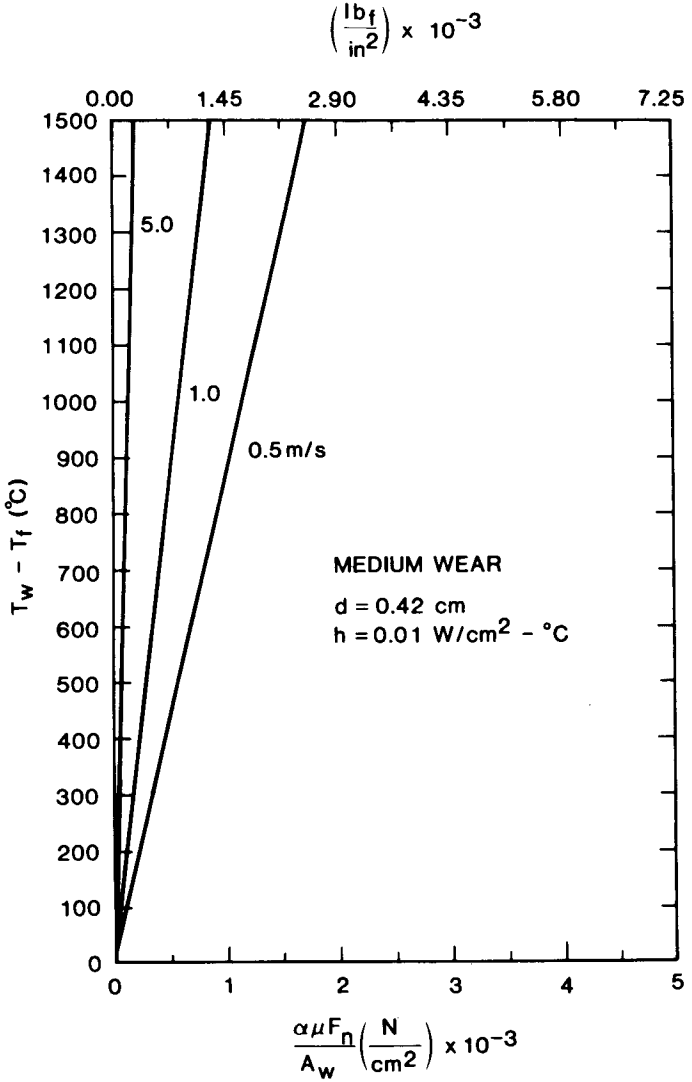

Figure B5

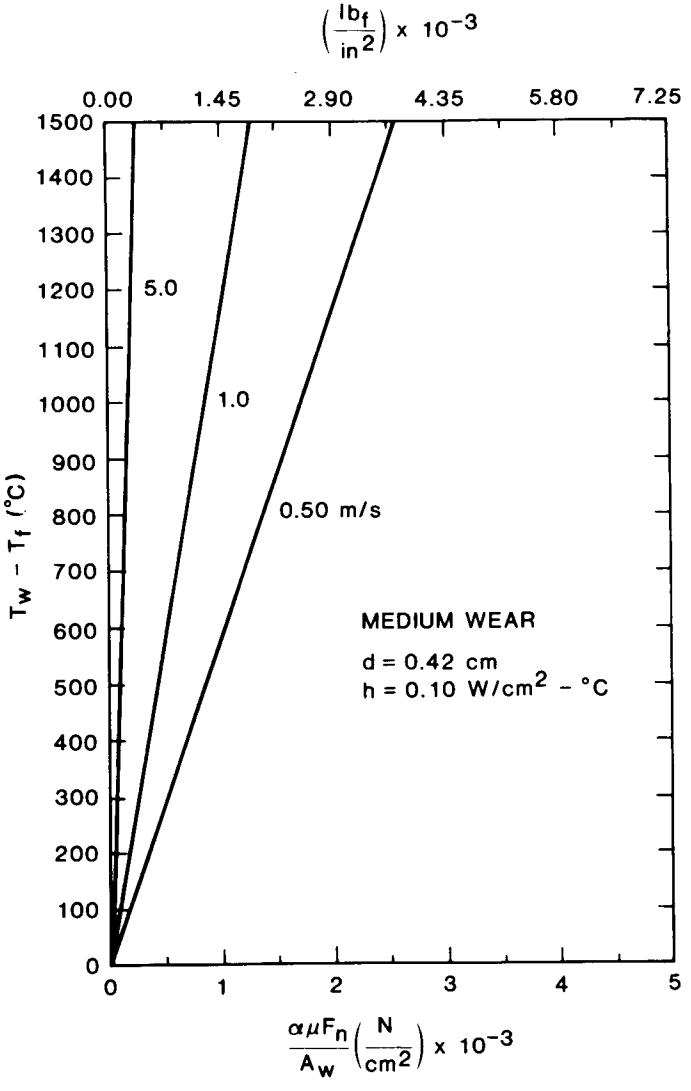

Figure B6

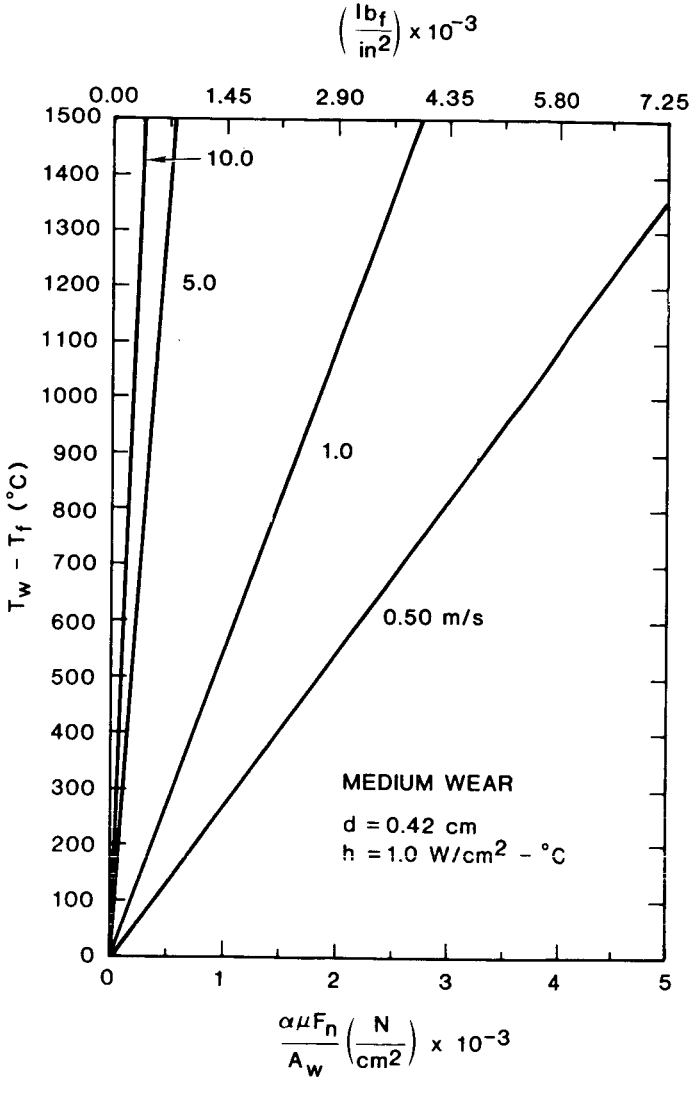

Figure B7

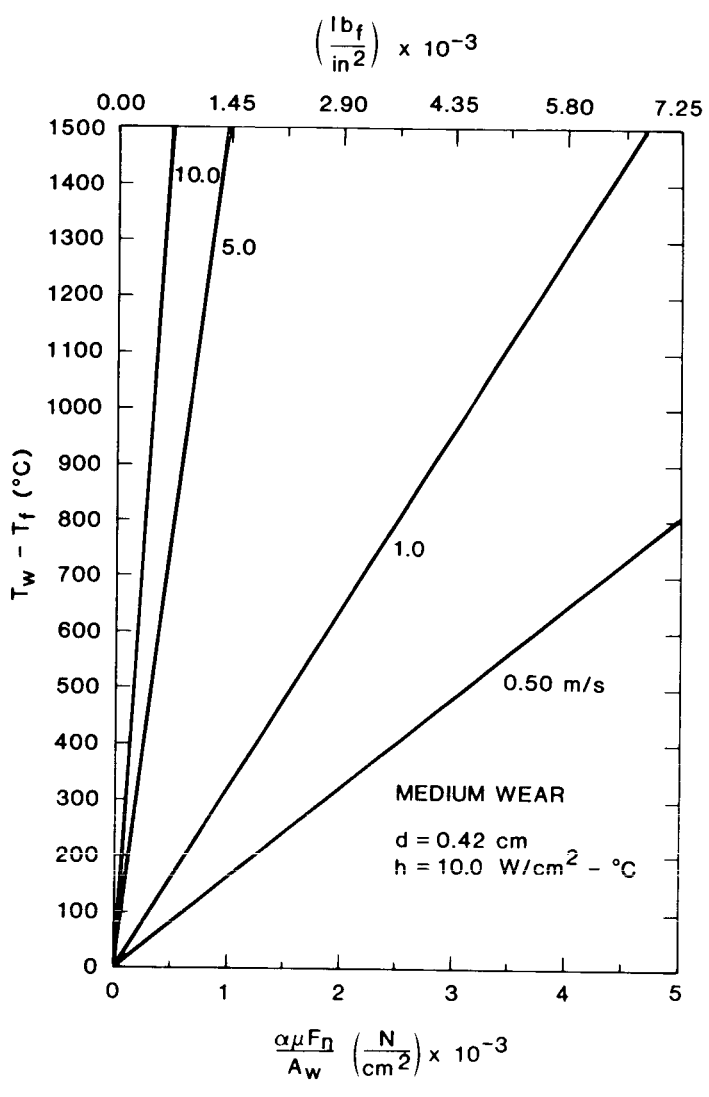

Figure B8

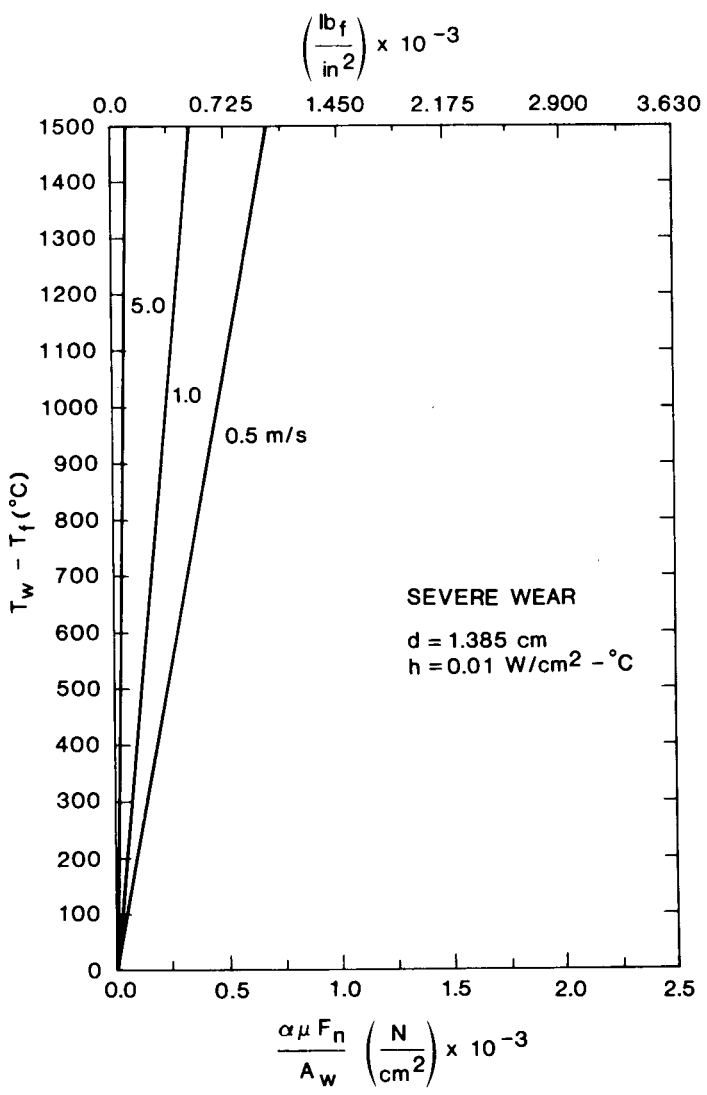

Figure B9

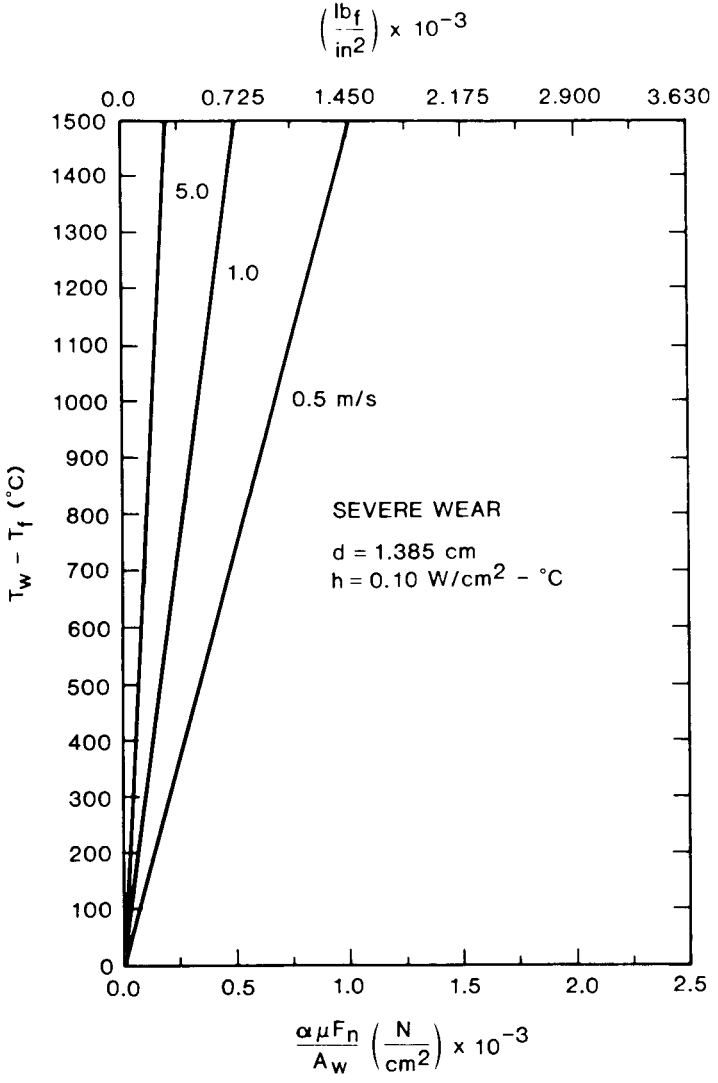

Figure B10

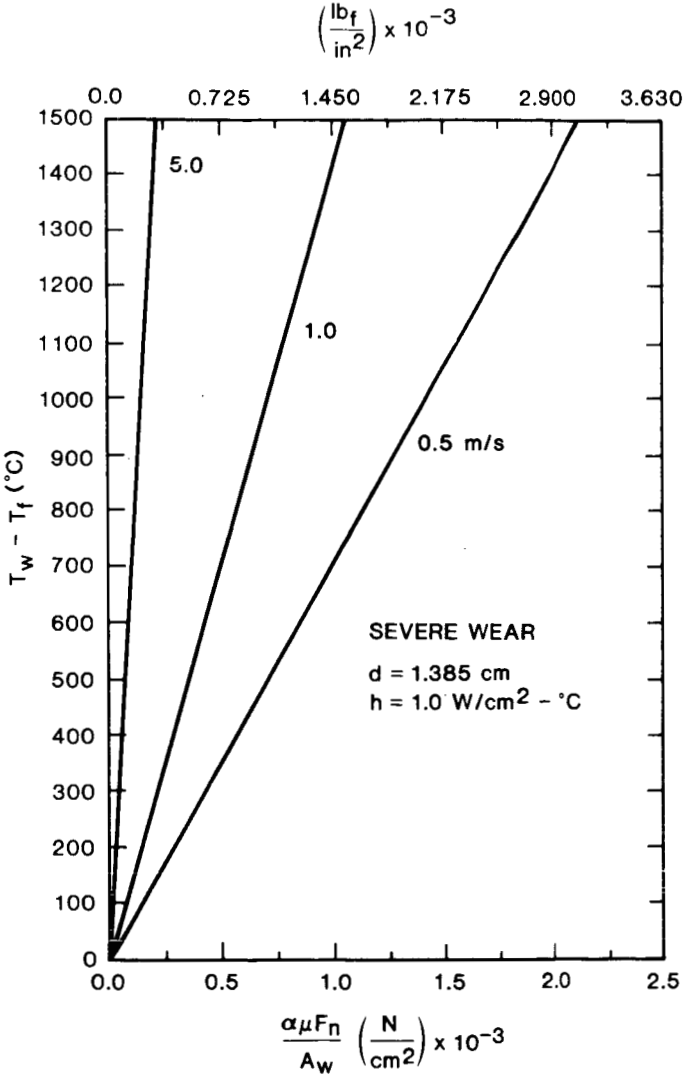

Figure B11

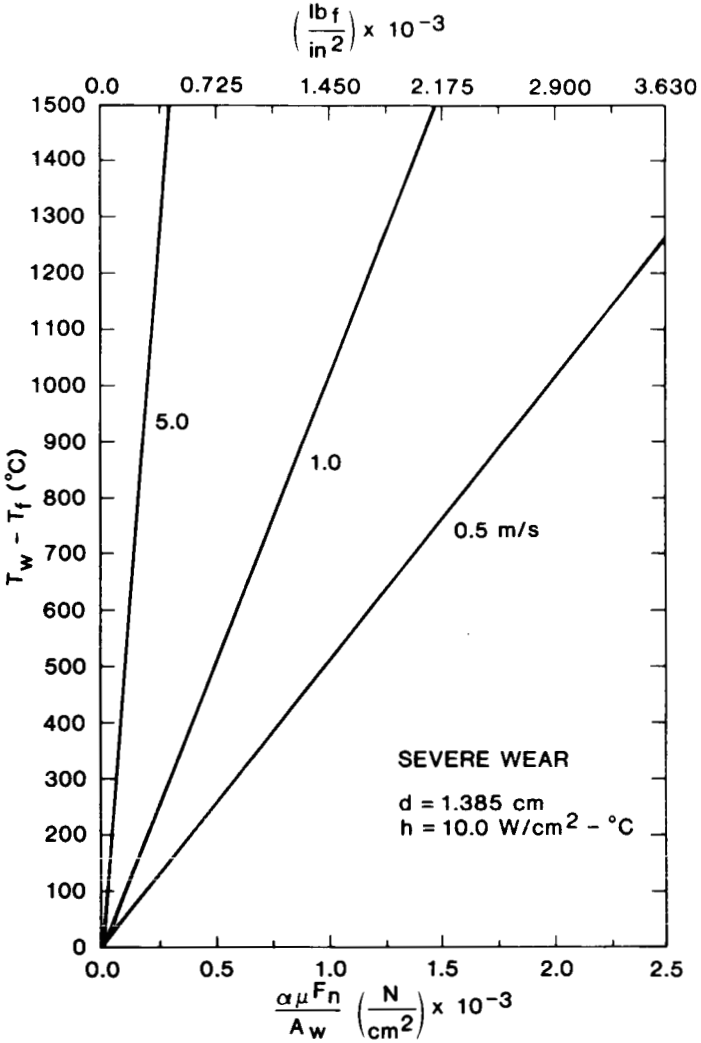

Figure B12

APPENDIX C

SAMPLE CALCULATIONS

OF WEARFLAT TEMPERATURES

APPENDIX C

SAMPLE CALCULATIONS OF WEARFLAT TEMPERATURES

Comparison of the Theory to the Hibbs Data for Tennessee Marble

i. Fixed parameters:

$d \tilde{=} 0.42$ cm - wearflat dimension

$\chi_2 = 0.01$ cm^2/s - rock thermal diffusivity

$k_2 = 0.019$ W/cm-°C - rock thermal conductivity

V = variable cm/s - cutting velocity

A = cooling nozzle area

ii. Approximation of h

Reynolds number of fluid flow over cutter is given by:

$$Re = \frac{\rho_f \, u \, D}{\mu_f}$$

$$u = \frac{Q}{A_{nozzle}} = \frac{6.3 \text{ gpm}}{\frac{\pi}{4}\left(\frac{1}{24}\right)^2 \text{ ft}^2} \times \frac{.1337}{60} = 10.3 \frac{\text{ft}}{\text{s}}$$

$D = .625$ in $= 0.052$ ft

$\mu_f/\rho_f = 1.057 \times 10^{-5}$ ft^2/s at 20°C

$$Re = \frac{(0.052)(10.3)}{1.057 \times 10^{-5}} \sim 5 \times 10^4 \quad Q = 6.3 \text{ gpm}$$

$$\sim 1 \times 10^4 \quad Q = 1.4 \text{ gpm}$$

From Figure 15:

h = 0 (1.0 W/cm^2-°C) for Re = 0 (4×10^4)

h = 0 (0.5 W/cm^2-°C) for Re = 0 (1×10^4)

iii. $F_c \sim F_f$

iv. Approximation of α

for d = 0.42 cm

h = 1.0 W/cm^2-°C f = 0.54 (Figure 8)

h = 0.5 W/cm^2-°C f = 0.68

for V = 1.1 m/s

$$\alpha = \left[1 + \frac{3\sqrt{\pi}}{2} \frac{k_2}{d} \left(\frac{Vd}{4\chi_2}\right)^{1/2} f\right]^{-1}$$

$$= \left[1 + \frac{3\sqrt{\pi}}{2} \frac{(0.019)}{(0.42)} \left(\frac{(110)(0.42)}{(4)(0.01)}\right)^{1/2} f\right]^{-1}$$

$\alpha = 0.31$ $\quad h = 1.0$ W/cm^2-°C

$\alpha = 0.26$ $\quad h = 0.5$ W/cm^2-°C

for $V = 0.44$ m/s

$\alpha = 0.42$ $\quad h = 1.0$ W/cm^2-°C

$\alpha = 0.36$ $\quad h = 0.5$ W/cm^2-°C

Alternatively, α may be found from Figure 10 for these same properties.

v. From equation 33: $T_w - T_f = (\alpha F_f V/A_w)f$

for Test No. 47 of Table 9

$F_f \cong F_c = 204.6$ N

$V = 0.44$ m/s

$A_w = (d)(1.0) = 0.42$ cm^2 for 2-D theory

$\alpha = 0.42$

$f = 0.54 \frac{°C}{W/cm^2}$

$T_w - T_f = (0.42)\frac{(204.6)(0.44)}{(0.42)}(0.54) = 48.61°C$

for $T_f \sim 20°C$

$T_w = 68.61°C$

The measured temperature was 65.5°C.

APPENDIX D

APPENDIX D

Calibration of Flow Channel

The flow channel used to measure convective heat transfer coefficients for a single PDC cutter in crossflow was designed for uniform flow through the test section. To verify this design goal, centerline velocities u_c were measured across a range of volumetric flow rates through the channel. The results are shown in Figure D1. Also shown in this plot is the curve for the mean velocity, $\bar{u}$, computed from the equation

$$\bar{u} = Q/A_u \quad , \tag{D-1}$$

where Q is the volumetric flow rate and A_u is the unobstructed (cross-sectional) flow area of the test section. Thus

$$A_u = (15.7 \text{ cm})(1.9 \text{ cm}) = 29.8 \text{ cm}^2 = 0.0298 \text{ m}^2 \quad .$$

The results shown in Figure D1 imply that minimal boundary layer development occurs in the test section, and therefore, the test section flow is relatively uniform. For example, the minimum value of the ratio $\bar{u}/u_c$ is 0.93 (at 2.5 L/s). On the other hand, fully developed flow in a rectangular duct, where the boundary layers extend from the walls to the center, is characterized by the equation [49].

$$\frac{\bar{u}}{u_c} = \frac{\pi^3}{96} \frac{\left[1 - \frac{192a}{\pi^5 b} \sum_{i=1,3,5,\ldots} \tanh(i\pi b/2a)/i^5\right]}{\sum_{i=1,3,5,\ldots} (-1)^{(i-1)/2}\left[1 - \frac{1}{\cosh(i\pi b/2a)}\right]/i^3} \tag{D-2}$$

where a is the half-width of the duct and b is its half-height. Substituting a = 15.7 cm/2 = 7.85 and b = 1.9 cm/2 = .95 cm into the above equation gives the result

$$\frac{\bar{u}}{u_c} = 0.077 \quad . \tag{D-3}$$

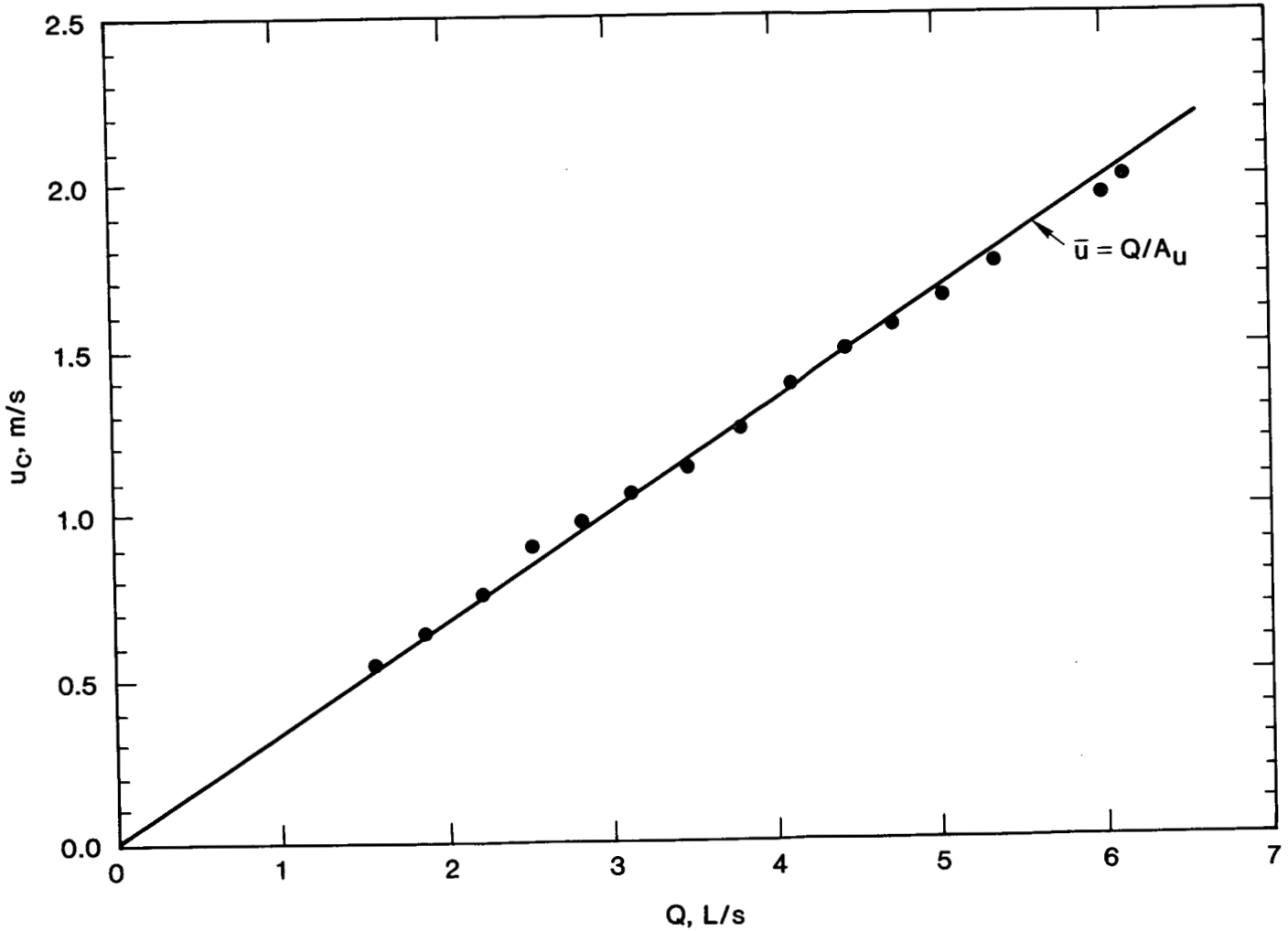

Figure D1. Measured Flow Channel Centerline and Mean Velocities

Comparing equation D-3 with the minimum value of $\bar{u}/u_c = 0.93$ measured in the flow channel illustrates that very little boundary layer development occurs in the test section.

Derivation of Heat Transfer Coefficient Equation

The electrical power supplied to the heat transfer gage, P_E, is converted to thermal power, P_T, by the electrical resistance of the gage. For a constant gage temperature T_G, all of this power must be transferred to the gage surroundings. Referring to Figure D2, the thermal power can flow in three directions: to the fluid via the gage encapsulant, to the surface to which the gage is mounted, and through the electrical leads. Thus

$$\begin{aligned} P_E &= P_T \\ i^2 R_G &= Q_c + Q_\ell \\ i^2 R_G &= h A (T_s - T_c) + Q_\ell \end{aligned} \qquad \text{(D-4)}$$

Here the electrical power has been expressed in terms of the measured current, i, and the predetermined gage resistance, R_G. The convected heat rate is expressed in terms of the heat transfer coefficient, h, the gage sensing area, A, and the difference between the temperatures of the gage encapsulant surface, T_s, and the fluid, T_f. The electrical lead and mounting surface heat losses have been lumped into the single term Q_ℓ.

It is desirable to express the convected heat rate in terms of the gage temperature T_G, rather than the gage encapsulant surface temperature, T_s. This may be done by noting that the convected heat rate is equal to the conducted heat rate between the gage grid and the encapsulant surface. Thus

$$h A (T_s - T_f) = \frac{k A}{t} (T_G - T_s) \quad , \qquad \text{(D-5)}$$

where k = thermal conductivity of phenolic encapsulant

t = thickness of encapsulant.

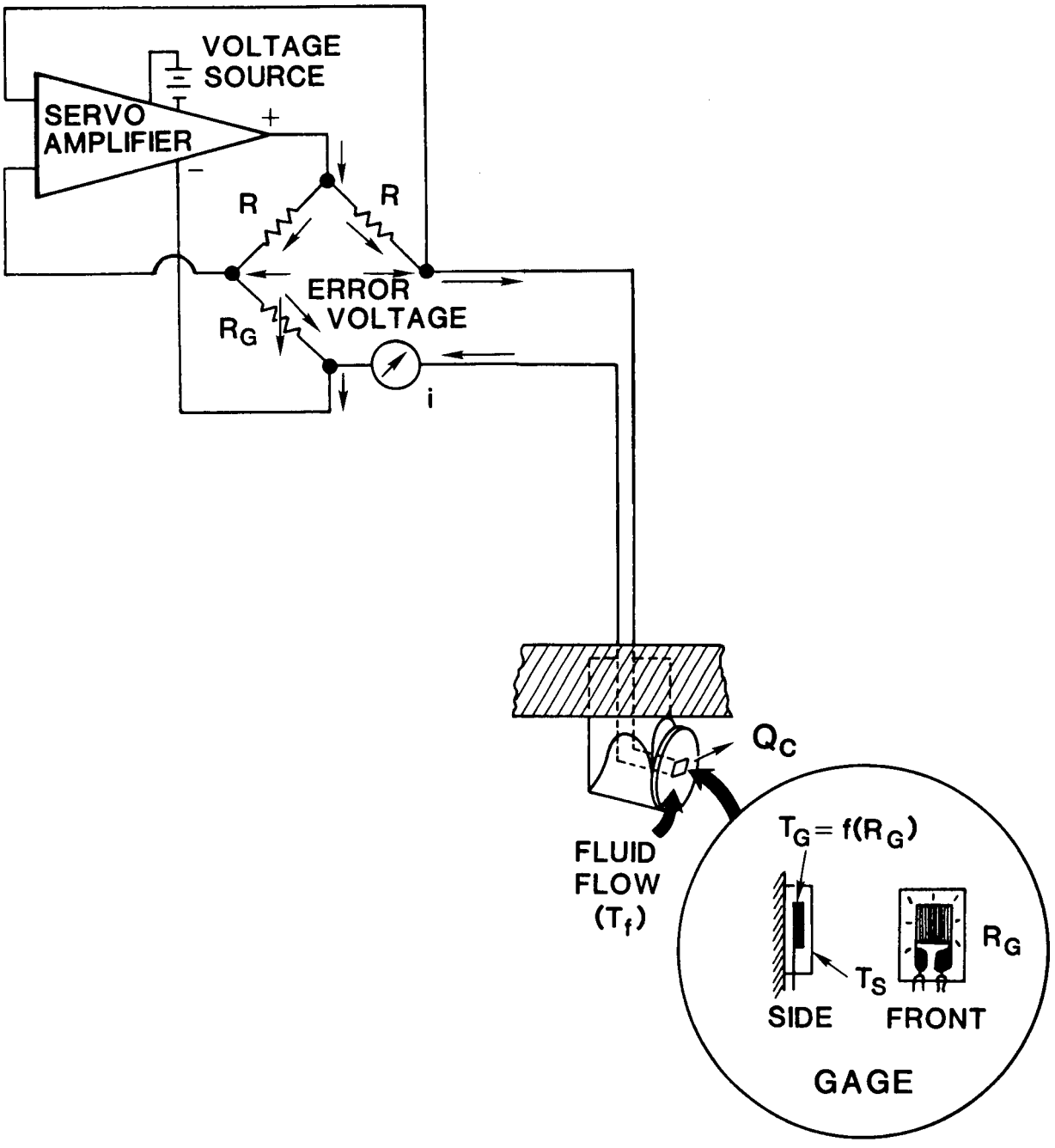

Figure D2. Details of Technique for Measuring Convective Heat Transfer Coefficients

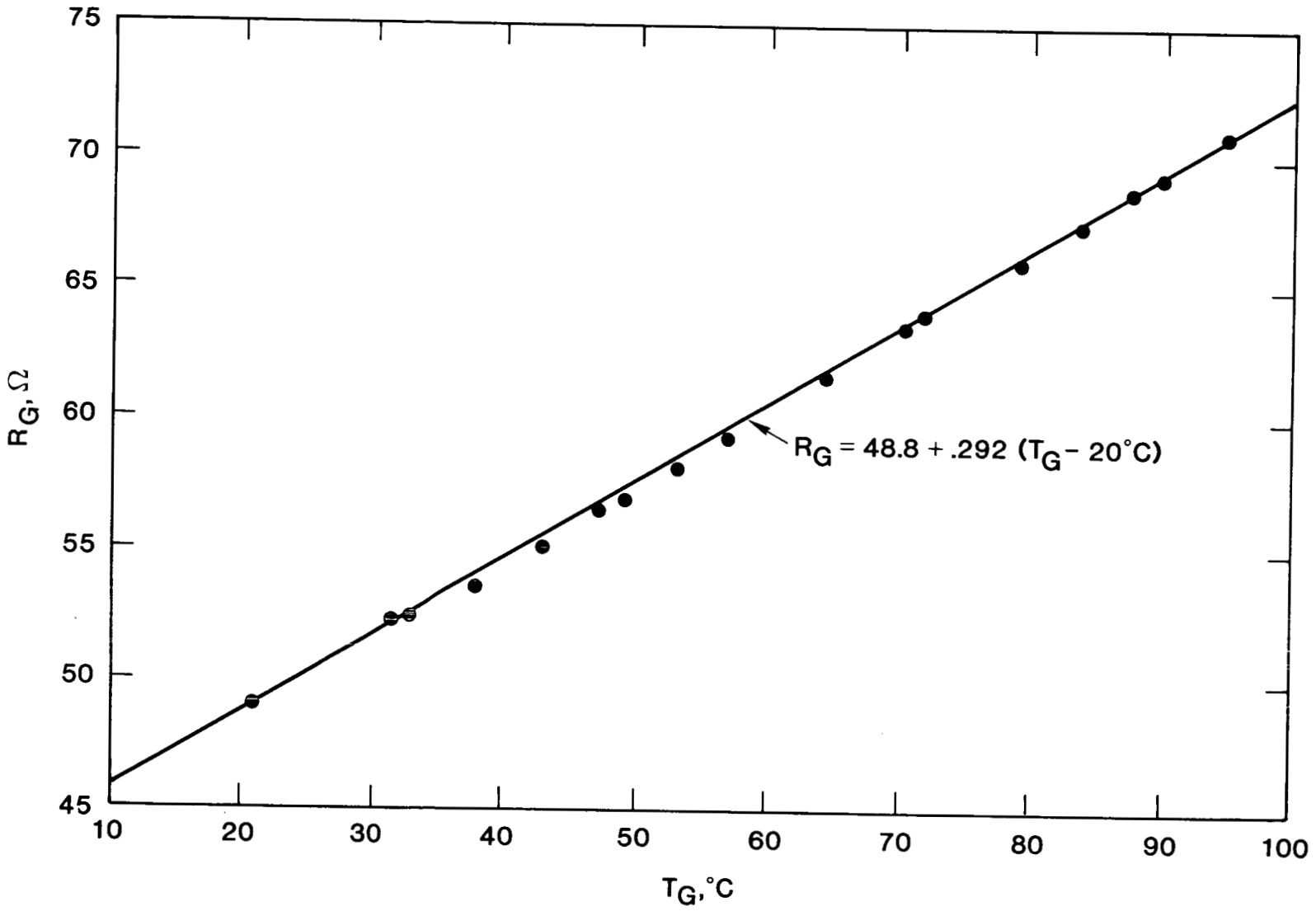

Figure D3. Heat Transfer Gage Electrical Resistance

Defining κ as the specific conductance of the encapsulant

$$\kappa = \frac{k\,A}{t} \quad , \tag{D-6}$$

solving for T_s, and substituting into equation D-4 gives the result

$$h = \frac{i^2 R_G - Q_\ell}{A(T_G - T_f) + (Q_\ell - i^2 R_G)/\kappa} \tag{D-7}$$

The quantities $\underline{i}$ and T_f are measured. The values of A (.039 cm^2) and κ (.058 W/°C) are known from physical properties of the gage. The value of T_G is predetermined; a nominal value of 60°C was chosen for the present study. The corresponding value of R_G is obtained from the calibration curve obtained in the present study and shown in Figure D3. This value is then set by adjusting the variable resistor shown in the circuit of Figure D2.

The only remaining quantity in equation D-7 is the lead and surface heat loss, Q_ℓ. This quantity was obtained by numerically modeling the gage-lead and gage-mounting surface interfaces with CINDA [50]. Since the heat transferred to the leads and mounting surfaces is eventually convected to the fluid via a different location on the mounting surface, Q_ℓ is presented in Figure D4 as a function of the heat transfer coefficient, which was assumed for this purpose to be constant over the mounting surface. At low values of h, the majority of the resistance heating flows into the leads and mounting surface. As $\underline{h}$ increases, Q_ℓ drops in diminishing proportion, until at large values of $\underline{h}$, Q_ℓ is only about 15% of the electrical power dissipated.

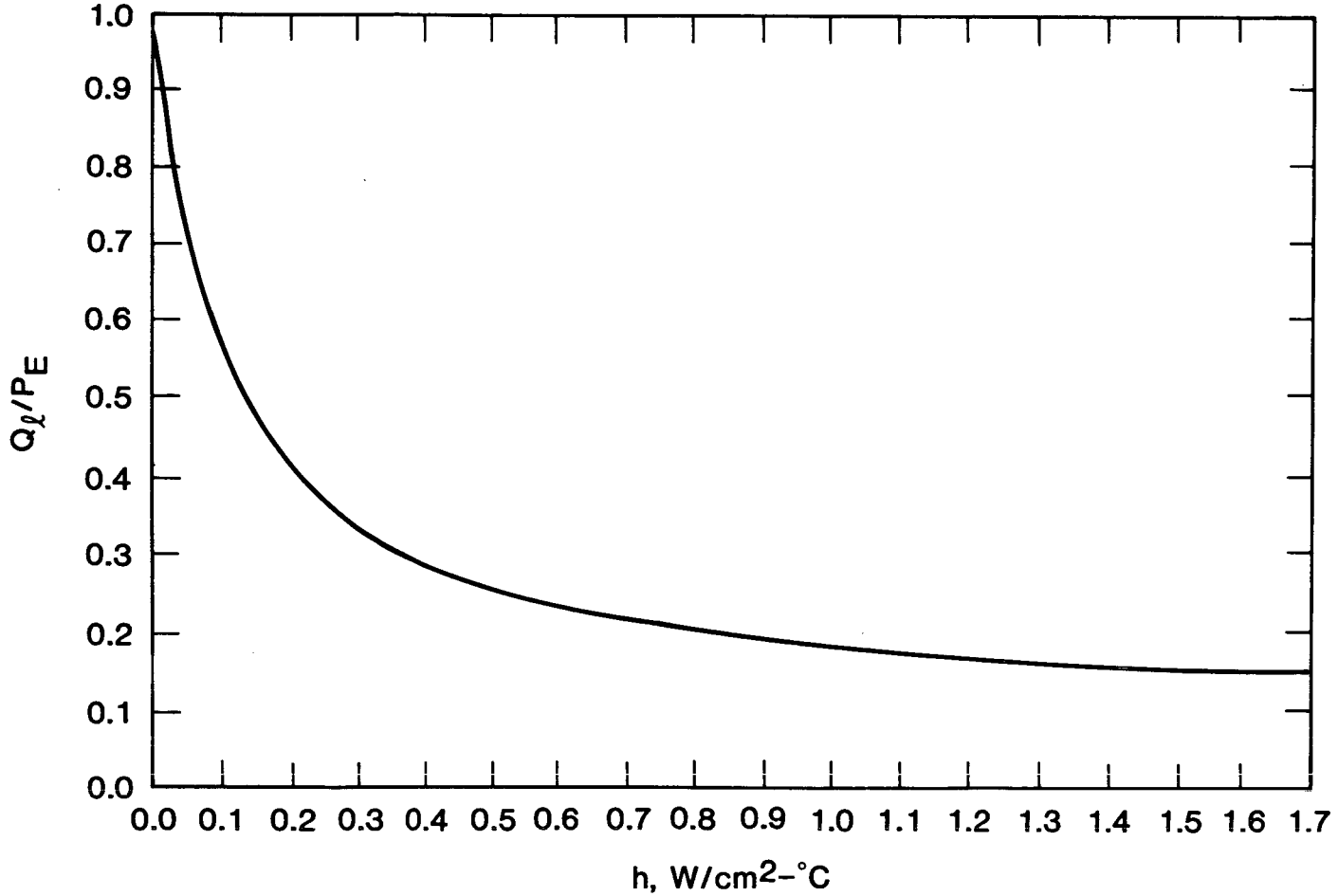

Figure D4. Relative Lead and Mounting Surface Heat Losses

DISTRIBUTION
TID-4500-R66-UC-66C (507)

Tom Anderson
Venture Innovations
P. O. Box 35845
Houston, Texas 77035

Ed Bingman
Shell Oil Company
Two Shell Plaza
P. O. Box 2099
Houston, Texas 77001

Larry Diamond, Vice President
Technical Services
Dyna-Drill
P. O. Box C-19576
Irvine, California 92713

John E. Fontenot
Manager, Mechanical Engineering
NL Petroleum Services
P. O. Box 60087
Houston, Texas 77205

Dr. Melvin Friedman
Professor of Geology
Center for Tectonophysics
and Dept. of Geology
Texas A&M University
College Station, Texas 77843

Wilton Gravley
Mobil Research & Development Corp.
Field Research Laboratory
P. O. Box 900
Dallas, Texas 75221

L. E. Hibbs, Jr. (2)
General Electric Company
P. O. Box 8, Building K-1
Schenectady, New York 12301

Earl G. Hoff, Director
Development & Operations
Phillips Petroleum Company
Geothermal Operations Headquarters
655 East 4500 South
Salt Lake City, Utah 84107

Jim Kingsolver
Manager, Geothermal Operations
Smith Tool
P. O. Box C-19511
Irvine, California 92713

U.S. Department of Energy
Geopressure Projects Office
Suite 8620, Federal Building
515 Rusk Street
Houston, Texas 77002
Attn: F. L. Goldsberry

James W. Langford
Manager, Research
Security Division
Dresser Industries, Inc.
P. O. Box 24647
Dallas, Texas 75224

Harvey E. Mallory
P. O. Box 54696
Tulsa, Oklahoma 74155

Gene Polk
NL Baroid
6400 Uptown Blvd., 365W
Albuquerque, New Mexico 87110

Del E. Pyle
Manager of Operations
Union Geothermal Division
Union Oil Co. of California
Union Oil Center
Los Angeles, California 90017

John C. Rowley
Los Alamos National Labs
Mail Stop 570
Los Alamos, New Mexico 87545

William D. Rumbaugh
Research and Development
Otis
P. O. Box 34380
Dallas, Texas 75234

Dwight Smith
Halliburton
Drawer 1431
Duncan, Oklahoma 73533

Tom Warren
Amoco Production Company
Research Center
P. O. Box 591
Tulsa, Oklahoma 74102

Dr. John Edwards
U.S. Bureau of Mines
Cochrans Mill Road
Pittsburgh Research Center
Pittsburgh, PA 15236

U.S. Department of Energy (3)
Geothermal & Hydropower Division
Forrestal Building, CE 324
1000 Independence Ave., SW
Washington, DC 20585
Attn: J. Bresee
D. Clements
D. Allen

DO NOT MICROFILM

1315 E. R. Hoover
3141 L. J. Erickson (5)
3151 W. L. Garner (3)
4000 A. Narath
4537 J. R. Tillerson
4700 E. H. Beckner
4740 R. K. Traeger
4741 J. R. Kelsey (15)
4741 C. C. Carson
4741 B. C. Caskey
4741 J. T. Finger
4741 D. A. Glowka (15)
4743 H. C. Hardee
4746 B. Granoff
4747 P. J. Hommert
4748 B. E. Bader
4750 V. L. Dugan
5500 O. E. Jones
5510 D. B. Hayes
5512 D. F. McVey
5512 A. Ortega (15)
5520 T. B. Lane
5521 D. V. Swenson
5522 L. M. Ford (3)
5530 W. Herrmann
5541 W. C. Luth
5830 M. J. Davis
5833 J. L. Jellison
5833 L. E. Pope
8214 M. A. Pound

☆U.S. GOVERNMENT PRINTING OFFICE: 1982-0-576-021/579